Stony Brook University

Water and Ion Transport in Lacrimal Gland: Models and Experiment

A Dissertation Presented

by

Wei Chieh Huang

to

The Graduate School

In Partial Fulfillment of the

Requirements

for the Degree of

Doctor of Philosophy

in

Physiology and Biophysics

Stony Brook University

August 2010

Stony Brook University

The Graduate School

Wei Chieh Huang

We, the dissertation committee for the above candidate for the
Doctoral of Philosophy degree,
hereby recommend acceptance of this dissertation.

Leon C. Moore Ph.D. – Dissertation Advisor
Professor
Department of Physiology and Biophysics

Peter Brink Ph.D. – Chairperson of Defense
Professor and Chairman
Department of Physiology and Biophysics

Chris Clausen Ph.D.
Associate Professor
Department of Physiology and Biophysics

Peter Reinach Ph.D. – Outside Member
Professor
Biological Sciences SUNY College of Optometry

This dissertation is accepted by the Graduate School

Lawrence Martin
Dean of the Graduate School

Abstract of the Dissertation
Water and Ion Transport in Lacrimal Gland: Models and Experiment
By
Wei Chieh Huang
Doctor of Philosophy
In
Physiology and Biophysics
Stony Brook University
2010

Tear secretion is a complicated process that involves two different cell types. The lacrimal acinar cell is thought to secrete a hypertonic primary fluid with a high K^+ concentration. This fluid is then modified by the ductal epithelia and transported to the avascular ocular surface. It is known that both sympathetic and parasympathetic input trigger protein release, but the role of adrenergic stimulation on water secretion in lacrimal gland remains unclear. **Therefore, the first goal of this dissertation is to examine the influence of α- and β-adrenergic activation on tear fluid production**.

Tear secretion requires coordination of different membrane channels and transporters. Walcott *et al*. showed the importance of basolateral Na^+-K^+-$2Cl^-$-cotransporter (NKCC1) on secretion rate. **The second goal is to develop an acinar cell mathematical model with cell volume regulation**. The model is used to examine whether NKCC1 alone is sufficient to generate hypertonic tear fluid with high KCl content when the cell is stimulated. Subsequently the model was expanded with acid-base regulatory transporters to investigate the interaction between volume- and pH-regulation systems. This effort led to the discovery that the sodium-bicarbonate transporter is expressed in lacrimal gland and participates in tear production.

Lastly, since acinar and duct cells express same membrane channels and transporters, it is likely that duct cells secrete a hypertonic fluid like acinar cell. **The third goal of this project is to develop a duct cell model and combine it with the acinar cell model**. The combined model was used to examine the flow dependence of tear composition. The predictions agree with measurements made in anesthetized rats.

Dedications

This dissertation is dedicated to my family for their support and inspiration.

Table of Contents

List of Symbols

Symbols	Description
V_c	Cell Volume
V_a	Apical Luminal Volume
V_L	Tubule Luminal Volume
V_{set}	Cell Volume Set Point
A	Major Axis
B	Minor Axis
a	Apcial Membrane
b	Basolateral Membrane
j	Tight Junction
o	Subscript Denoting “Exit”
A	Membrane Area
J^w	Water Flux
J^i	Solute Flux
$J_{chemical}$	Carbonic Anhyrase Flux
t	Time
i	Subscript Denoting “Solutes”
C^i	Concentration
E	Membrane Potential
Et	Transepithelial Potential
I	Membrane Current
F	Faraday's Constant
Z_i	Valence Charge
P	Membrane Permeability
σ	Reflection Constant
E_T	Total Amount of Enzyme
τ	Time Constant
k	Transporter Binding Rate Constants

K_d	Water Dehydration Rate Constant
K_h	Water Hydration Rate Constant
P_{CO2}	CO_2 Partial Pressure
K	Dissociation Constant
H_T	Total Free H^+

List of Figures

List of Tables

Acknowledgement

I would like to thank my advisor, Dr. Leon C. Moore for his help and support. Thank you for giving me this wonderful chance to work in your lab. Thank you for your patience when I was having slow moments in the lab. In addition to learning science, I learned to think thoroughly and look at a problem from different aspects before making conclusions. You have my highest respect as a mentor, a professor, a scientist, and a person. I am honored to be your student, and your advice will benefit me for the rest of my life.

To my dissertation chairman Dr. Peter R. Brink. Thank you for your support since the day I joined the department. I still remember your helpful advice throughout all these years.

I would like to thank my committee member, Dr. Chris Clausen. To me, you are the talking encyclopedia who knows almost everything in the world. Thank you for telling all those interesting stories. More importantly, thank you for spending many days teaching me computation modeling and troubleshooting my code.

To my dissertation outside committee member, Dr. Peter Reinach, thank you for coming all the way for my dissertation defense.

I would like to thank Dr. Irene C. Solomon for her generous support when I first joined the department. Thank you for getting me into the department. Thank you for all the helpful advice you have given me throughout my graduate life.

I would also like to thank Aija Birzgalis for all of her help. Thank you for teaching me all that I needed to know about conducting animal research. Thank you for always being there to set up the equipment for the experiments.

To my labmates and friends, Aniel Nieves-Gonzalez and Dr. Juan Cordovez, thank you for all your help, especially for troubleshooting my code when I got stuck.

I would like to thank my wife, Hui Jing Yu, who is always by my side since we were in high school. Thank you for introducing me to the graduate program in Physiology and Biophysics, and thank you for all your support and love. When you are there you make my days easier and happier.

Chapter 1. Summary of Key Findings

The following are the major findings of this research:

1. We demonstrated that adrenergic stimulation does not trigger tear secretion in anesthetized mice.
2. We showed that an acinar cell model with Na^+-K^+-$2Cl^-$ cotransporter (NKCC1) as the only basolateral loading pathway is sufficient to account for the generation of hypertonic tear fluid with high K^+ concentration, but fails to explain residual tear secretion during NKCC1 inhibition.
3. We established that the acinar cell secretion of hypertonic tear fluid requires a) muscarinic-induced increases apical K^+ and Cl^- conductances, b) cation-selective tight junctions with $P_{Na} >> P_K \geq P_{Cl}$, c) low apical membrane water permeability.
4. We found that muscarinic-induced cellular alkalization in acinar cells is due to a two-fold increase in NHE activity.
5. We simulated the effects of transporter inhibition on resting I_{sc} and found evidence suggesting compensation between cell volume and pH regulation transport pathways.
6. We established that the pNBC transporter is expressed in lacrimal gland, and that its activity can account for the residual I_{sc} during NKCC1 and NHE blockade.
7. We analyzed the dynamics of the I_{sc} response to muscarinic stimulation and found evidence of differential regulation of both NKCC and pNBC, possibly via a PKC-dependent pathway.

8. We found that the primary secretion from the acinar cell model is hypertonic with a high K^+ concentration that depends strongly on the cytosolic Cl^- concentration.
9. We analyzed rat tear samples and found that the ionic composition was flow dependent in a manner consistent with the predictions of our duct cell model.
10. We demonstrated that apical K^+-Cl^- cotransporter (KCC1) in duct cells strongly influences basal tear secretion, but had no effect on tear flow or composition when the cells were stimulated
11. We established that the rate of tear production depends strongly on the ratio of apical membrane area in duct cells to that of acinar cells.

Finally, this project is a good example of the synergism between mathematical modeling and experimental work in an investigation of a complex problem. A mathematical model is nothing more than an explicit representation of a hypothesis in a computable form that provides detailed and quantitative predictions about system behavior. The underlying hypothesis is tested by comparison of the model predictions to measured behaviors. Although agreement between model prediction and data bolster confidence in the adequacy of the hypothesis and the model, often more is learned when the model fails to predict known behaviors. Systematic analysis of the failure is highly informative, in that it often reveals shortcomings in the underlying hypothesis, errors in the model, or sometimes even flaws in the experimental data. Correction of the underlying cause of the failure results in real progress. In this project, our models failed to predict measured behaviors in three instances, and in each case new insight was

gained. The first led to a deeper understanding of the interactions between the cell-volume and pH-regulation transport pathways. The second revealed the involvement of the pNBC transporter in lacrimal gland, which lead us to immunocytochemistry studies confirming the existence of the transporter. And third, it led us to perform experiments to characterize the flow dependency of tear ionic composition.

Chapter 2. Lacrimal Gland Function and Dry-Eye Disease

2.1 Lacrimal Gland Anatomy and Functions

In humans, the lacrimal gland is an almond-shaped exocrine gland that is located on top of the anterior and lateral parts of the orbit of the eye. Like other exocrine glands, such as salivary gland and pancreas, the lacrimal gland is composed of many lobes. Within each lobe, acinar cells are arranged into tubuloacinar structures such that the fluid secreted by the acinar cells drains into a small duct. Multiple small ducts converge into larger ducts. The larger ducts then join together at the main lacrimal duct, which directs secretions onto the surface of the eyes.

The lacrimal glands secrete tear-specific proteins and the majority of the water and electrolytes that bathe the ocular surface. The secretory epithelium mainly consists of acinar cells (80% of the mass the gland), and the remaining are lacrimal duct cells (12% of the total mass), myoepithelial cells and plasma cells (1). The columnar acinar cells are thought to be the primary secretory cells in the lacrimal gland. They are arranged into a spherical epithelium and connected by tight junctions that separate basolateral and apical membranes. On the apical aspect of the cell, the cytosol is filled with secretory granules that contain tear-specific proteins and other secretory products. Stimulation of basolateral-membrane receptors triggers apical exocytosis and the subsequent release of the vesicular contents into the lumen. Water secretion by acinar cells facilitates delivery of luminal content to the ocular surface. Many different proteins are secreted from acinar cells. Proteins that protect the cornea from pathogens include: IgA, lactoferrin, lysozyme, and peroxidase; proteins and humoral substances that support

cell growth are: retinol, epidermal growth factor (EGF), transforming growth factor, and endothelin-1. Synthesis of these proteins is controlled by circulating hormones, except for IgA which is secreted by plasma cells and transported into and stored in acinar cells. Protein secretion is regulated by neural reflexes.

Unlike acinar cells, duct cells do not contain secretory granules and, thus, their role in protein secretion is thought to be limited. The only known protein secreted from duct cells is EGF (2). Very little is known about the mechanism of water and electrolyte secretion by lacrimal duct cells. Only one study reported that lacrimal duct cells modify primary secretion of the acinar cells to generate a hypertonic fluid. Gene expression analysis shows that duct cells express the same membrane channels and transporters as acinar cells, including apical aquaporin 5 (AQP5), K^+ and Cl^- channels and basolateral Na^+-K^+-$2Cl^-$ cotransporter (NKCC1), Na^+-H^+ exchanger (NHE), and Cl^--HCO_3^- exchanger (AE1) (3). Also, both duct cells and acinar cells showed similar levels of alkalization (4) and cytosolic Ca^{2+} oscillation (5-6) in response to carbachol (muscarinic agonist) stimulation. These findings strongly suggest that duct cells may secrete a fluid that is similar, if not identical, to the acinar cell secretion.

2.2 Neural Regulation of Lacrimal Secretion

Lacrimal gland secretion is regulated by neural input. External stimuli trigger activation of sensory nerves in the cornea and conjunctiva which in turn activates the efferent limb via a simple reflex arc in the central nervous system. In response, the efferent limb sends signals from both sympathetic and parasympathetic nerves to stimulate lacrimal gland secretion. Activation of parasympathetic nerves leads to release

of the neurotransmitters acetylcholine and vasoactive intestinal peptide (VIP), which causes water and protein secretion. Activation of sympathetic nerves releases the neurotransmitter norepinephrine which also triggers protein secretion from the lacrimal gland.

2.2.1 Muscarinic Activation of Lacrimal Gland Secretion

Acetylcholine is released from parasympathetic nerves and activates secretion from both acinar (1) and duct cells (3) by binding to M_3 muscarinic receptors on the basolateral membranes. Activated M_3 receptors interact with the $G_{q/11}$ subtype of G-proteins, which then activates phospholipase C (PLC) to break down phosphatidylinositol bisphosphate (PIP_2) into 1,4,5-inositol trisphosphate (IP_3) and diacylglyerol (DAG). IP3 then binds to its receptor (IP_3R) which is located on the endoplasmic recticulum (ER). Activation of IP_3R leads to release of cytosolic Ca^{2+} from intracellular stores for downstream signal transduction. Cytosolic Ca^{2+} levels are maintained by enhanced Ca^{2+} influx. The rise of cytosolic Ca^{2+} activates Ca^{2+}/calmodulin-dependent protein kinases which stimulate protein secretion. This is accomplished by increasing the rate of secretory vesicle fusion with the apical membrane. Moreover, increased Ca^{2+} also causes the opening of apical membrane K^+ and Cl^- channels. This increases ion efflux into the acinar lumen, with water following via osmosis.

In additional to IP_3, DAG activates specific protein kinase C (PKC) isoforms that are bound to the basolateral membrane. Phosphorylation of PKCα activates downstream signal transduction molecules which are involved in water, electrolytes and protein

secretions. Two other isoforms are also activated by DAG: PKCε and –δ. They are thought to be involved in Ca^{2+} handling in lacrimal acinar cells, and they play inhibitory role in termination of stimulated secretion (7)

2.2.2 VIP Activation of Lacrimal Gland Secretion

VIP is another important cholinergic agonist that is known to stimulate protein secretion in lacrimal glands. VIP binds to receptors (predominately VIPR1 in lacrimal acinar cells) on the basolateral membrane. VIPR1 interacts with a G-protein (Gs), which in turn activates adenylyl cyclase (AC). Phosphorylation of AC generates cyclic-AMP (cAMP) from ATP. The rise of cytosolic cAMP levels activates protein kinase A, which causes water, electrolyte, and protein secretion. VIP stimulated secretion is terminated by cAMP phosphodiesterase.

2.2.3 Sympathetic Stimulation of Lacrimal Gland Secretion

Norepinephrine is released from sympathetic nerves and it can bind to both α_1- and β-adrenergic receptors on lacrimal gland cells. Activated α_1-adrenergic receptors interact with a G-protein ($G_{q/11}$). This causes a small increase in cytosolic Ca^{2+} (much smaller than muscarinic stimulation), but the mechanism for the rise in Ca^{2+} level is not clear (1). However, one study showed that activation of α_1-receptors increase cyclic-ADP-ribose (cADP-ribose) levels. cADP-ribose binds to ryanodine receptors located on the ER membrane which leads to Ca^{2+} release and increased exocytosis (1). Activated $G_{q/11}$ also forms DAG via an unknown pathway; DAG activates PKCα, -ε, and -δ. PCKε has stimulatory effect on lacrimal acinar cells for protein secretion, while PKCα, and –δ

inhibits α_1-adrenergic stimulation. This could be one of the mechanisms that terminate secretion.

β-adrenergic stimulation does not cause an increase in cytosolic Ca^{2+}, but does raise protein secretion via a cAMP-dependent pathway (8). A dose-response study of lacrimal gland protein secretion showed a higher EC_{50} in response to β-adrenergic stimulation compared to α_1-adrenergic and activation. This could be due to the fact that most of the β-adrenergic receptors are located in the cytosol in lacrimal gland (9).

2.3 Dry-Eye Disease

The function of tear secretion is to provide nutrients and to protect the avascular ocular surface from the outside world. A significant impairment of tear secretion leads to discomfort and a feeling of dryness in the eyes, a disorder known as dry-eye disease. If untreated, it will lead to dryness of the corneal epithelium, damage to the cornea, increased chance of foreign invasion, and, in severe cases, it can lead to loss of vision. There are two types of dry-eye disease: aqueous-deficient and evaporative dry-eye. Aqueous-deficient dry-eye is mainly due to reduced water secretion from the main lacrimal gland. Evaporative dry-eye is associated with meibomian gland dysfunction. Reduction of lipid output from meibomian gland leads to increased evaporation of the aqueous layer of tear fluid, and dry eye results.

Currently there is no truly effective therapy for dry-eye diseases because the etiology of this disease is ill-defined. Available treatments, which only prevent further damage to the ocular surface, include: topical autologous serum eye drops, artificial tears, punctual plug occlusion, humidified goggles, and immunosuppressants such as

cyclosporine. There are 10 million people in United States alone who have been diagnosed with dry-eye diseases (14). Sjögren's Syndrome (SS), which is one type of aqueous-deficient dry eye, affects more than three million people (14). SS is an autoimmune disorder that is characterized by lymphocytic infiltration in lacrimal gland tissue. In lacrimal gland (as well as in salivary gland), there is a marked increase in numbers of memory B and T cells in the tissue, and this is associated with extensive destruction of acinar and duct cells (10). Also, there is increased expression of cytokines (interlukin1α and $-\beta$) and pro-oncogenes (tumor necrosis factor α). These processes eventually lead to a decrease of water output, possibly due to a number of different mechanisms, including loss of acinar and duct cells, destruction of innervating nerves, inhibition of neurotransmitter release from neurons, inhibition of neurotransmitter receptors in exocrine gland, inhibition of sensory nerve activity. It is well documented that lymphocytic infiltration is one of the most important hallmarks of SS, but the precise mechanism that triggers the immune response remains unknown. Because it has been reported that post-menopausal females are ~10 times more likely to be diagnosed with dry-eye symptoms than males, it has been hypothesized that reduction of circulating androgen levels may be a trigger for immune response in lacrimal and salivary glands.

2.3.1 Androgen Influence of Lacrimal Gland Function

In rabbits, it has been demonstrated that lacrimal gland function can be influenced by circulating androgen levels. Lacrimal gland function was assessed after ovariectomy and compared to a sham-surgery group. The results showed increased total DNA degradation due to cell death (11) and decreased β-adrenergic receptors (12). Moreover,

the same group found glandular atrophy in ovariectomized rabbits (11), and this is due to necrosis of lacrimal acinar cells. Importantly, these changes were prevented by dihydrotestosterone (DHT) treatment. This supports the concept that androgen has positive effects on lacrimal gland function. One possible explanation is that circulating androgen is anti-inflammatory (13), reducing the progression of lymphocytic infiltration in lacrimal glands. In general, females have stronger immune response in comparison to males, and this could be linked to circulating estrogen levels (14). It is known that estrogen has pro-inflammatory function, such as the promotion of polyclonal B cell activation (15) and autoantibody formation (16). During menopause, circulating androgen levels in females decrease, thereby altering the ratio between circulating androgen and estrogen levels. The imbalance of anti-/pro-inflammatory modulators may lead to stronger immune responses which may eventually trigger the onset of dry-eye disease.

2.3.2 Effect of Pro-inflammatory Cytokines in Lacrimal Gland Function

Lacrimal gland function is further compromised by elevated cytokine levels. Autoantibodies against β-adrenergic and M_3-muscarinic receptors have been detected in serum of both nonobese diabetic (NOD) mice, a murine model of SS (17), and in primary SS patients (18). It has been further demonstrated that this M_3-receptor autoantibody binds to the second extracellular loop of the membrane receptor. As a result, increased Ca^{2+} signaling was observed in MRL/lpr mice, another SS murine model (19). This increase is thought to be transient, and is followed by membrane receptor desensitization and internalization (20). Eventually, this process leads to a down-regulation of membrane receptor density that compromises water and electrolyte secretion in the

lacrimal glands. In addition, elevated cytokine levels could also target the nerves that innervate exocrine glands. Immunocytochemistry on axon proteins or neural peptides reveals marked neural rarefaction in regions with lymphocytic infiltration in salivary gland biopsy samples from SS patients, while the innervation of normal regions is preserved (21). In contrast to this finding, Zoukhri *et al*. showed that lacrimal gland innervation is not altered during the progression of SS in a murine SS model (7), and that reduction of water secretion could be due to impaired neurotransimitter release (22). There is much evidence that indicates that lymphocytic infiltration is the primary cause of dry-eye diseases, and lack of circulating androgen could be one of the major determinants of the strength of the immune response. The primary trigger for the immune response may be viral infections (23), or genetic factors (24). However, it is clear that no single mechanism can fully account for the pathophysiology of dry-eye disease. The etiology of dry-eye diseases remains to be fully elucidated, and it is likely to be multi-factorial.

2.3.3 Water Secretion in Dry-Eye Disease

One of the major symptoms of dry-eye disease or SS is reduced water secretion. Although artificial tears can provide moisture, any reduction of water secretion could lead to reduced delivery of tear-specific proteins and nutrients from the lacrimal acini to the cornea. Decreased fluid secretion from lacrimal gland has been observed in New Zealand Black/White (NZB/W) mouse, another SS murine model, prior to the onset of lymphocytic infiltration (25). This suggests that an increased immune response is not sufficient to explain the reduced water secretion. Moreover, biopsies from SS patients revealed impaired cellular trafficking of aquaporin-5 (AQP5) in lacrimal gland acinar

cells (26). Also, it has been reported that the expression pattern of different PKC isoforms are altered in SS patients (27). PKC is one of the most important signal transduction mediators in lacrimal gland secretion (2); besides its role in protein secretion, PKC also regulates membrane cotransporters in exocrine glands, such as the Na^+-K^+-$2Cl^-$ cotransporter (NKCC1) (28) and the pancreas isoform of the electrogenic Na^+-HCO_3^- cotransporter (pNBC1) (29). Reduction in the activities of these key transporters could influence the ionic gradient across the epithelium, thus affecting water secretion rate. One possible therapeutic approach is to target signal transduction pathways, in addition to immunosuppression, to restore water secretion in injured lacrimal glands. Although it is known that muscarinic stimulation causes water secretion in lacrimal gland (30), the basic mechanism of generation of this hypertonic fluid with high KCl content has not been fully elucidated. Therefore, to understand dry-eye disease, it is crucial to gain a better understanding of what the basic mechanisms of water and electrolyte transport are. To accomplish this, we have developed mathematical models of both acinar and duct cells to examine the contributions of different membrane transporters on water and electrolyte secretions; the model simulations are subsequently validated using experimental data. This work is divided into three parts as follow:

1. Development of a mathematical model of a single lacrimal acinar cell that includes representation of a volume regulatory system. This simple model will allow us to examine if the NKCC1 transporter alone is a sufficient explanation for the high K^+ and Cl^- concentrations in lacrimal fluid. Model

simulations will be compared with experimental measurements from Walcott, *et al*. (30).

2. Expand the mathematical model to include a pH regulatory system. Here, we will use the model to look at the contributions of volume regulatory and pH regulation systems in fluid secretion. Moreover, we hypothesize that the electrogenic pNBC1 is present in lacrimal acinar cells. We intend to use the model to simulate short-circuit current experiments and compare the results with data from Selvam, *et al.* (64), and confirm pNBC1 expression and localization using immunofluorescence methods on sectioned mouse lacrimal glands.
3. Develop a lacrimal duct cell model with pH and volume regulation systems. The model simulations are then compared to in vivo tear secretion measurements. With this model, we can explore the potential role of an apical KCC1 transporter in K^+ and Cl^- secretion in duct cells.

Chapter 3. Adrenergic-Induced Water Secretion in Lacrimal Gland?

3.1 Introduction

A recent study conducted by Ding *et al*. showed that there is sympathetic innervation in mouse lacrimal gland (9). The sympathetic innervation pattern varies between different regions of the gland. This suggests that there may be differential activation of lacrimal acinar cells for secretion. It is known that muscarinic activation causes both water and protein secretion. In the same study, Ding *et al*. showed that adrenergic stimulation elicits protein secretion. They reported that α-adrenergic activation resulted in protein secretion rates similar to muscarinic exposure, but lower rate of protein secretion followed β-adrenergic activation (9). Since sympathetic stimulations induce protein secretion, it is also important to determine the role of adrenergic agonists on water secretion in lacrimal gland. Therefore, the goal of this study is to examine the effects of α- and β-adrenergic agonists on lacrimal water secretion.

3.2 Materials and Methods

3.2.1 In Vivo Tear Secretion Measurements

Experiments were conducted using C57 (Teconic) mice. The animals were housed in an approved animal facility, and all procedures were approved by IACUC Committee at SUNY Stony Brook.

The animal was anesthetized by intraperitoneal injection of a mixture of ketamine, xylazine, and acepromazine (100, 5, 2.5 mg/Kg, respectively) and placed on a heated surgical table; body temperature was monitored and maintained at 37^{o}C. The right

femoral artery was cannulated to monitor blood pressure. A cannula was inserted into the trachea to prevent aspiration of saliva. The left jugular vein was cannulated for isotonic saline infusion at 0.5 mL/hr/100 g body weight and supplemental anesthetics when needed.

The animal was then placed on its side with the head immobilized by non-penetrating steel pins. The lacrimal gland and duct were exposed with a small incision along an axis between the outer junction of eyelids and the ear. The surrounding connective tissue was cleared from the gland by blunt dissection. The exposed lacrimal gland was continuously superfused with mock interstitial fluid (Krebs-bicarbonate-Ringer, KBR, solution) containing (in mM) NaCl 105.1, Na Acetate 16, Na_2HPO_4 0.6, $MgSO_4$ 1.19, KCl 4.84, glucose 5.55, urea 24.99, NaH_2PO_4 0.13, Hepes 5.0, 1% dialyzed BSA, and $CaCl_2$ 2.2 nM pH adjusted to 7.4. The superfusate was maintained at 37^oC. To avoid fluid spreading, the lacrimal gland was covered by two layers of cellulose fiber mesh (Kimwipe®) that were cut to the shape of the lacrimal gland. The first fiber mesh was placed directly on top of the lacrimal gland. The superfusion pipette is then positioned ~0.5 mm above the first layer at the dorsal aspect. The second mesh was then placed on top of the superfusion pipette. With the aspiration pipette position at the distal aspect, it ensured that the superfusate fully covered the gland. Agonists and drugs were added to the superfusate; the system has a wash-in time ~ 30 – 40 seconds.

The lacrimal duct was sectioned as far distally as possible, and the end of the duct was placed into a microcapillary tube with known volume (Microcaps, Drummond Scientific). Tear flow rate was measured by monitoring the meniscus movement along

the tube by a CCD camera. The average water secretion rate was determined by computing increased length of the fluid column and multiplying by the unit volume per length of the capillary tube.

After 15 minutes of recovery, the duct was placed into the microcapillary tube and superfusate was switched to KBR solution containing 10 μM carbachol, a muscarinic agonist. After 3 – 5 minutes, the superfusate was switched back to KBR solution until the secretory rate returned to zero. Then the gland was exposed to 10 μM phenylephrine (PE), a α-adrenergic agonist, or isoproterenol (ISO), β-adrenergic agonist, for four mintues. The viability of the gland was then accessed with another carbachol exposure.

3.2.2 Cell Culture Preparation and Cell Volume Study

Lacrimal glands were removed and placed in soybean trypsin inhibitor (STI) and cut into small pieces with a sharp scalpel blade. The small pieces were then washed in Hanks Balance Salt Solution (HBSS) for 15 minutes at 37^{o}C. The pieces were incubated with mixture of collagenase, DNAase and hyaluronidase in Dulbecco's Modified Eagle's Medium at 37^{o}C for 25 minutes. The tissue was then centrifuged at 1200 rpm for 5 minutes. The suspension was then passed through a sterile mesh filter to remove large fragments. Then the filtered suspension was then centrifuged again. The pellet was then resuspended in culture medium, and 0.5 mL aliquots were plated in small petri dishes with the bottom coated with Matrigel®. The cells were then incubated at 37^{o}C overnight and used the next day.

After washing the cells with mammalian Tyrode's solution (in mM: 125 NaCl, 20 $NaHCO_3$, 4 KCl, 1 $MgCl_2$, 1 $CaCl_2$ 10 glucose and 5 Hepes, adjusted to pH 7.4 after

equilibration with 95% O_2/CO_2), the cells were placed in a chamber of an inverted microscope and continuously perfused with an isotonic Tyrode's solution (~320 mOsm) at 37^{o}C. Agonist-induced cell volume changes were recorded in time-lapse videos to 30 seconds interval at 40X magnification with DIC optics. After 2 minutes, the cells were locally exposed to the agonist solutions (10 μM carbachol, 10 μM PE, and 10 μM ISO) via a glass micropipette. Positioning of the micropipette was achieved with the aid of a micromanipulator, and pipette pressure was controlled with a Gauer manometer. The agonist solution was stained with 0.1% FD&C green (a membrane-impermeable vital dye) to verify the movement of agonist solution. The solution is removed via an aspiration pipette which was placed downstream from the cell of interest. After 5 minutes, agonist injection was stopped. The cell of interest was visually inspected for intracellular blue/green staining. Such staining indicated loss of cell membrane integrity and, if present, the experimental results were discarded. The time-lapse experiment stopped at 8 minutes. Images of the cells were analyzed using Image J software (www.rsb.info.nih.gov). Cells were treated as ellipsoid, and cell volume (V) was calculated as: $V = \frac{4}{3}\pi AB^2$, where A and B are the lengths of major and minor axes. Relative cell volume was then computed as the ratio to baseline cell volume.

3.2.3 Statistical Analysis

Comparisons between two groups were performed with a pair- or two-sample t test. Comparison with more than two groups was performed with a one-way analysis of variance, followed by Student-Newman-Kuels multiple-comparison tests using SigmaStat software (Systat, Inc).

3.3 Results

3.3.1 PE and ISO Exposure Failed to Elicit Water Secretion

Topical exposure to 10 μM PE or ISO did not stimulate water secretion in 12 animals. However, carbachol was able to induce water flow as showed in Figure 3-1. The insensitivity to PE or ISO exposure was also observed even the agonists dosages were increased to 100 μM for up to 10 minutes (not shown).

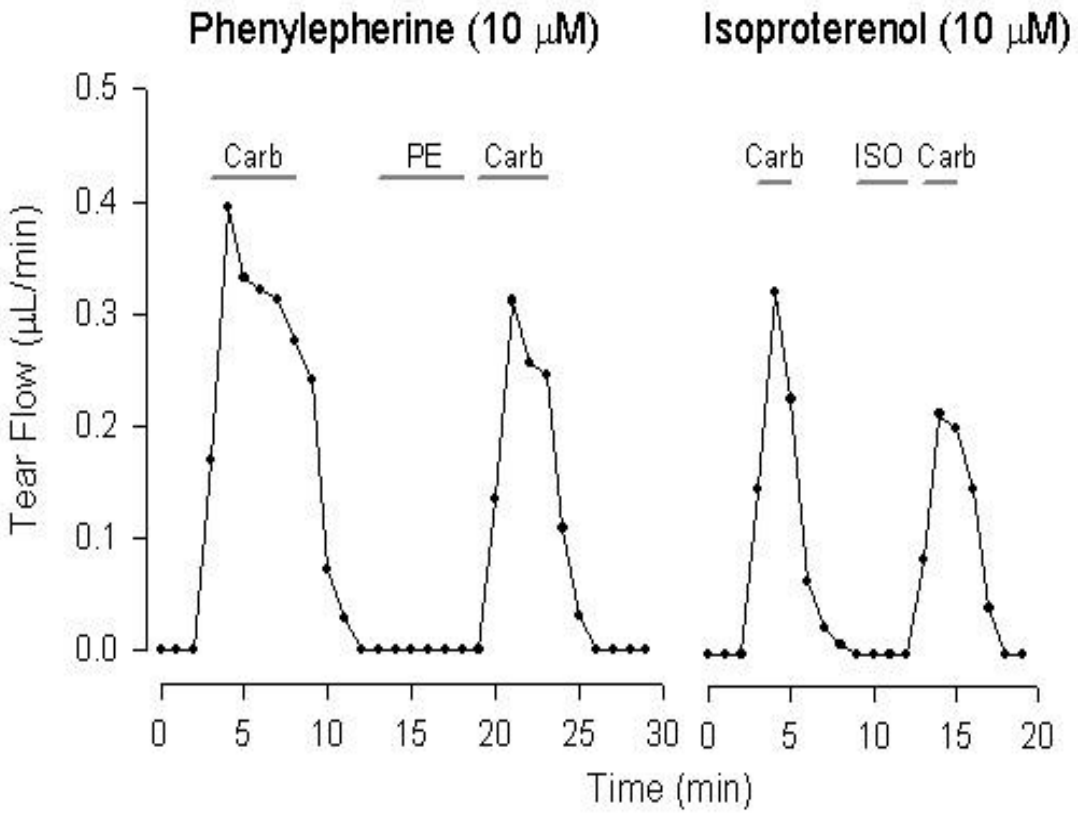

Figure 3-1. These are sample responses of water secretion when the lacrimal glands were stimulated. Exposure to 10 μM carbachol caused water secretion in anesthetized mice. Peak water flow was observed within the first minutes of agonist exposure. However, exposure to PE or ISO did not stimulate water secretion in these animals, even when the agonist dosages were increased by 10-fold.

3.3.2 Agonists-Induced Cell Volume Changes

Cell shrinkage is an indicator of the onset of KCl secretion in isolated lacrimal acinar cells, cell shrinkage was observed when the cells were exposed carbachol, but this was not observed in cells that were exposed to PE or ISO (Fig 3-2). Figure 3-3 illustrates typical images that were analyzed. Exposure to carbachol causes a significant reduction of cell volume, whereas cell shrinkage was not observed in response to adrenergic agonists. However, in some cells, adrenergic agonist exposure triggered visible cytokinesis and changes in cell shape, which is consistent with the onset of protein secretion.

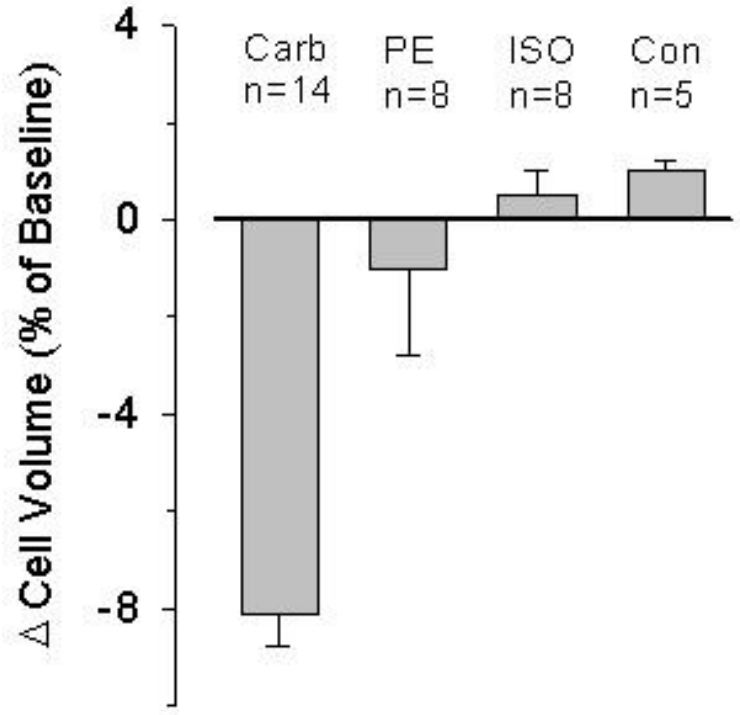

Figure 3-2. Carbachol causes ~10% cell volume reduction in isolated lacrimal acinar cells. In agreement with water flow measurements, PE and ISO had no significant effect on cell volume.

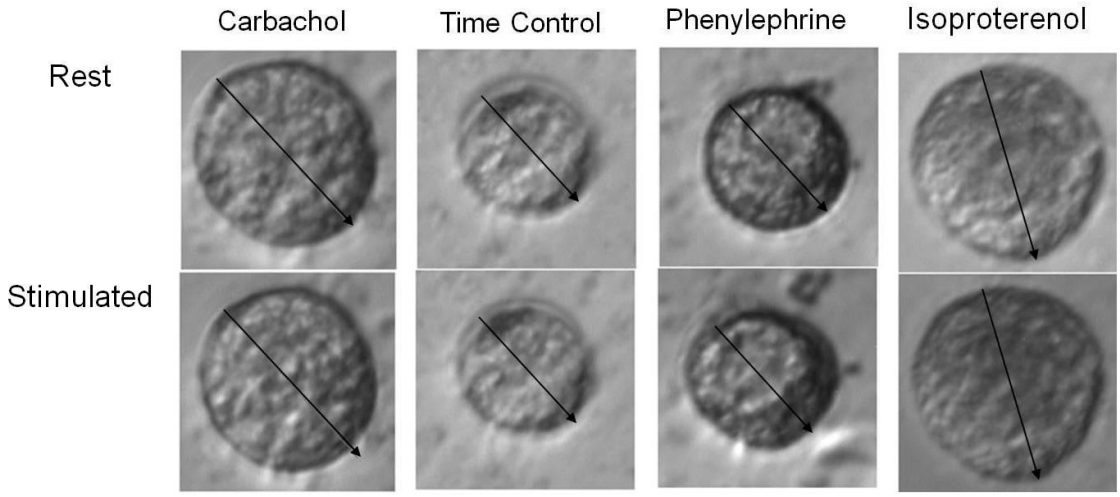

Figure 3-3. Micrographs illustrating exposure to adrenergic agonists only changed cell shape, but not cell volume. The upper row shows the baseline image of the cell, and the lower row shows the cell volume/shape change after 5 minutes agonist exposure. Note, the arrows for each cell are the same length, and it is used to highlight the cell volume changes. Note that 4 different cells are shown, and the upper and lower images in each column are the same cell.

3.4 Discussion and Conclusions

Although it has been demonstrated that lacrimal gland protein secretion can be triggered by either α_1-adrenergic or β-adrenergic activation, exposure to PE or ISO did not stimulate tear flow in anesthetized mice. However, exposure to adrenergic agonists in some cells did elicit the onset of visible cytokenesis and changes in cell shape. This observation, and the heterogeneity of sympathetic innervation of the lacrimal gland, suggests that there may be differential activation of lacrimal gland fluid and protein secretion, such that the amount of protein secreted and perhaps the spectrum of secreted proteins may depend on the balance of parasympathetic and sympathetic input. This issue deserves further study. However, since this dissertation focuses on water and electrolyte secretion, the influence of sympathetic input will not have to be considered.

Chapter 4. Water and Electrolyte Secretion in Lacrimal Gland

As described in Chapter 2, the extraorbital lacrimal gland secretes the majority of the aqueous layer of the tear film. This layer provides a favorable (osmolarity and pH) environment to maintain the health of the ocular surface. Fluid composition measurements of the final secretion from lacrimal gland in several animal models (30-32) and human tear samples collected from conjunctival sac (32) reveal that tear fluid is hypertonic with high K^+ and Cl^- concentrations as compared to plasma (Table 4-1). This indicates that lacrimal fluid is actively secreted rather than passively formed by diffusion.

Table 4-1. Experimental measurements of lacrimal fluid composition from different species. Rat (31), Rabbit (32), Mouse (30), and Human (33).

	Na^+ (mM)	K^+ (mM)	Cl^- (mM)
Rat	135 ± 5	46 ± 3	123 ± 1
Rabbit	107 ± 4	42 ± 4	126 ± 5
Mouse	144 ± 5	38 ± 5	149 ± 16
Human	146 ± 1.5	14.9 ± 0.9	128 ± 1.2
Plasma	140	4	105

Like other exocrine glands, lacrimal acinar cells are the major sites of water and electrolyte secretion. Immunohistology (3, 30) and electrophysiological studies (34) have identified several important membrane channels and cotransporters that are involved in generation of hypertonic fluid (Fig 4-1). When the acinar cell is at rest, cytosolic Cl^-

concentration is held above equilibrium by the electroneutral Na^+-K^+-$2Cl^-$ cotransporter (NKCC1). Upon muscarinic stimulation, cytosolic Ca^{2+} is increased. Besides facilitating protein secretion, this also activates Ca^{2+}-activated K^+ and Cl^- channels on the apical membrane. Luminal K^+ efflux depolarizes the apical membrane; this generates an electrochemical gradient that favors Cl^- efflux. Accumulation of luminal anions (proteins and negative charged solutes) generates a net negative transepithelial potential (negative with respect to basolateral membrane), which causes Na^+ to diffuse across the epithelium through paracellular junctions. Water follows the movement of ions via osmosis.

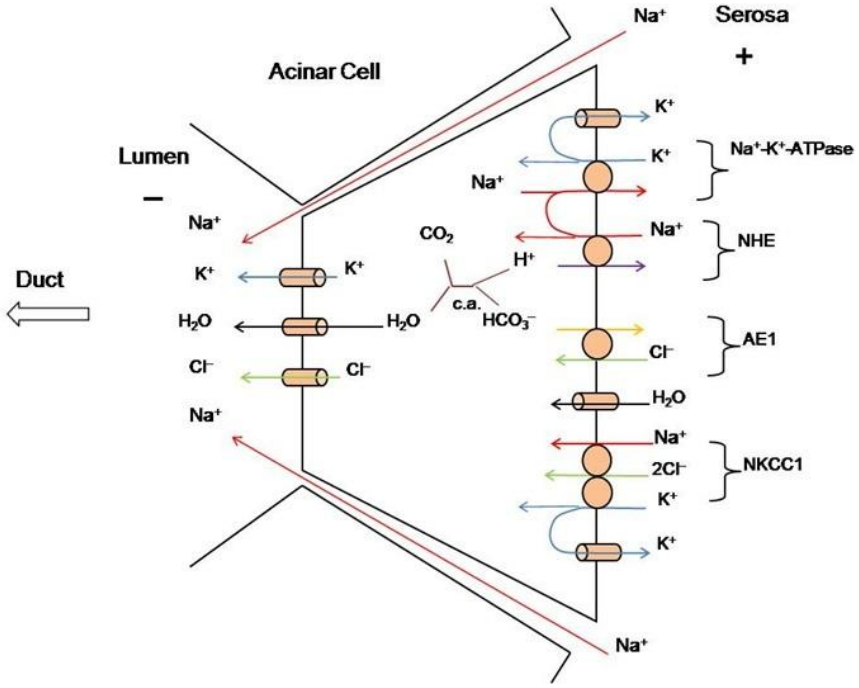

Figure 4-1. A schematic illustration of water and electrolyte secretion in the lacrimal acinar cell. Localization of membrane channels and transporters are based on existing data. Cytosolic Cl^- level is maintained above equilibrium by the basolateral NKCC1 and the parallel actions of NHE and AE1. Opening of apical K^+ and Cl^- channels allows KCl efflux into the lumen. Na^+ diffuses into the lumen via paracellular junctions, and water follows by osmosis. Thus, a net flow of water is established across the epithelium.

The challenge for these cells is to maintain a high cytosolic Cl^- concentration during continued stimulated secretion. Two separate mechanisms are thought to be involved. It has been demonstrated that the activity of volume-regulatory transporter, NKCC1, increases when acinar cells are exposed to muscarinic agonists, which increases the uptake of KCl across the basolateral membrane. The pH-regulatory pathway, which includes the Na^+-H^+-exchanger (NHE) and Cl^--HCO_3^- cotransporter (AE1), work in tandem to increase basolateral NaCl uptake. The excess Na^+ is then removed by Na^+-K^+-ATPase in exchange for K^+. Taken together, both of these processes facilitate net KCl uptake. Water and electrolyte secretion in lacrimal gland is a complex process that requires coordination of different cell membrane components. In order to understand the precise mechanism of water transport across the lacrimal epithelium, it is important to understand the function and regulation of each component that is involved in the secretory process.

4.1 Ca^{2+}-activated-Cl^- Channel

The primary function of Cl^- channels in secretory epithelia is to facilitate transcellular Cl^- movement. In lacrimal gland, the main Cl^- passive conductance is via Ca^{2+}-activated-Cl^- channels (35). Although the molecular structure of this channel is not yet resolved, studies have demonstrated that cytosolic Ca^{2+} levels influence the kinetics of the channel, in that free cytosolic Ca^{2+} binds to the channel and increases channel open probability (10, 35). In addition, the binding of Ca^{2+} is modulated by membrane voltage. Nilius *et al*. showed that the half-maximal activation by Ca^{2+} decreased from ~650 nM at -80 mV to ~300 nM at +100 mV (36). This is consistent with the notion that

K^+ efflux depolarizes the apical membrane and facilitates Cl^- efflux from the cell. Moreover, the current-voltage curve shows an outward rectifying current with increasing clamping voltage and the slope of the rectifying current becomes steeper with increasing cytosolic Ca^{2+} levels (35). In lacrimal acinar cells, exposure to acetylcholine has an nonhomogeneous Ca^{2+} response (37). Results from cytosolic Ca^{2+} imaging and patch-clamp measurements show that the luminal, but not the basolateral, Ca^{2+}-dependent current is synchronized with the initiation of the Ca^{2+} response. Resting current densities predicted by the same group showed that K^+ and Cl^- currents are 13 times and 6 times larger in the luminal membrane (compared to basolateral membrane) respectively. These findings suggest that the Ca^{2+}-dependent Cl^- channel is mainly located on the apical membrane. The open probabilities for these channels are enhanced by muscarinic stimulation, and this is one of the critical requirements for acinar cell secretion. Further, in isolated mouse lacrimal acinar cells, Walcott *et al*. showed that secretion-induced cell shrinkage, an indicator of the onset of secretion, is blocked by flufenamic acid, a Cl^- channel inhibitor (30). Together, these results suggest that Cl^- channel activation is Ca^{2+}- and voltage-dependent, and explains how muscarinic stimulation, by increasing cytosolic Ca^{2+} levels and depolarizing the apical membrane facilitates apical Cl^- channel opening.

Intracellular pH (pH_i) also affects apical Cl^- current. Electrophysiological measurements of the influence of pH on apical Cl^- current showed that increasing pH_i activates the Ca^{2+}-activated-Cl^- channels (38). Suppression of Cl^- current by cell acidification is possibly due to competition between H^+ and Ca^{2+} for binding to the channel (39) and this would lower channel open probability. Therefore, efficient

regulation of intracellular pH is a critical requirement for lacrimal acinar cell electrolyte and fluid secretion.

4.2 Ca^{2+}-activated K^+-Channel (Maxi-K channel)

One unique feature of lacrimal gland acinar cell is the expression of Maxi-K channels on both the apical (40) and the basolateral membranes (41). However, there is evidence that the majority of the channels are localized on the luminal side (37). This finding agrees with electrophysiological measurements by Marty *et al*., which demonstrated that increasing intracellular Ca^{2+} concentration by muscarinic stimulation or via a Ca^{2+} ionophore activates three currents in lacrimal acinar cells: a K^+ current, a Cl^- current, and a nonselective cation current (34). The tetraethylammonium-sensitive (42) outward-rectifying K^+ current is attributed to the passive conductance of the Maxi-K channel in lacrimal glands (43). Like the apical Cl^- channel, the Maxi-K channel is regulated by both membrane voltage and cytosolic Ca^{2+}: membrane depolarization causes the channel to open and increased cytosolic Ca^{2+} concentration increases the channel open probability (42).

The Maxi-K channel is one of the most important mechanisms for generating high K^+ luminal fluid in the lacrimal gland. In the exocrine pancreas and salivary gland, the vast majority of K^+ channels are localized on the basolateral membrane. Stimulation of these channels facilitates basolateral Cl^- influx by depolarizing the membrane, and Cl^- leaves the cell through apical Cl^- channels. This ensures vectorial transepithelial Cl^- movement when the cells are stimulated. Measurements of the composition of pancreatic juice (44) and the primary secretion of salivary gland (45) show that luminal K^+

concentration is close that of to plasma. This suggests that in these exocrine glands, K^+ may just diffuse passively across the epithelium. Unlike the pancreas and salivary gland, the lacrimal gland secretes K^+ via the apical Maxi-K channel. This was demonstrated by Walcott *et al*. who reported that exposure to charybdotoxin, a Ca^{2+}-activated K^+-channel inhibitor, blocked carbachol-induced cell shrinkage in isolated mouse acinar cells (30). Together, there is strong evidence that muscarinic stimulation activates both K^+ and Cl^- channels in the apical membrane of lacrimal acinar cells, and that these two channels are essential for agonist-induced secretion. These findings also suggest that the primary secretion from lacrimal acinar cells has a K^+ concentration that is much higher than plasma.

4.3 The Influence of Cell-Volume Regulation on Water and Electrolyte Secretion in Lacrimal Gland

The cell-volume regulation system in lacrimal acinar cells consists of the NKCC1 transporter, the volume-sensitive K^+ and Cl^- channels, and NHE. NKCC1 is activated in response to cell shrinkage or exposure to muscarinic stimulation. Thus, basolateral KCl uptake increases. When acinar cells are at rest, this transporter is thought to play an important role in maintaining a high cytosolic Cl^- concentration. This was demonstrated by Walcott *et al*. (30) who investigated the effects of furosemide, a NKCC1 inhibitor, on cell volume. Cell volume slowly decreased over 20 minutes of furosemide exposure, and the addition of carbachol further reduced cell volume at a much faster rate (30) (Fig 4-2). This observation supports the concept that NKCC1 is a major Cl^- loading pathway in resting acinar cells. This also indicates there is a significant Cl^- leakage pathway in

resting acinar cells, which could account for the basal resting rate of tear fluid secretion. Moreover, lacrimal fluid secretion *in vivo* is reduced by ~30% when lacrimal glands are topically exposed to furosemide (30) (Fig 4-3). This suggests that NKCC1 is also involved in stimulated secretion. In contrast to NKCC1, volume-sensitive K^+ and Cl^- channels are responsive to cell swelling. Opening of these channels leads to KCl efflux, which is the basis of a regulatory volume decrease. However, the role that these channels play in generation of a hypertonic KCl secretion remains unclear.

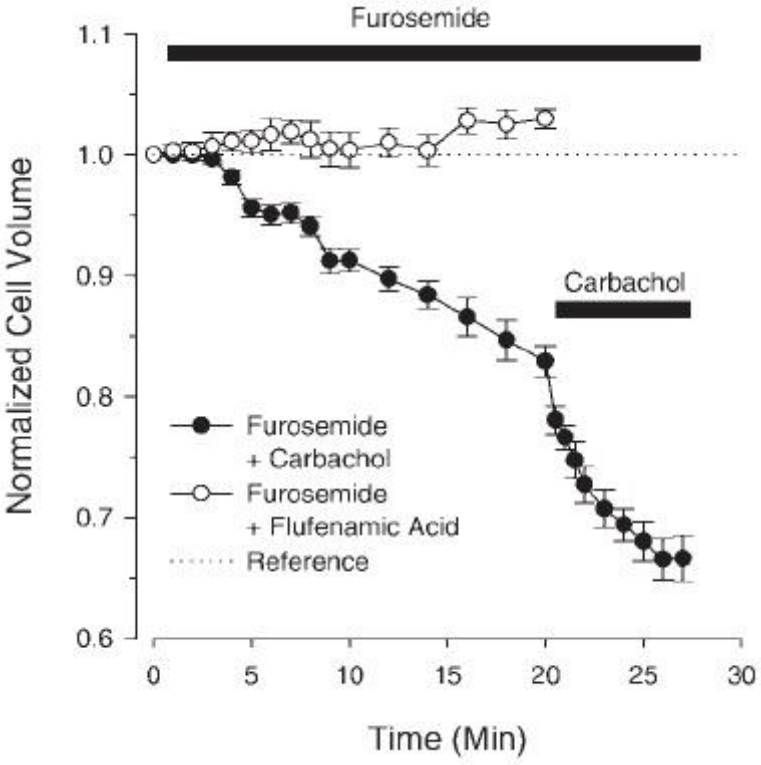

Figure 4-2. In isolated mouse lacrimal acinar cells, 20 minutes furosemide exposure slowly decreases cell volume. This could be due to Cl^- leakage from the cell. Carbachol increases the rate of cell shrinkage. This suggests that NKCC1 is an important Cl^- loader in acinar cells at rest and when stimulated. This graph is from Walcott *et al*. (30).

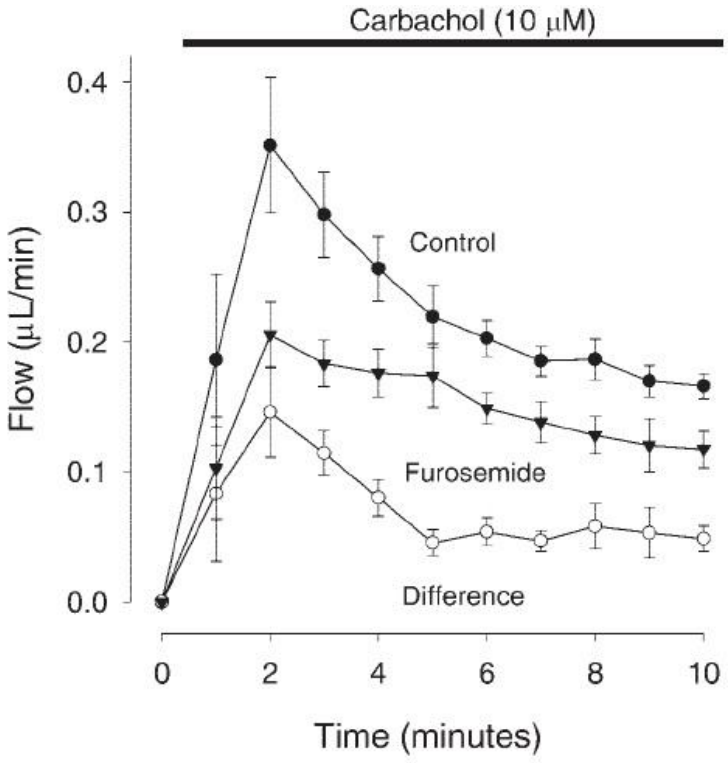

Figure 4-3. In anesthetized animals, Walcott et al. reported that exposure to furosemide 20 minutes prior to carbachol stimulation causes a ~30% reduction in water secretion rate (30).

4.3.1 NKCC Regulation

The molecular structure of NKCC1 consists of 12 transmembrane domains with both N- and C-termini located inside the cell, and a glycosylated extracellular loop, which is the target for loop-diuretics which inhibit NKCC1 activity (46). The membrane transporter activity is controlled by at least two mechanisms: level of protein phosphorylation, and cytoskeleton. It has been reported that there are three threonines which are possible phosphorylation sites that are located on the N-terminus of NKCC1 (T184, T189, and T202) (47). Out of the three sites, phosphorylations of T184 and T189 are linked to physiological changes in the brain and spinal cord (48-49). Moreover,

NKCC1 activity is also modulated by protein phosphatase (PP) 1 (47) and 2a (50) activity. Increase PP1 and 2a activities inhibited NKCC1 transport by reducing the level of protein phosphorylation in the transporter. Therefore, it is likely that NKCC1 transport is modulated by the balance of phosphorylating kinase and PP activities.

In a yeast two-hybrid system, Piechotta *et al*. have identified potential kinases, Ste20/SPS1-related, proline alanine-rich kinase (SPAK) and oxidative stress-response protein 1 (OSR1), for NKCC1 phosphorylation (51). SPAK, OSR1, and PP1 are downstream regulatory targets of WNK (WNK 4(1) and WNK 3). WNKs activate in response to decreases in cytosolic Cl^- concentration and, perhaps, cell shrinkage (52). This causes phosphorylation of SPAK and OSR1 and inhibition of PP1, thereby activating NKCC.

NKCC1 activity is also regulated by cytoskeleton structure (53). It has been shown that actin filaments are depolymerized when the cell is swollen, and polymerized when the cell is under hypertonic stress (54). It has been demonstrated that SPAK and OSR1 were unable to bind to depolymerizing actin filaments (55). Therefore, NKCC1 was not phosphorylated.

4.3.2 NHE and Cell Volume Regulation

The NHE is one of the most important pH regulatory proteins in the cell. It controls cytosolic pH by removing excess free H^+ in exchange for Na^+ in an electrically neutral manner. In addition to the role in controlling pH, NHE is also involved in cell volume regulation. It has been demonstrated that under hyperosmotic stress, there is no detectable cytosolic acidification prior to an increase in Na^+ uptake via NHE in rat thymic

lymphocytes (56). This suggests osmotic activation of NHE occurs via some unknown pathways that remain to be elucidated. Moreover, it has demonstrated that regulatory volume increase (RVI) behavior is sensitive to amiloride in isolated rat lacrimal acinar cells (57). Increased H^+ extrusion causes cellular alkalization, which is thought to activate AE1 for HCO_3^- removal in exchange of Cl^- (57). So, cellular uptake of NaCl results and cell volume is then restored.

4.3.3 Cell Volume Sensitive K^+ and Cl^- Channels

In isolated lacrimal acinar cells, it has been demonstrated that Ca^{2+}-activated-K^+ and -Cl^- channels are responsible for regulatory volume decrease (RVD) under hyposmotic stress (58-59). The properties of these channels were described earlier in this chapter. These channels are regulated by cytosolic Ca^{2+} concentration. During hypotonic shock, membrane stretch causes opening of non-selective cation channels which increases Ca^{2+} influx; and Kotera *et al*. showed that depletion of extracellular Ca^{2+} inhibits the cell swelling-induced Cl^- current (58). This could be one of the mechanisms the cell distinguishes between carbachol- and swelling-induced KCl secretions, where muscarinic exposure requires Ca^{2+} release from intracellular storage. It also could stimulate different signal transduction pathways. Since swelling-induced K^+ and Cl^- efflux is closely associated with each other (60), it is possible that K^+ current is regulated in the same fashion.

4.3.4 KCC Regulation

The electroneutral KCC isoform 1 is expressed in many cells. It serves a house-keeping function by helping to maintain constant cell volume. When under hypotonic

stress, activation of KCC1 leads to the extrusion of K^+ and Cl^-, which reduces cell volume back toward normal, a process known as a RVD. There are data indicating that KCC1 activation is linked to cytoskeletal detection of cell membrane deformation or stretching due to swelling (60); this effect can be inhibited by cytochalasin B, which blocks monomer addition to the fast-growing actin chain (61). Besides disturbances in cell volume, KCC1 is also thought to be activated in respond to elevated cytosolic Cl^- concentration. When too much Cl^- is present, WNK kinases are inactivated, which leads to dephosphorylation of PP1, SPAK and OSR1. This leads to dephosphorylation of the regulatory sites of both NKCC1, which reduces its activity, and KCC, which increases its transport activity (52).

4.4 The Influence of pH Regulation on Water and Electrolyte Secretion in Lacrimal Gland

Like the cell-volume regulation system, the pH regulatory system also plays an important role in lacrimal gland tear secretion. Fluctuations of lacrimal fluid pH could lead to tear-specific protein dysfunction and have detrimental effects on the ocular surface. It is known that NHE is localized on the basolateral membrane (62), as is the AE1 transporter (3), and carbonic anhydrase (CA) (63). Although there is no evidence directly indicating an influence of the pH regulation system on fluid secretion in lacrimal gland, it is thought that the parallel actions of NHE and AE1 supplements Cl^- uptake during stimulated secretion. In rabbit lacrimal acinar cell monolayers, resting short-circuit current (I_{sc}) was measured in the presence of bumetanide, an NKCC1 inhibitor, and amiloride, an NHE inhibitor. Compared to control conditions, blocking NKCC1 or

NHE along is not sufficient to reduce resting I_{sc} (64). This suggests the NHE and AE1 transporters can compensate for NKCC1 inhibition and vice versa. Also, *in vivo* secretion measurements showed ~30% reduction of water secretion rate with the presence of furosemide (30). This could be explained by two reasons: i) the degree of inhibition is unknown because the antagonist is applied topically; and ii) part of the secretion rate is sustained by Cl^- uptake via the pH regulatory pathway.

4.4.1 Carbonic Anhydrase (CA) in Lacrimal Gland

Carbonic anhydrase is a protein that facilitates the reversible hydration of CO_2. The end products are H^+ and HCO_3^-. CA is widespread in many tissue and it has as many as eleven isozymes; four of these isozymes are cytosolic which includes I, II, III, and VII; four are membrane-bound: IV, IX, XII, and XIV; two are present in mitochondria: VA and VB; and one is secreted from cells (VI) (65). CA VI is expressed in the secretory granules in both rat and rabbit lacrimal acini (63). Also, Ogawa *et al*. have found CA I and II in interlobular ducts (65). In salivary gland, CA II is found to be located in the cytosol of acinar and duct cells (66). In addition, a transport metabolon is formed by binding of CA II to the C-terminus cytoplasmic tail of AE1. It has been demonstrated that AE1 mutants that are unable to bind CA II have significantly lowered transport activity in HEK 293 cells (67). Application of acetazolamide, a CA inhibitor, inhibits AE1 mediated Cl^-/HCO_3^- exchange in HEK293 cells (67) and salivary acinar cells (68). Moreover, in intact lacrimal gland, acetazolamide application also inhibits 50% of lacrimal fluid flow (Fig 4-4). These results indicate that inhibition of CA II not only causes reduction of the rate of intracellular HCO_3^- generation, it also decreases AE1

activity. Taken together, these results strongly suggest that HCO_3^- transport is another mechanism that may be involved in lacrimal fluid secretion.

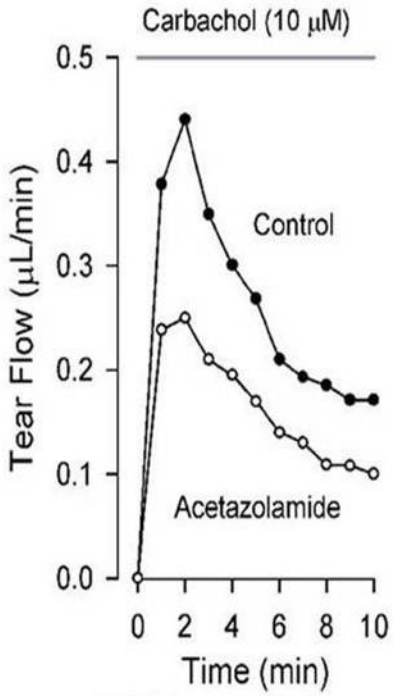

Figure 4-4. In anesthetized animals (n = 3), inhibition of carbonic anhydrase topically causes a ~50% reduction of water secretion. This could be due to inhibition of Cl^- uptake through AE.

4.4.2 NHE Regulation

The NHE plays an important role in preventing cytosolic acidification by removing protons in exchange for Na^+ at a ratio of 1:1. This house keeping protein senses an increase in intracellular H^+ concentration and facilitates proton extrusion. This is important because, as a byproduct of cellular metabolism, H^+ accumulates inside cells. In addition, negative charges on the cell membrane drive H^+ diffusion into the cell down the electrochemical gradient. These protons are buffered by intracellular HCO_3^- and

other buffers (proteins, phosphoates, and etc) at resting pH. However, the buffering capacities of these processes are limited, and as cytosolic H^+ concentration rises NHE is activated by the binding of free H^+ to an allosteric modifier located on the transmembrane region of the NHE (71).

NHE consists of 14 transmembrane domains (TD). TD 8 and 9 are conserved among different isoforms of NHE, and they are thought to be the Na^+ and H^+ binding sites of the protein (69). Moreover, there are numbers of serine and threonine residues located on the C-terminus that are possible sites for regulation (70). Although energy is not required for NHE transport, depletion of cellular ATP inhibits NHE activity (71). This could be due to some upstream regulatory protein activities that are energy dependent. The precise mechanisms of NHE regulation remain to be elucidated.

Based on density distribution data, NHE is thought to be localized on the basolateral membrane in lacrimal acinar cells (62). Excess free protons are removed via the basolateral membrane in exchange for Na^+, thereby stabilizing intracellular pH. Ammonium perturbation experiments show a rapid intracellular pH (pH_i) recovery upon removal of ammonium (72). pH recovery is slowed down significantly in the presence of amiloride, an NHE inhibitor, or removal of extracellular Na^+. These findings suggest that NHE is the major pH regulatory protein in the lacrimal acinar cell. Basolateral extrusion of free H^+ causes cellular alkalization. This increases cytosolic HCO_3^- levels, and this increases HCO_3^- removal in exchange for Cl^- via AE1. This could be another mechanism for net Cl^- uptake that supplements NKCC1 activity during stimulated secretion.

4.4.3 AE Regulation

The electroneutral anion exchanger (AE1) consists of 14 transmembrane domains (73). This transporter facilitates extrusion of HCO_3^- in exchange of Cl^- at a 1:1 ratio. The N-terminus contains binding sites for kinase regulations, whereas the C-terminus contains acid motifs that are binding regions of CA for transport metabolon formation (73). AE1 is sensitive to stilbene derivatives, 4-acetamideo-4'-isothiocyanostiblene-2,2'-disulfonic acid (SITS) and 4,4'-diisothiocyanostibene-2,2'-disulfonic acid (DIDS) exposure.

Lambert *et al*. have demonstrated the existence of AE in lacrimal acinar cells by measuring Cl^- influx during K^+-channel inhibition and with the membrane potential held at 0 mV (74). This was confirmed by Ubels *et al*. who found AE1 localized on the basolateral membrane using immunocytochemistry on both lacrimal acinar and duct cells (3). In isolated rat lacrimal acinar cells, it has been shown that AE1 activity is modulated by pH_i and transmembrane Cl^- (K_m ~10 mM $[Cl]_o$) and HCO_3^- gradients (74-75). Moreover, it has been reported that Cl^--HCO_3^- exchange is increased with muscarinic receptor-induced increased intracellular Ca^{2+} in salivary acinar cells (68). The regulation of the transporter could be linked to CaMKII, like NHE. Yet, the precise mechanism remains unclear. Taken together, these findings suggest that AE1 facilitates Cl^- uptake during stimulated lacrimal secretion, which provides an alternative role for Cl^- entry.

4.4.4 pNBC Regulation

The pancreatic isoform of electrogenic sodium bicarbonate cotransporter (pNBC1) is expressed in many exocrine glands, such as pancreas and parotid acini of

salivary gland (76-77), as well as in the cornea (78-79). The stoichiometry of pNBC1 is 2 HCO_3^-: 1 Na^+, which was calculated using reversal potential measurements (80). Compared to pNBC1, the kidney isoform of this cotransporter (kNBC1) has a coupling ratio of 3:1, despite the fact that they have similar molecular structures. Moreover, the stoichiometry of the kidney isoform of NBC1 can be shifted by cAMP-mediated protein kinase A (PKA)-phosphorylation of Ser^{982} (81). This indicates cAMP could be an important modulator in NBC activities. It has been reported that carbachol-induced increases of pNBC1 activity occurs through a Ca^{2+}/calmodulin-activated PKC-dependent mechanism (29). Since both pNBC and AE are encoded from the SCL4A4 gene, their molecular structure is thought to be very similar. Like AE1, there are many regulatory sites on the cytoplasmic tail of pNBC1 that allow for enzymatic modifications. Yet, the regulatory mechanisms remain to be elucidated.

To date, there has been no evidence showing that pNBC1 is expressed in lacrimal gland. However, there is evidence which indicates the presence of an amiloride-insensitive pH_i recovery pathway in lacrimal acinar cells (72). These mechanisms are both Na^+-dependent and independent. The Na^+-dependent pathway is possibly due to pNBC1-mediated loading of HCO_3^-, while the Na^+-independent pathway could be due to CO_2 hydration by CA and increased AE1 uptake. One of the goals of this dissertation is to identify pNBC1 in sectioned mouse lacrimal glands, and to investigate its physiological role in muscarinic stimulated water secretion, by using the mathematical model in the simulation of the short-circuit measurements in rabbit lacrimal acinar cell monolayers reported by Selvam *et al*. (64).

4.5 Water and Electrolyte Secretion in Lacrimal Duct Cells

Little is known about the function of lacrimal duct cells in fluid secretion. Immunocytochemistry shows that these cells and acinar cell express similar proteins (Fig 4-5). This suggests that acinar and duct cells could have similar function in fluid secretion. Exposure to muscarinic agonists results in the formation of a hypertonic primary secretion from acinar cells. This high K^+ and Cl^- fluid passes through the lacrimal duct system where it remains hypertonic with a high K^+ concentration. The mechanism of how duct cells maintain the hypertonic primary secretion is not clear. Apical expression of AQP5 in duct cell membranes suggests that duct cells secrete fluid. Moreover, it has been noted that duct cells express more basolateral NKCC1 than acinar cells (30). Further, the presence of the K^+-Cl^- cotransporter (KCC1) on duct cell apical membranes provides an additional pathway for KCl secretion (3). Together, these findings suggest that duct cells may have more fluid transport capacity than acinar cells, and that the secreted fluid is similar in composition to the fluid secreted by the acinar cells.

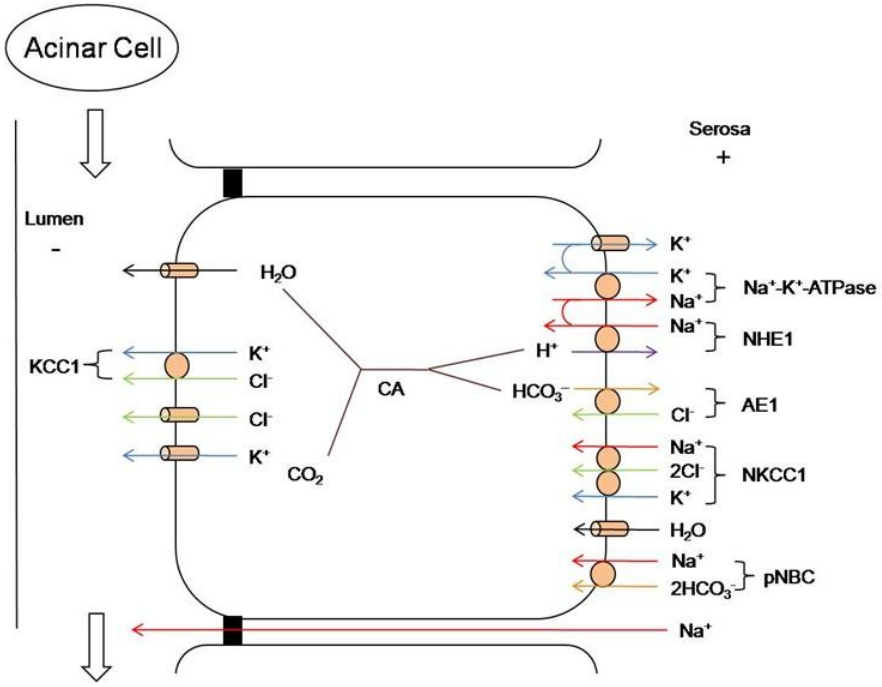

Figure 4-5. Schematic illustration of ion transport pathways in a lacrimal duct cell. Like the acinar cell, the duct cell expresses a similar array of membrane channels and transporters. One key difference is the apical expression of KCC1 (3) which could be an important mechanism for the generation of a high KCl secretion.

Chapter 5. Model Description

The lacrimal acinar cell model was developed based on the urinary bladder epithelial cell model described by Latta *et al*. (82). The acinar cell model is based on a set of differential equations (state equations) that describes cell volume and intracellular ion concentrations with respect to time. Water is assumed to be the largest constituent of the cytosol. Therefore, movement of water via osmosis into or out of the cell determines cell volume. Solute fluxes across the cell membrane are determined by the electrochemical gradients, parameters of membrane transporters, and active transport.

The analysis of this model starts with the description of a single cell in the lacrimal epithelium with the assumption that all of the lacrimal acinar cells behave the same. The cell model is divided into two configurations: 1) single cell mode, which is a single isolated acinar cell where the apical and basolateral membranes are bathed in the same extracellular medium and 2) compartment mode, where an acinar cell is adjacent to with a small apical compartment corresponding to the lumen of the acinus. This latter configuration was used to simulate secretion *in vivo* where the composition of luminal fluid is determined by the ratio of apical water and solute fluxes.

Compartment mode is also used to simulate voltage-clamp experiments in confluent acinar cell monolayers, in which case both apical and basolateral bathing solutions have the same composition with the volume of the apical lumen compartment being set to value much larger than cell volume to ensure that apical and paracellular fluxes do not cause alternations of the luminal composition. The serosal bathing solution

is also assumed to have constant composition. Finally, the transepithelial voltage is held at 0 mV.

The intracellular and extracellular solutions are assumed to be well stirred. Therefore, the solutions are homogenous, and unstirred-layer effects are not taken into account. Figure 5-1 shows a schematic of the model with orientation of water and solute fluxes, where *A* denotes membrane area, *J* denotes solute and water fluxes, *C* denotes solute concentration, and *E* represents membrane voltage. Refer to the Appendix I for model parameters.

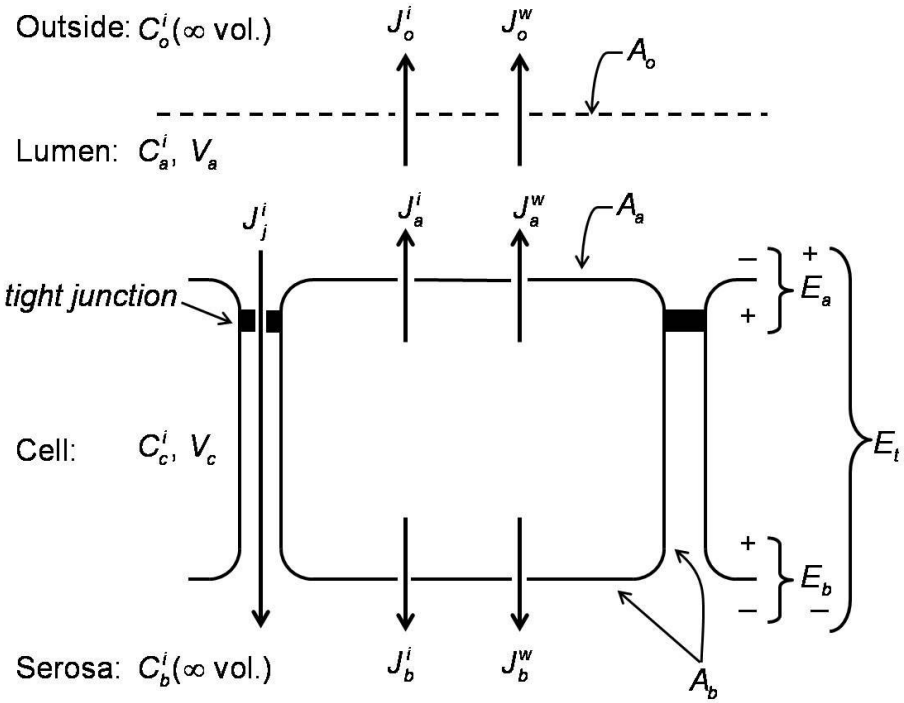

Figure 5-1. Schematic representation of the general model of acinar cell transport. The straight arrows denote the positive direction of water or solute fluxes. Membrane potential is oriented that + inside while – outside of the cell. e.g. A positive value of E_t means that the luminal compartment is positive with respect to the serosa. In the case of short-circuit current simulation of monolayer experiments, V_a is considered infinite.

5.1 State Equations

Cellular influx or efflux of water flux follows the law of conservation of mass. This yields a differential equation describing cell volume, V_c (cm^3), as a function of membrane water flow with respect to time:

$$dV_c/dt = -A_a J_a^W - A_b J_b^W \qquad (5\text{-}1)$$

A positive value of water flux represents an efflux of water. Superscripts *a* and *b* denote apical and basolateral membrane respectively.

Similar to water movement across the membrane, intracellular solute concentrations are also governed by mass conservation. They are determined by the apical and basolateral membrane solute fluxes and water flows:

$$V_c \frac{dC_c^i}{dt} = -A_a J_a^i - A_b J_b^i - C_c^i \frac{dV_c}{dt} \qquad (5\text{-}2)$$

Here, superscript *i* represents each solute species. Notice that equation (5-1) and (5-2) are coupled to each other, and both apical and basolateral solute fluxes share common intracellular concentrations. Therefore, alteration of ion concentration of one solute will lead to change in osmolarity and fluxes across the membranes. More importantly, changes in electrolyte concentrations could lead to charge imbalance. Therefore, another constraint of the cell model is that all compartments must remain to maintain electrically neutral (e.g. $\sum_i z_i C_c^i = 0$).

Other equations for the basic cell model includes water fluxes and basolateral Na^+,K^+-ATPase. Water fluxes across the cell membranes are determined by the osmotic gradients and the water permeabilities:

$$J_{a,b}^{W} = (C_{a,b} - C_c)\sigma_{a,b}P_{a,b}^{W} \tag{5-3}$$

where $P_{a,b}^{W}$ are the water permeabilies across apical and basolateral membrane. $\sigma_{a,b}$ are the unitless reflection constants. Basolateral Na^+-K^+-ATPase activity is described by a voltage-dependent competitive-binding model (83) and the pump parameters are appropriate for cardiac ventricular cell model (83).

5.2 Water/Solute Luminal Fluxes

Recall that the model has two configurations. For simulations with a luminal compartment (*in vivo* simulations), lumen composition is determined by apical- and junctional- solute/water flows to/from outside:

$$V_a \frac{dC_a^i}{dt} = A_a(J_a^i - J_k^i) - A_o J_o^i \tag{5-4}$$

Lumen volume (V_a) is assumed to be constant, hence water flow from apical membrane to lumen is: $J_o^W = \frac{A_a}{A_o} J_a^W$. An equal volume flow leaves the compartment and advects luminal solutes. If apical water flow reverses, solute is advected into the lumen from the outside compartment. This is described by the following:

$$\begin{aligned} &J_o^W \geq 0 : J_o^i = J_o^W C_a^i \\ &J_o^W < 0 : J_o^i = J_o^W C_o^i \end{aligned} \tag{5-5}$$

5.3 Volume Regulation System

When the cell is under hypertonic stress, NKCC1 activity increases. The NKCC1 transporter facilitates cellular loading of Cl^- above its electrochemical equilibrium. Net solute uptake through this cotransporter also causes cell swelling due to subsequent water influx. A schematic of the NKCC model is shown in Figure 5-2A. This kinetic description of the NKCC1 transporter was developed by Lytle *et al*. (84). Besides NKCC1, patch-clamp studies have demonstrated that lacrimal acinar cells express volume-sensitive K^+ and Cl^- channels that are responsive to hypotonic stress (58-59). Increased solute permeabilities of these channels causes cellular extrusion of Cl^- and subsequent cell shrinkage due to water efflux. In the lacrimal gland model, NKCC1 and the volume-sensitive K^+ and Cl^- channels are located on the basolateral membrane. For simplicity, the regulation of NKCC1 activity and channel permeabilities are mediated by changing the amount E_T and channel permeabilities via piecewise continuous linear functions (Fig 5-2B). Cell swelling increases membrane K^+ and Cl^- permeabilities, thereby dumping KCl. Cell shrinkage increases NKCC1 transport, thereby causing net solute uptake. Cell volume is compared with a volume set point (V_{set}) to determine the adjustments in transporter activities. In response to volume changes, E_T of NKCC or K^+ and Cl^- channel permeability gradually increase until they reach saturation (vertical dashed line), where the cotransporter is running at their maximum level, while keeping the other one at its minimal activity to uptake/unload solutes. To simulate signaling and diffusion delays, changes in transporter activity, channel permability, and solute

concentrations are include a first-order delay for the NKCC1, the following expression is employed:

$$\frac{dE_T}{dt} = (E_T - E_T^{Guess})\tau \tag{5-6}$$

where τ is the time constant for the transporter/channel to activate, and E_T^{Guess} is the initial guess value for NKCC1 activity (refer to **Section 5.5.1** for time delay computations). A similar equation is used for the volume-sensitive channels. Refer to Appendix III for parameters values of the volume regulation system.

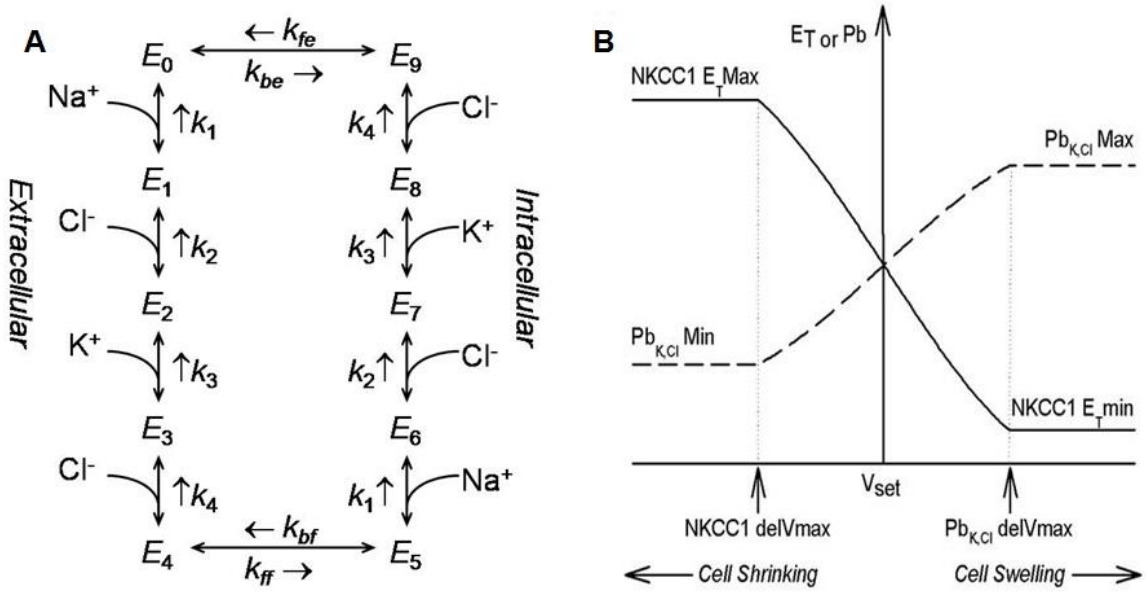

Figure 5- 2. A: The activity of NKCC1 is represented by 10-state sequential binding equations at equilibrium. It facilitates movement of Na^+, K^+ and 2 Cl^- into the cell. B: Schematic illustration of the piecewise continuous function that determines the transporter activity (E_T) for both NKCC1 and K^+ and Cl^- channel permeabilities as a function of change in cell volume. Cell volume is compared to volume set point (V_{set}) to determine if the cell is swelling or shrinking. When the level of volume change is larger than the maximum tolerance (vertical dashed lines), the appropriate volume regulatory system will run at the maximum E_T while the other stays at its minimum.

Another important volume regulatory protein is the electroneutral KCC1 transporter. This membrane transporter is only expressed in lacrimal duct cells. It is activated in response to cell swelling, and this transporter facilitates KCl extrusion like the volume-sensitive K^+ Cl^- channels. A schematic of model is showed in Figure 5-3. The E_T for this transporter is also governed by a piecewise function as showed in figure 5-2B, where cell swelling will increase KCC activity until it reaches the maximum rate while keeping NKCC1 activity at minimum.

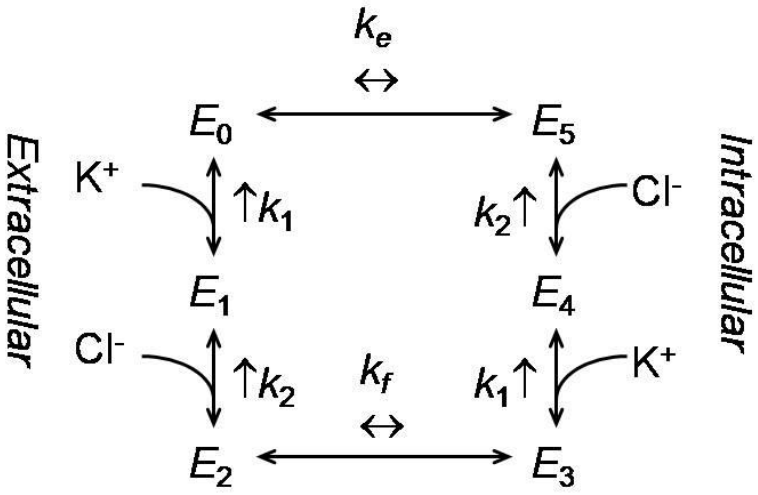

Figure 5-3. Schematic illustration of the of KCC1 co-transporter model. The activity of this cotransporter is represented by 6-state sequential binding equations at equilibrium. This transporter moves K^+ and Cl^- out of the cell to facilitate cell volume reduction.

5.4 pH Regulation Systems

pH regulatory systems include: three intrinsic buffer systems, the NHE and AE cotransporters, and CO_2 hydration. The three intrinsic buffers, ammonia, bicarbonate, and phosphate, are in equilibrium as follows:

$$
\begin{aligned}
B_{ammonia} &= C_{NH_3} + C_{NH_4^+} \\
B_{bicarbonate} &= C_{H_2CO_3} + C_{HCO_3^-} \\
B_{phosphate} &= C_{H_2PO_4} + C_{HPO_4^{2-}} \\
H_T &= C_{NH_4^+} + C_{H_2CO_3} + C_{H_2PO_4} + C_{H^+}
\end{aligned}
\tag{5-7}
$$

The total free hydrogen concentration (C_{H^+}) is calculated using the isohydric principle:

$$
H_T = C_{H^+} + \sum_j \frac{C_{H^+} + B_j}{C_{H^+} + K_a^j} \tag{5-8}
$$

where j denotes the buffer systems (ammonia, bicarbonate, and phosphate), B is the total buffer concentration, and K_a is the equilibrium constant.

CO_2 hydration, which is catalyzed by carbonic anhydrase, is represented as a chemical flux in the model:

$$
J_{chemical} = \frac{V_L}{A_a + A_b}(K_d[H_2CO_3] - K_h[CO_2]) \tag{5-9}
$$

where V_L is volume of the cell or luminal space, A_a and A_b are apical and basolateral membrane area, K_d and K_h are dehydration and hydration rates that represents carbonic anhydrase activity. CO_2 is assumed to be highly permeable, thus constant in all compartments. Therefore, cytosolic CO_2 concentration depends on blood CO_2:

$$
[CO_2] = 0.03(\frac{mM}{mmHg}) \times P_{CO_2} \tag{5-10}
$$

where P_{CO_2} is the partial pressure of CO_2.

The NHE model was developed by Weinstein and the model parameters are those found in rat proximal tubule models (85). In brief, this model extrudes H^+ or NH_4^+ coupled to Na^+ movement into the cell; this causes cellular alkalization. It has an internal modifier that adjusts transporter activity as a function of intracellular H^+ concentration. A schematic of NHE model is showed in Figure 5-4.

The AE model was developed by Chang *et al*. and the model rate constants used were obtained by fitting the model to kinetic measurement in human red blood cell at body temperature (86). This model removes one mole of HCO_3^- in exchange for one mole of Cl^- , thereby acidifying the cell. A schematic of the AE1 model is shown in Figure 5-5.

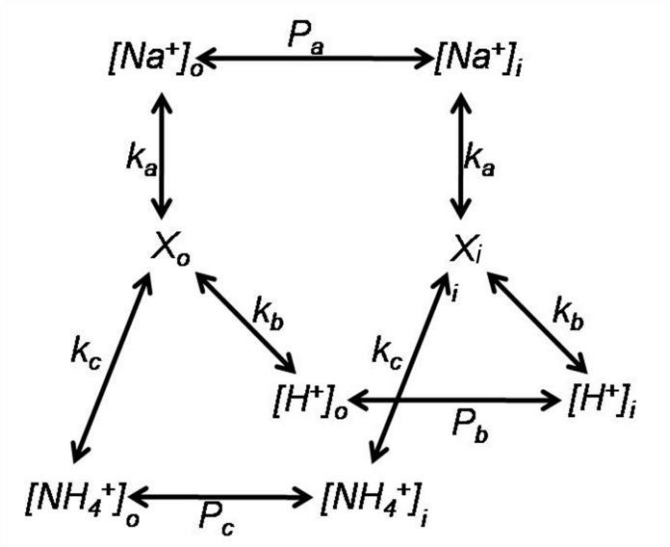

Figure 5-4. Schematic illustration of the NHE1 model developed by Weinstein (85). This transporter facilitates extracellular (denoted *o*) uptake of Na^+ in exchange of intracellular (denoted *i*) H^+. Na^+ and H^+ fluxes are determined by the bound ion permeabilities, which can be modified according to cytosolic H^+ level. The model parameters are from a rat proximal tubule model.

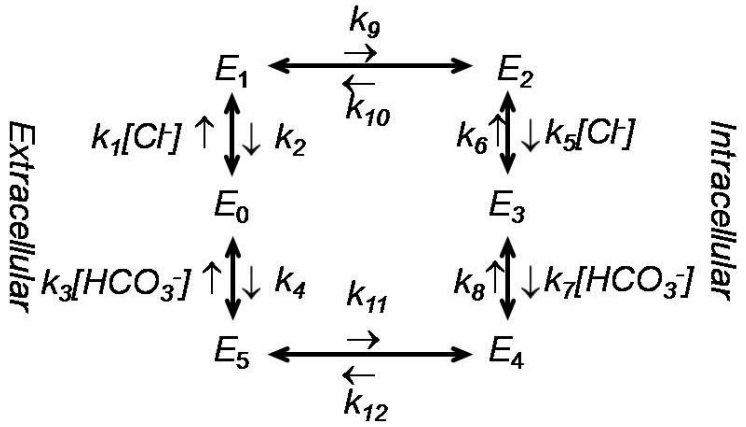

Figure 5-5. Schematic illustration of the AE1 model developed by Chang *et al* (86). This transporter facilitates removal of cytosolic HCO_3^- in exchange of Cl^-. Model parameters are from a rat distal tubule AE model.

The model of the pancreatic isoform of the electrogenic Na^+-HCO_3^--cotransporter (pNBC1) was developed by Gross *et al*. and the model parameters are from rat kidney isoform NBC model (87). The model was modified to obtain a Na^+:HCO_3^- coupling ratio of 1:2. This model facilitates uptake of Na^+ and HCO_3^-, thereby alkalizing the cell. Na^+ and HCO_3^- transport is governed by a six-state ordered kinetic model (Figure 5-6). This model assumes that one substrate binds to the carrier before another one can bind and each binding step is voltage dependent. Since this model transports two HCO_3^- for every Na^+, the sequential steps of binding and releasing two moles of HCO_3^- are put together by multiplying by the coupling ratio. Translocation of the transporter occurs only when it is fully loaded or empty.

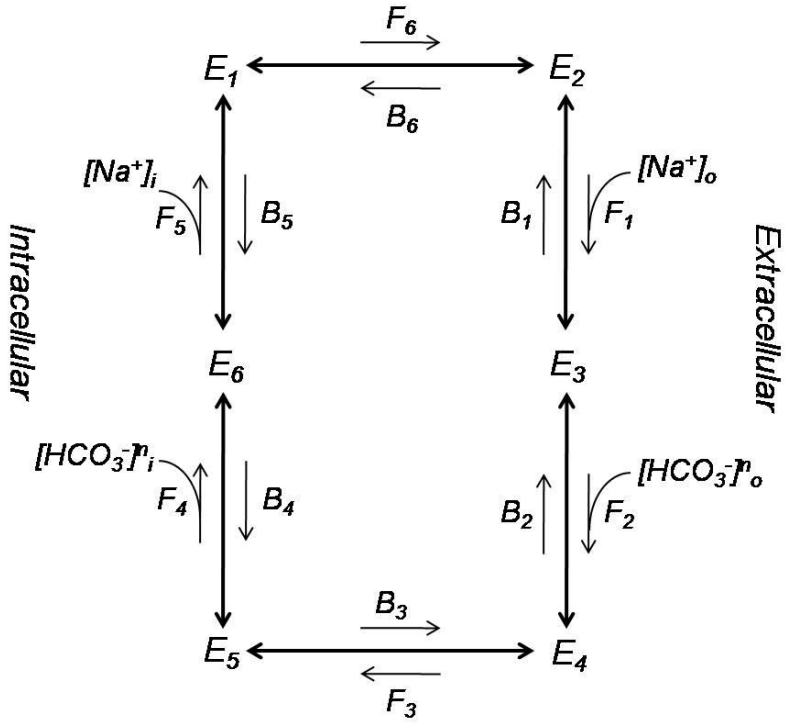

Figure 5-6. Schematic of the pNBC1 model. The pNBC1 model is modified from the kNBC model developed by Gross *et al*. (87). This electrogenic transporter facilitates Na^+ and HCO_3^- uptake with coupling ration of 1:2. The parameters for the model are based on a rat proximal tubule kNBC model but modified to reflect the stoichiometry of the pancreatic isoform.

5.5 Numerical Methods

The model was solved using MATLAB® (see www.mathworks.com). All computations were done using double precision arithmetic, and were performed on a Dell XPS laptop computer with an Intel® Core™ 2 Duo processor running at 2.4 GHz on a 64-bit Windows 7 platform. Typical simulations took between 10 and 20 seconds in real time.

5.5.1 Numerical Solutions for State Equations

The model consists of 28 coupled differential equations. The state equations were solved using ODE15S, a library routine in MATLAB® that is an adaptive routine designed for stiff systems; note that the system of equations is stiff owing to the fact that water transport occurs much more rapidly than solute transport. ODE15S was set to maintain relative and absolute tolerances at better than 10^{-3} and 10^{-6} respectively.

Evaluation of the model is achieved by integrating the state equations from the initial time (t_0) to final time (t_f) with the time increment that was computed by the ODE solver. Input for the ODE system consists of initial values of cytosolic and luminal solute concentrations and initial guess values for NKCC1, volume-sensitive KCl permeabilities, and diffusion delays. The solutions of the state equations consist of the cytosolic and luminal solute concentrations as well as time delays arising at different time points.

5.5.2 Computation of Membrane Voltages

The passive fluxes of each electrolyte across the membranes are dependent on the membrane potentials: apical membrane voltage (E_a) is needed for computing apical fluxes and basolateral membrane voltage (E_b) is needed to compute basolateral fluxes. The transepithelial potential E_t (= $E_a - E_b$) is needed for computing paracellular fluxes. The fluxes are computed using the Goldman-Hodgkin-Katz constant field flux equation with membrane permeabilities $P^i_{a,b,j}$. Membrane currents are then calculated $I^{a,b,j} = FA^{a.b.j}\sum_i z_i J^i_{a,b,j}$.

Membrane potentials were computed at each iteration step in the ODE solver. Since it is an epithelial cell model, E_a and basolateral E_b were computed simultaneously. Membrane potentials are computed numerically to ensure zero net cellular current (including passive, membrane transporters, and paracellular currents) by solving numerically the following expression:

$$f\begin{bmatrix} E_a \\ E_b \end{bmatrix} = \begin{bmatrix} F(A_a \sum_i z_i J_a^i + A_a \sum_i z_i J_j^i) \\ F(A_b \sum_i z_i J_b^i) \end{bmatrix} = \begin{bmatrix} 0 \\ 0 \end{bmatrix} \qquad (5\text{-}11)$$

where F is Faraday's constant and z_i is solute valence. Eq. 5-11 was solved using a two-dimensional Newton's method, with derivatives computed numerically via finite differences. Convergence to a solution occurred when the relative changes in the membrane potentials were less than 10^{-10} (i.e., 10 significant digits).

5.5.3 Computation of Intracellular, Extracellular, and Luminal pH

The H^+ concentration in each compartment was computed using a polynomial root-finding method. Briefly, multiplying Eq. 5-8 by the denominator terms in the sum yields a polynomial in terms of C_H. For our case where we considering three buffer systems (see Eq. 5-7), the polynomial is third order. The positive real root was determined using the MATLAB library routine ROOTS. Give C_H, it was then a simply matter to compute the acidic and basic species using the known equilibrium constants (K_a) of each buffer.

5.5.4 Computation of Solute Fluxes

As mentioned above, passive solute transport was assumed to obey the Goldman-Hodgkin-Katz constant-field flux equation, an equation that reduces to simple diffusion

for nonelectrolyte species. Nevertheless, the equation includes a term of the form $x/(\exp(x) - 1)$, where x includes membrane potentials. To avoid computational singularities when $x = 0$, and numerical inaccuracy when $|x| \approx 0$, care was taken to write appropriate code to avoid such problems. The code was based on MATLAB library routine EXPM1, which is used to compute accurately $\exp(x) - 1$.

5.5.5 Computation of Transporter Model Fluxes

The model consists of several kinetic transporter models: NKCC1, AE1, KCC1, and pNBC1. Kinetics of these models were described by *n*-sequential binding equations, where *n* represents number of binding steps, all of which are in equilibrium. Each binding step was computed as the calculating the difference between the forward and backward reactions. This will produce a system of linear equations, an *n*+1 by *n*+1 matrix, where the additional arise from concentration of total transporter protein in the membrane. An example of this linear system for the AE1 transporter is:

$$\begin{bmatrix} -k_2 & 0 & 0 & 0 & 0 & k_1[Cl^-]_o & -1 \\ k & -k_{10} & 0 & 0 & 0 & 0 & -1 \\ 0 & k_6 & -k_5[Cl^-]_i & 0 & 0 & 0 & -1 \\ 0 & 0 & k_7[HCO_3^-]_i & -k_8 & 0 & 0 & -1 \\ 0 & 0 & 0 & k_{12} & -k_{11} & 0 & -1 \\ 0 & 0 & 0 & 0 & k_4 & -k_3[HCO_3^-]_o & -1 \\ 1 & 1 & 1 & 1 & 1 & 1 & 0 \end{bmatrix} \begin{bmatrix} E_1 \\ E_2 \\ E_3 \\ E_4 \\ E_5 \\ E_6 \\ j_{AE1} \end{bmatrix} = \begin{bmatrix} 0 \\ 0 \\ 0 \\ 0 \\ 0 \\ 0 \\ E_T \end{bmatrix} \quad (5\text{-}12)$$

where k are the binding and unbinding constants for each step. Eq. 5-12 is an example of the kinetic model shown in Figure 5-5. Solution of Eq. 5-12 was done using the build-in linear system solvers in MATLAB. The evaluations of NKCC1, KCC1, and pNBC1 were done using similar method. NHE fluxes were computed using the same equations and constants described by Weinstein (85).

Chapter 6. Is NKCC Alone Sufficient to Account for the Generation of Hypertonic High KCl Tear Fluid?

6.1 Introduction

Muscarinic stimulation of the lacrimal gland produces a hypertonic fluid containing high K^+ and Cl^- concentrations compared to plasma. Electrophysiological measurements have shown increased apical K^+ and Cl^- conductance upon carbachol stimulation (6). In mice, tear secretion has a biphasic pattern as shown in Figure 6-1; tear flow rises to a peak and the declines to a plateau. The plateau phase flow is sustained by anion efflux through the apical membrane and by ion uptake by basolateral membrane transporters. NKCC1 is expressed on the basolateral membranes of mouse lacrimal acinar cell (30), and this transporter is an important volume regulator that facilitates Na^+, K^+, and Cl^- uptake. *In vitro* application of furosemide, which blocks NKCC1, to resting isolated acinar cells causes a slow decline in cell volume to ~50% of normal. This suggests that basal NKCC1 activity is necessary to compensate for the slow apical leakage of Cl^- in resting cells. Moreover, *in vivo* tear secretion studies showed that blocking NKCC1 reduces tear flow (30). These data suggest that NKCC1 plays an important role in tear secretion, yet the contribution and effects on tear flow of the regulation of this transporter by disturbances in cell volume and muscarinic stimulation is unknown. Therefore, we used the mathematical model of an acinar cell to examine interactions between cell volume regulation and water secretion in the lacrimal gland.

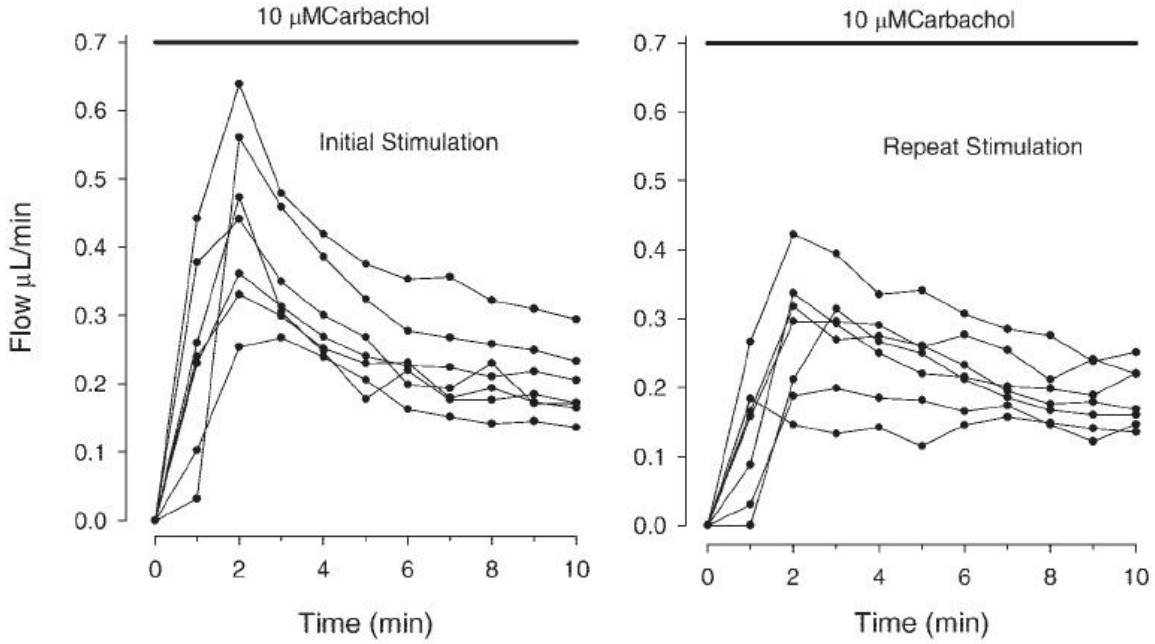

Figure 6-1. Experimental results from Walcott *et al*. (30). The left panel shows the lacrimal gland secretory response for initial topical carbachol exposure in anesthetized animals. Peak secretion is achieved within the first two minutes then followed by a plateau. The right panel shows the response to a second stimulation after 10 minutes of rest. Note that the peak secretion response is altered, while the plateau response remains unchanged.

6.2 Simulation Approaches

Refer to the section **Model Description** (Chapter 5) for a detailed description of the mathematical model of an acinar cell. In brief, simulation can be done in two model configurations: isolated cell mode, which is used to simulate *in vitro* experiments in cultured cells, and compartment mode, which is used to simulate *in vivo* tear flow measurements in mice. In this aim, the cell model incorporates passive conductances, Na^+-K^+-ATPase, NKCC1 and volume-sensitive K^+ and Cl^- channels. Model simulations are compared to experimental measurements in isolated C57 mouse acinar cells, and tear

secretion responses measured in anesthetized C57 mice in response to topical application of drugs and agonists. Most of the data are from Walcott, *et al*. (30).

6.3 Volume Regulation Parameter Determination

To determine if the model behaves like an acinar cell in culture, model simulations were compared with experimental measurements. First we looked at the model behavior in single isolated cell configuration. Cell volume perturbation experiments are simulated using the model and compared with *in vitro* experiments (Fig 6-2). When isolated lacrimal acinar cells were placed in a hypotonic solution, RVD occurred (Panel B). This behavior is also exhibited in the cell model (Panel A). RVI during hypertonic shock is also seen in both isolated cell and the cell model (Panel C and D). Application of furosemide abolished RVI and cell volume remained reduced even after the hypertonic perturbation is removed. This suggests that NKCC1 is the major membrane transporter that is involved in volume regulation. The magnitude of response in the cell model is similar to observations in *in vitro* studies. This indicates the total amount of enzyme (E_T) values for the NKCC1 and K^+ and Cl^- channel permeabilities and the cell volume regulation parameters are appropriate (Parameters are listed in Appendix III).

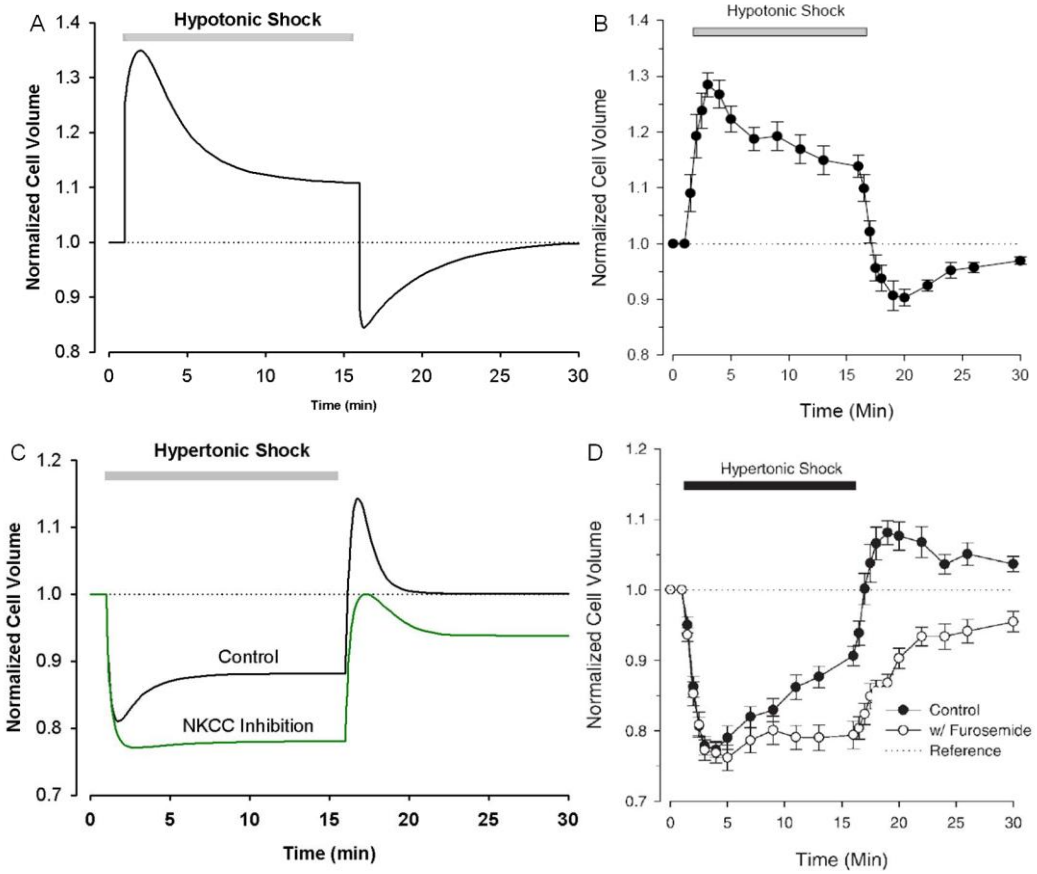

Figure 6-2. In isolated lacrimal acinar cells, an RVD response is elicited after hypotonic stress (B). This behavior is simulated using the cell model (A). An RVI occurred after exposure to hypertonic stress (D) (30). This behavior is simulated using the cell model (C, black). The RVI response is reduced in the presence of furosemide (D open circle). This suggests that NKCC is the predominant cell volume regulatory protein in these cells. Cell volume stayed down even when the hypertonic stress is removed. This behavior is simulated using the cell model with 80% NKCC inhibition (C, green curve).

6.4 Secretion-Induced Cell Shrinkage

Muscarinic stimulation of isolated acinar cells also induces a cell volume reduction. This behavior is also demonstrated by the model (Fig 6-3); panel B shows that carbachol induces cell shrinkage (filled circles). This effect can be inhibited by application of charybdotoxin, a maxi-K channel blocker, and flufenamic acid, a Cl^- channel blocker (open circles and filled squares, respectively). The model predicts

similar behavior when K^+ and Cl^- conductance are reduced (Panel A). When unstimulated acinar cells were exposed to furosemide, cell volume gradually decreases. Application of carbachol further reduces cell volume (Panel D, filled circle). The isolated cell model predicts a similar response (Panel C). Taken all together, the isolated cell model is able to simulate the measurements from cell volume perturbation experiments and the effects of carbachol stimulation *in vitro*. Therefore, the parameters (see Appendix III) for the volume regulatory system seem appropriate for lacrimal acinar cells.

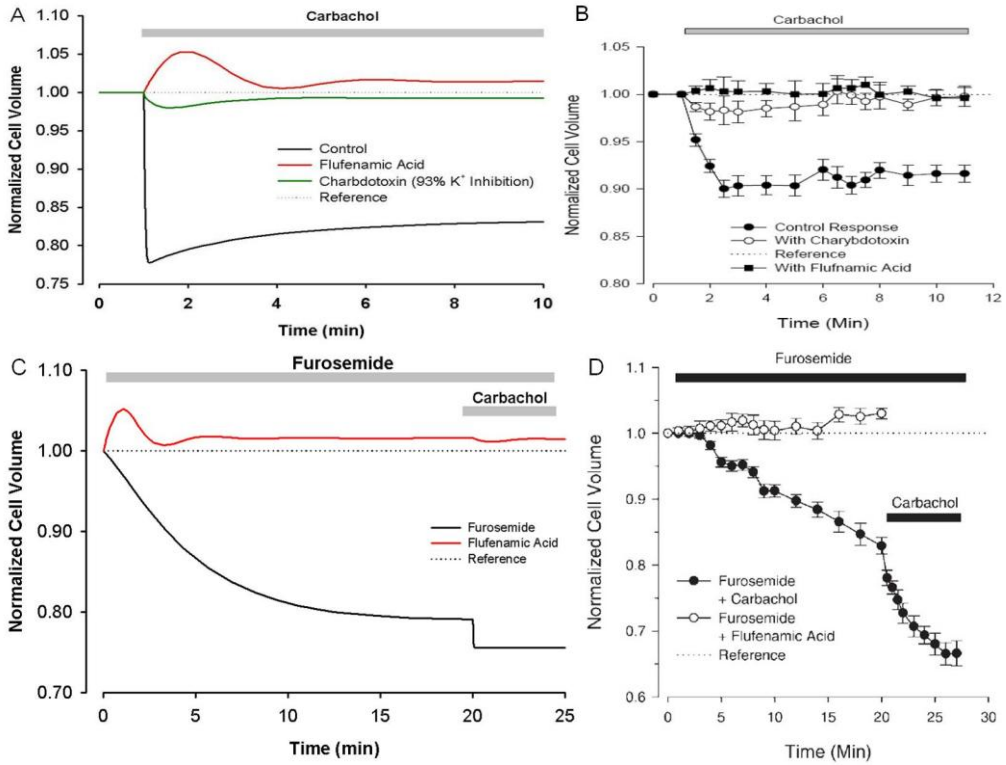

Figure 6-3. Secretion-induced cell volume change as reported by Walcott *et al*. (30). Carbachol exposure causes ~10% cell volume reduction in isolated lacrimal acinar cells, and the cell volume change is inhibited or even partially reversed in the presence of charybdotoxin, a Maxi-K channel inhibitor (B, open circles), and flufenamic acid, a Cl^- channel inhibitor (B, filled squares). The acinar cell model predicts similar behaviors (A). Resting cell volume is reduced in the presence of furosemide, and this is inhibited by flufenamic acid (D). The cell model is also able to simulate this behavior (C).

6.5 *In Vivo* Water and Electrolyte Secretion Simulation

Simulations were done in compartment mode to simulate *in vivo* tear secretion with low apical water permeability (see Appendix I). The action of carbachol was simulated by increasing apical K^+ and Cl^- permeabilities. To sustain high cytosolic K^+ and Cl^- concentrations, NKCC1 activity had to be increased. This causes a rapid rise in fluid secretion (Fig 6-4) followed by waning to a plateau. This behavior is similar to the *in vivo* tear measurement (Fig 6-1, left panel). The effect of different levels of NKCC1 inhibition (simulation of simultaneous furosemide/carbachol exposure) on tear secretion is non-linear. The initial peak was not changed, while the plateau phase of tear fluid decreased monotonically with increasing NKCC1 inhibition. Note that 99% NKCC1 inhibition significantly reduced water secretion rate (Fig 6-4). Over time, the secretion rats drop to near zero (not shown). This degree of tear flow inhibition was not observed *in vivo* (see Fig 6-1). This suggests that 1) there are furosemide-insensitive pathways that contribute to tear secretion, or 2) the exposure of the *in situ* gland to topical furosemide was not uniform or complete. The effects of repeated stimulations on tear flow were also simulated using the model (Fig 6-5). The degree of peak attenuation decreases as the intervals between simulations increases. The model predicts that this phenomenon is due to slow luminal K^+ removal at low tear flows rather than slow cytosolic Cl^- recovery (Fig 6-5). A higher K^+ concentration in the lumen reduces the driving force for apical K^+ and Cl^- efflux, thus, peak tear flow is attenuated.

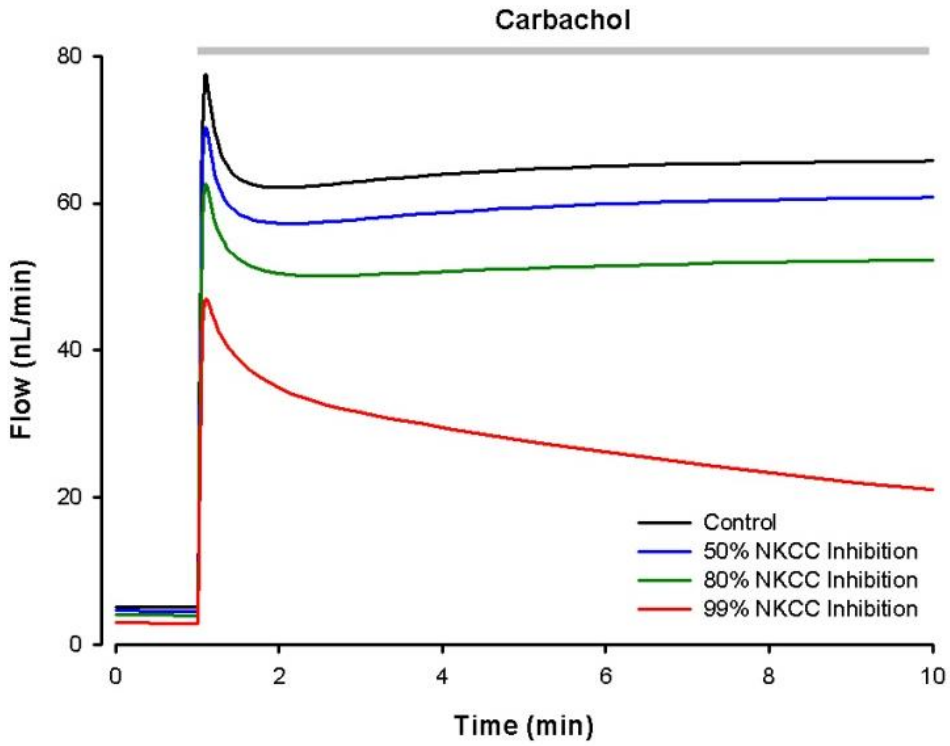

Figure 6-4. Lacrimal fluid flow is simulated using the model in compartment mode. The simulations predict a biphasic flow response that is similar to *in vivo* measurements (Figure 6-1 left panel). Carbachol triggers a rapid rise in fluid secretion. Different levels of NKCC1 inhibition reduced tear flow rate at a highly non-linear fashion. At 99% NKCC1 inhibition (red), water flow continues to decrease to almost zero (not shown), which does not agree with *in vivo* measurements (30).

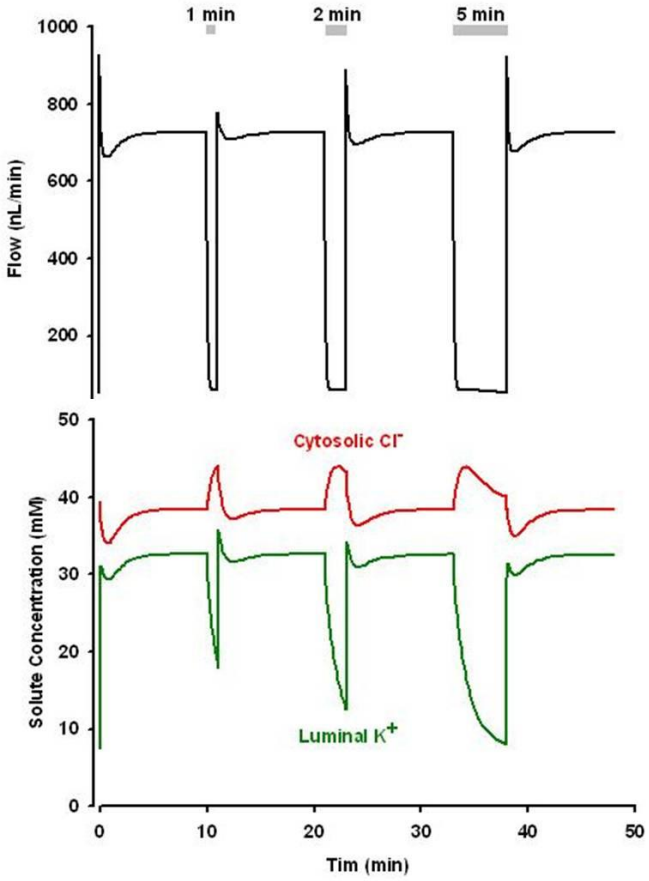

Figure 6-5. Top: Repeated exposure of lacrimal glands to carbachol was also simulated using the model in compartment mode and compared to *in vivo* measurement (Figure 5-1 right panel). The degree of peak attenuation decreases as the intervals between stimulations increases. Bottom: Peak attenuation is possibly due to slow wash out of K^+ (green) from the luminal compartment rather than slow replenishment of cytosolic Cl^- (red) via NKCC1.

5.6 Single Cell Versus Compartment Mode

When exposed to carbachol, isolated acinar cells undergo a ~10% cell volume reduction. However, measuring cell volume changes during stimulated secretion in an intact epithelium is technically challenging and has not been done. Therefore, we used the model in compartment mode to simulate the effects of carbachol exposure and compare the behaviors of single-cell and compartment configurations in terms of water

flow, cell volume, cytosolic concentration, and membrane voltage. Upon carbachol stimulation, the isolated cell model shows a ~15% reduction of cell volume, while in compartment model, cell volume only falls by 3% (Fig 6-6). This can be explained by the difference in cytosolic solute concentrations (Fig 6-6). With the model in compartment mode, cytosolic Na^+, K^+ and Cl^- concentrations were maintained relatively constant. However, in isolated single-cell mode, there is a marked reduction in the Cl^- concentration. This difference in cytosolic Cl^- behavior is related to the substantial difference in the membrane potentials between the two models (Fig 6-7). In the isolated cell model, the onset of secretion is associated with transient depolarization followed by a persistent hyperpolarization. Thus, it leads to more K^+ and Cl^- efflux and cell volume loss. In contrast, the compartment model shows a sustained depolarization in the apical membrane. This potential difference sets up the electrochemical gradient for apical K^+ and Cl^- efflux, and for Na^+ to diffuse via the tight junctions into the lumen. These electrolytes accumulate in the luminal space where they set up an osmotic gradient that drives basolateral-to-apical water flux. So, the model with a luminal compartment shows a sustained net water flow across the apical membrane upon stimulation (Fig 6-8), while the isolated single cell only showed a transient net water efflux (Fig 6-8). This is due to the fact that in an isolated cell, both apical and basolateral membranes are exposed to the same solution, and there is no osmotic gradient.

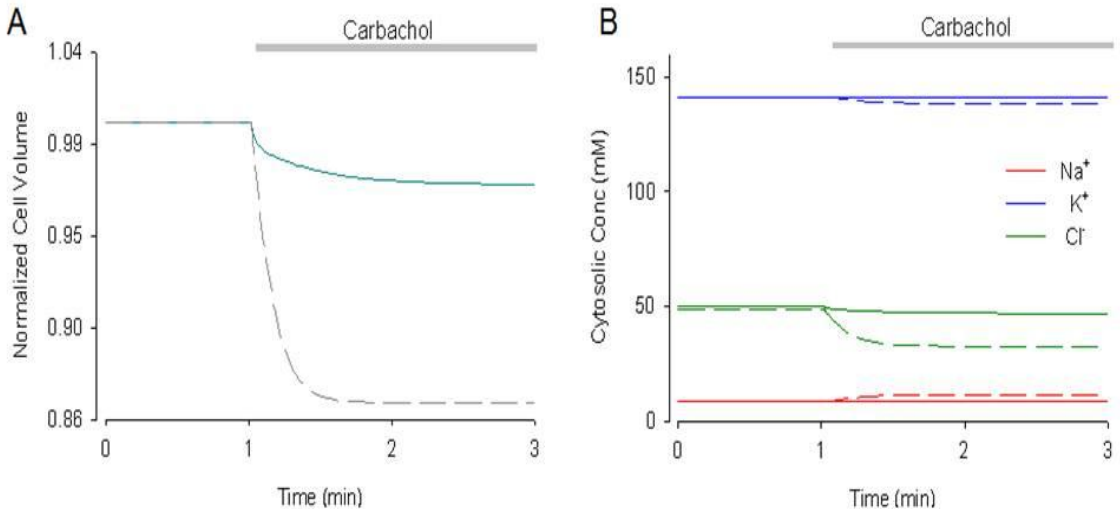

Figure 6-6. In isolated single-cell mode (dashed line), the model predicts that cell volume will be reduced by 13% after exposed to carbachol. However, in compartment mode (solid line), cell volume is decreased by 3% (Panel A). This is due to differences in the changes in cytosolic ion concentrations (Panel B).

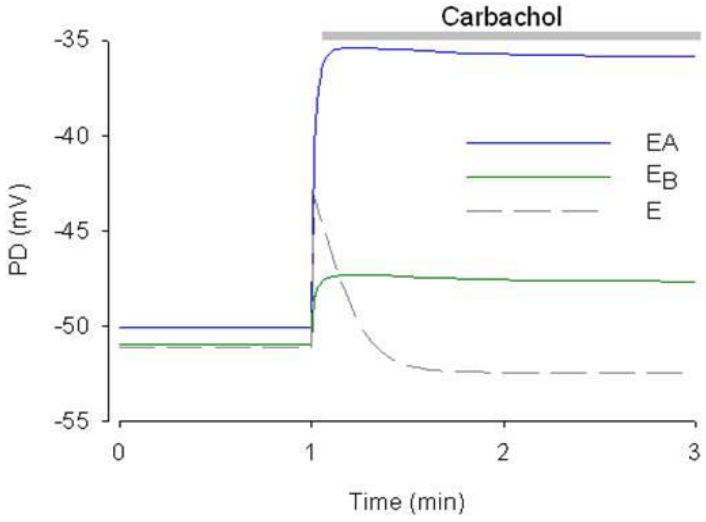

Figure 6-7. In the isolated single cell model (dashed line), carbachol induces a transient depolarization followed by persistent hyperpolarization, which leads to K^+ and Cl^- efflux and cell volume loss. In contrast, the model with a luminal compartment (solid line) shows the development of a small transepithelial difference because the apical membrane remains depolarized during carbachol exposure.

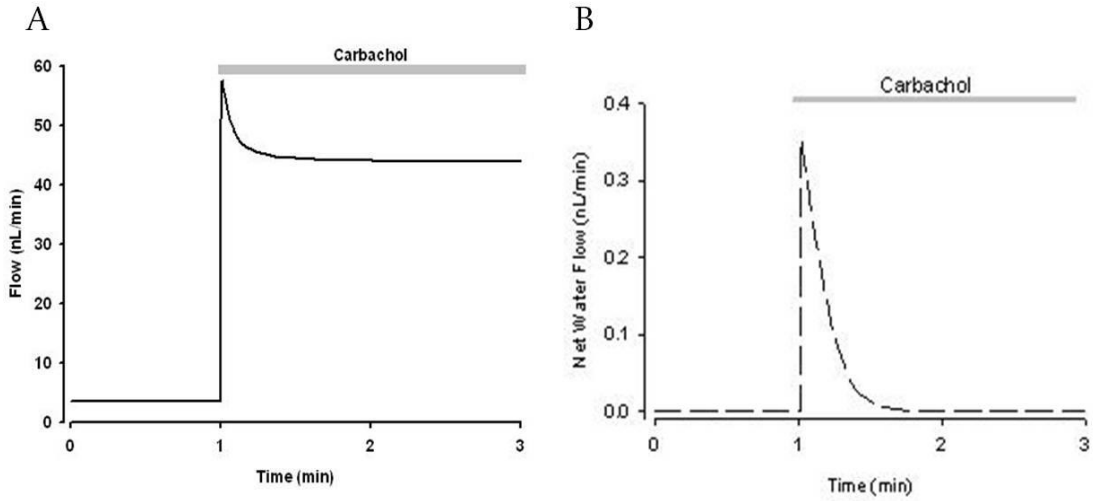

Figure 6-8. Panel A: Water secretion in compartment mode is sustained by the osmotic differences across the epithelium. Panel B: Only a transient net water out flow is observed in isolated single cell simulations because the bathing solution is the same on both apical and basolateral membranes.

6.7 Conclusions

In general, the model yields predictions that agree reasonably well with results in both *in vitro* and *in vivo* measurements. Notice that in compartment-mode simulations, the magnitude of tear flow and the duration is different in comparison to *in vivo* experiments. This is due to the fact that tear secretion is simulated using only one acinar cell in compartment mode. The same tear flow magnitude can be achieved by multiplying the simulated flow rate with number of acinar cells with the assumption that all the acinar cells in the same lacrimal gland behave the same. Strong (99%) NKCC1 inhibition reduced tear secretion to a level lower than observed in *in vivo* measurements. This suggests that there could be furosemide-/bumetanide-insensitive pathways involved in tear secretion.

The predictions of the model are that generation of a hypertonic secretion and reasonable cell volume regulation requires: 1) agonist-induced increase in apical K^+ and

Cl^- permeabilities (1000-fold increase in this model); 2) sufficient basal NKCC1 activity to maintain cytosolic Cl^- concentration above equilibrium; 3) a rise in NKCC1 activity during fluid secretion.

Chapter 7. Mathematical model of lacrimal acinar cell with pH and volume regulation

7.1 Introduction

Upon muscarinic activation, rat lacrimal glands secrete hypertonic fluid containing high K^+ and Cl^- and ~20 mM HCO_3^- (31). In addition, when rat lacrimal acinar cells are exposed to carbachol, cellular acidification occurs immediately followed by alkalization (Fig 7-1). After removal of the agonist, cellular pH slowly returns to resting levels (4). The later phase of this response is thought to reflect an increase in the activity of NHE, which loads Na^+ into the cell while facilitating H^+ extrusion, thus raising pH and increasing cytosolic HCO_3^-. To stabilize intracellular pH, AE1 is also activated to remove excess HCO_3^- in exchange for Cl^- (4). Overall, the NHE and AE1 work in parallel to load Na^+ and Cl^- into the cell. Simulations from Chapter 5 suggest that muscarinic stimulation also causes increase NKCC1 activity, which drives Na^+, K^+, and Cl^- uptake. To explore whether the acid-base transport and cell volume regulation pathways exhibit reciprocal compensation when one is blocked, Selvam, *et al*. measured short circuit current, I_{sc}, through a confluent monolayer of cultured lacrimal acinar cells (Fig 7-2) (64). I_{sc} did not significantly decline when either one of the pathways was inhibited. This indicates compensation between these two mechanisms, and that there is another transport pathway that is insensitive to both amiloride and bumetanide. The goals of this aim are 1) to expand the cell volume regulation model to include acid-base transport in order to examine the contributions of, and compensation between, these two pathways of tear secretion, and 2) to determine if the transport pathway responsible for

the residual current when the NKCC and NHE transporters are blocked arises from sodium-bicarbonate cotransport.

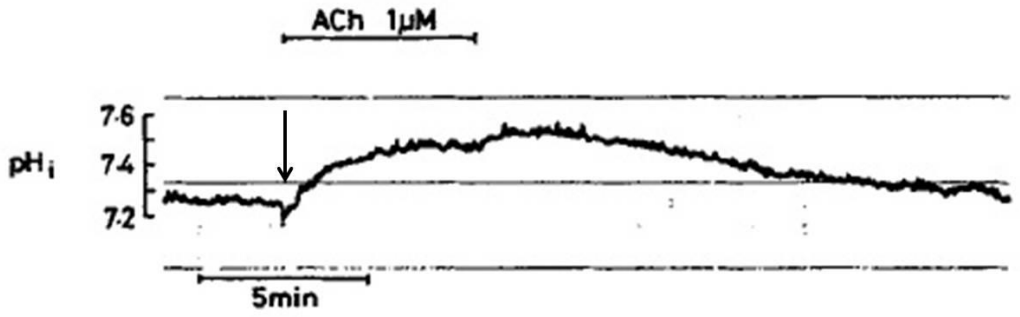

Figure 7-1. pH response of an isolated mouse lacrimal acinar cell measured by Satio *et al*. (4). Upon muscarinic agonist exposure, rapid acidification occurred (arrow); this could be due to HCO_3^- efflux via the non-selective Ca^{2+}-activated-Cl^- channel. Cytosolic pH then rises because of increased NHE activity. Cytosolic pH slowly recovers when the agonist is removed.

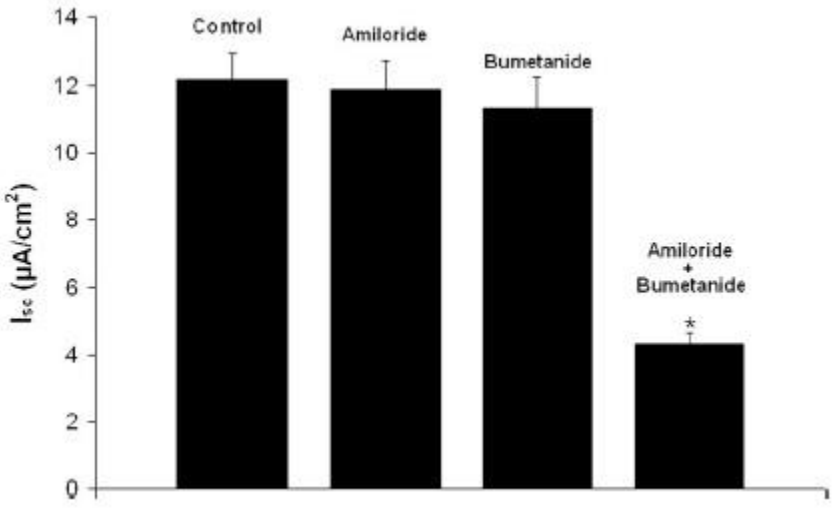

Figure 7-2. Resting short-circuit current (I_{sc}) measured in rabbit lacrimal acinar cell monolayers by Selvam *et al*. (64). Inhibition of NHE or NKCC alone is not sufficient to reduce I_{sc} magnitude. However, dual inhibition causes significant reduction of I_{sc}. This suggests there is compensation between NHE and NKCC uptake mechanisms and that there is a third transport pathway involved.

7.2 Materials and Methods

7.2.1 Model Description

The lacrimal acinar cell mathematical model was expanded by incorporating NHE, AE1, and CO_2 hydration. Refer to **Model Description** (Chapter 5) for schematics of NHE, AE1, and CO_2 hydration. The isolated single-model configuration was used for comparison with measurements with isolated rat acinar cells (4). The voltage-clamp model was used to simulate voltage-clamp experiments in cultured rabbit acinar cell monolayers for short-circuit measurement experiments (64). In this setting, both apical and basolateral bathing solutions are the same. Also, luminal volume is set to a value much larger than cell volume to ensure apical and paracellular fluxes do not significantly alter luminal ion compositions. The bathing solution of the cell is assumed to have infinite volume, thus transepithelial transport does not alter the bath composition and the transepithelial voltage is held at 0 mV. The compartment-mode of the model is used to simulate tear secretion and to predict the relative contributions to fluid secretion by the NKCC1, NHE, AE1, and pNBC.

7.2.2 Immunohistology

Mouse lacrimal gland and pancreas were removed and fixed in 4% paraformaldehyde overnight at 4^{o}C. These tissues were then placed in 30% sucrose in buffer at 4^{o}C for at least 12 hours. The tissue was frozen in tissue medium and sectioned on a cryostat at 10 m. Sectioned tissues were collected on slides and stored at -20^{o}C until staining. Tissues were rehydrated in buffer containing 0.6% Triton X-100 for 30 minutes. The tissues were then treated with nonspecific donkey serum (Santa Cruz

Biotech) for 1 hour at room temperature. The slides were then drained, washed, and exposed to primary antibody, rabbit anti-rat pNBC1 IgG (Alpha diagnostic) at concentration of 40 g/mL. After overnight incubation at 4°C, the slides were treated with secondary antibody, Alexa Fluroa 488 (donkey anti-rabbit, Invitrogen) at 1:100 dilutions, for 1 hour at room temperature. The sections were examined using a Zeiss epifluorescence microscope and photographed using a Zeiss AxioCam digital camera.

7.3 Transepithelial Resistance (TER)

In four rabbit lacrimal acinar cell monolayers, Selvam *et al*. measured total transepithelial resistance (64). At rest, TER was 205.4 ± 21.6 $\Omega \times cm^2$; and when stimulated by 100 M carbachol on the basolateral membrane, TER decreased to 147.9 ± 11.4 $\Omega \times cm^2$ (personal communication with Dr. Shivaram Selvam). To account for this observation, we conducted a voltage-clamp simulation with the cell model in compartment mode, with the transepithelial membrane voltage held at 0 mV. Small membrane currents were computed by applying a brief (1 second) 5 mV bipolar pulse to the model, and TER was computed from Ohm's Law. With the chosen membrane and junctional ion permeabilities, the model was able to generate TER of 238.3 $\Omega \times cm^2$ at rest and 131.9 $\Omega \times cm^2$ when stimulated. The good agreement between model and experimental data further demonstrate that the model parameters are appropriate, and yield transport rates similar to those exhibited by the acinar cell monolayers *in vitro*.

7.4 Stimulated pH response

In isolated mouse lacrimal acinar cells, Satio *et al*. (Fig 7-1) measured cytosolic pH response after exposure to carbachol (4). In single cell mode, the model shows a

similar pH response when exposed to carbachol (Fig 7-3). The rapid release of HCO_3^- upon opening of Cl^- channel causes cell acidification. This activates the NHE, thus resulting in cellular alkalization. Upon removal of the agonist, there was a prolonged recovery of cell pH. The isolated single acinar cell model exhibited similar behavior when the activities of the basolateral NHE and pNBC1 transporters were increased. The extended alkalization after agonist removal was due to slow HCO_3^- removal.

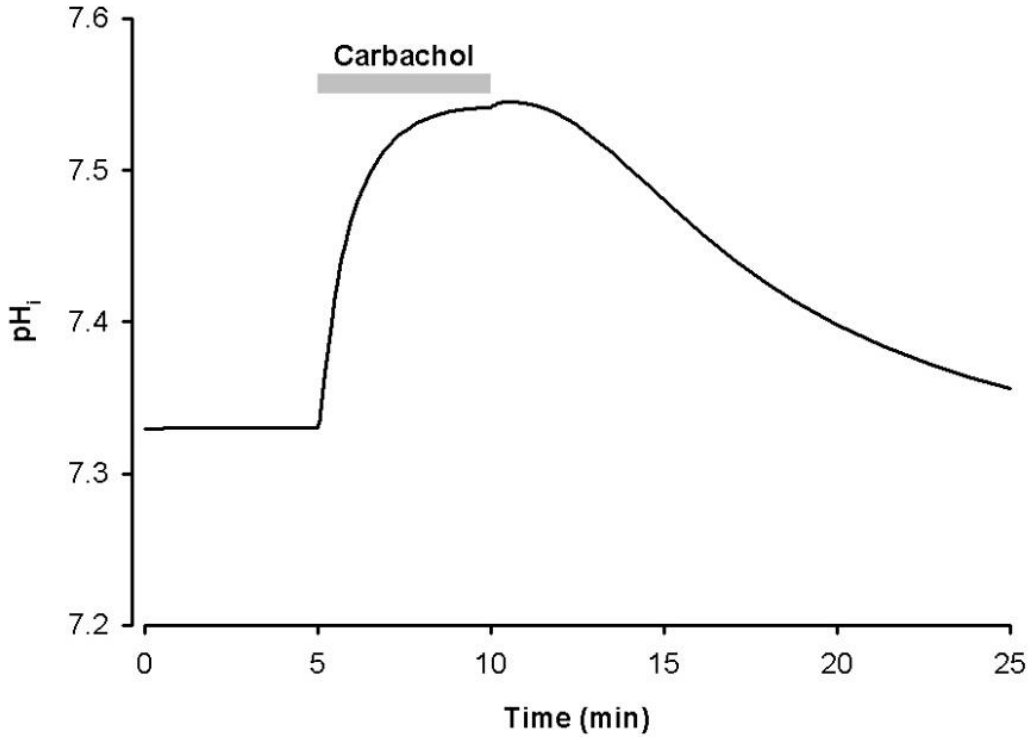

Figure 7-3. In single cell mode, the cell model is able to simulate the pH response *in vitro*. Cytosolic pH is alkalized upon muscarinic-agonist exposure. This is achieved by doubling the NHE activity. Cytosolic pH shows a very slow recovery after the stimulus is removed.

7.5 Results

7.4.1 Resting Short-Circuit Current (I_{sc})

Studies have shown that there are volume-regulation (3, 30, 38, 58) and pH-sensitive (3, 5) transport pathways in lacrimal acinar and duct cells. Since these are localized on the basolateral membrane, it is possible that they work in parallel to maintain high cytosolic Cl^-. Selvam *et al*. examined the compensatory relationship of these pathways by measuring I_{sc} in rabbit lacrimal acinar monolayers (64). No significant change occurred in I_{sc} occurred when either NKCC or NHE was inhibited. This indicates that these two pathways compensate for each other, and the results support the idea that these two transporters are involved in maintaining high cytosolic Cl^- levels at rest. To account for this behavior, I_{sc} was computed using the cell model in voltage-clamp (compartment) mode, where the luminal and basolateral composition was the same. I_{sc} values (normalized to control) were computed with E_T NKCC and E_T NHE values listed in Appendix III and IV (Fig 7-4A). With 99% NHE inhibition, the model predicted that I_{sc} was fully compensated by an increase in NKCC1 activity. Unlike actual measurements from monolayer (Fig 7-4B), the cell was unable to maintain I_{sc} when 99% of NKCC1 activity was inhibited. This suggests that, at rest, the model uses NKCC1 as the primary Cl^- uptake pathway. Since NHE and AE work in parallel to facilitate net NaCl uptake, we attempted to increase E_T NHE and E_T AE together to restore I_{sc} to control values during NKCC blockade. This could be achieved by increasing NHE and AE activities by 6-fold (Fig 7-4C). This increase in NHE and AE activity could be

triggered by the marked reduction in cell volume that occurs when the NKCC transporter is blocked.

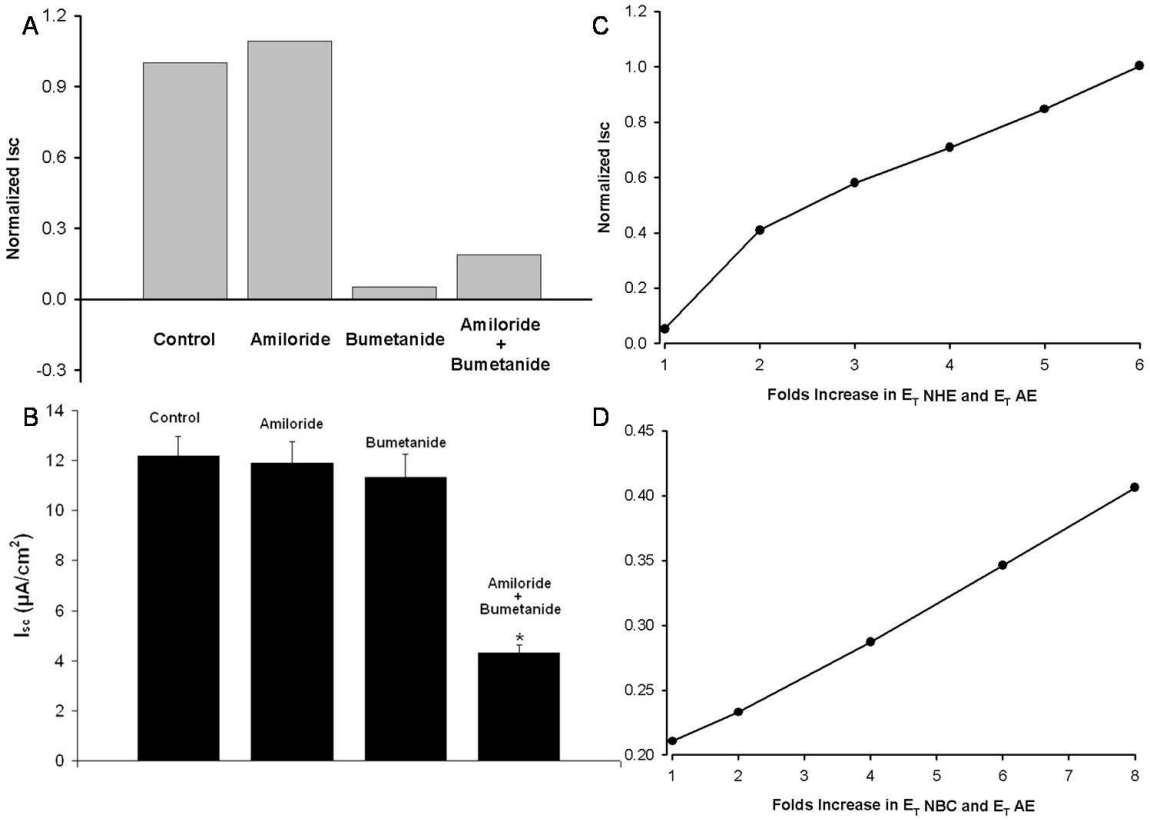

Figure 7-4. A: Resting I_{sc} is predicted by the acinar cell model in voltage-clamp mode. I_{sc} was compensated when 99% NHE activity was inhibited, due to increased NKCC1 transport. When 99% NKCC1 activity was inhibited, with basal level of NHE and AE activities, the model did not exhibit any compensation and I_{sc} fell to near zero. B: Resting I_{sc} response measured by Selvam *et al*. C: When 99% NKCC1 activity was inhibited in the model, a 6-fold increase in NHE and AE1 activities was needed to restore I_{sc} to the measured level. However, when both NKCC1 and NHE are inhibited, the model predicts lower I_{sc} than measured. D: When both NKCC1 and NHE activities were reduced, I_{sc} could be restored to ~40% of control, similar to the Selvam results, with an 8-fold increase in AE and pNBC1 activity. These two transporters act together to facilitate net NaCl uptake.

7.4.2 Na^+-HCO_3^--Cotransporter and I_{sc}

Although antagonizing NKCC1 or NHE alone did not show significant I_{sc} change, Selvam *et al*. showed that dual inhibition reduced I_{sc} by ~60% (64). However, the model failed to account for this observation in that I_{sc} was reduced by ~80% (Fig 7-2A, amiloride + bumetanide). As a result, cytosolic HCO_3^- level decreases, and AE transport was reduced. Further, I_{sc} could not be restored by just increasing AE activity. This suggests there is an amiloride and bumetanide-insensitive transport pathway in lacrimal acinar cells.

The antibody labeling study showed pNBC1 expression on both acinar and duct cells (Fig 7-5). The apical and basolateral membrane of both acinar and duct cells are identified with hematoxylin and eosin staining (personal communication with Dr. Leon Moore) on sectioned mouse lacrimal gland (7-5A). Like pancreatic ducts, there is strong basolateral staining for pNBC1 on lacrimal acinar and duct cells, but not on the apical membranes (Fig 7-5D). To represent this pathway, a published kNBC1 model (87) was modified to a pNBC1 model and incorporated into the basolateral membrane of the cell model. With pNBC1, the model was able to restore I_{sc} when E_TNBC and E_TAE increased by 8-fold (Fig 7-4D). pNBC1 provides an additional source of cytosolic HCO_3^-, which is exchanged for Cl^- via the AE1 transporter. The Na^+ is pumped out of the cell in exchange for K^+. As a result, cytosolic Cl^- is partially restored and I_{sc} rises.

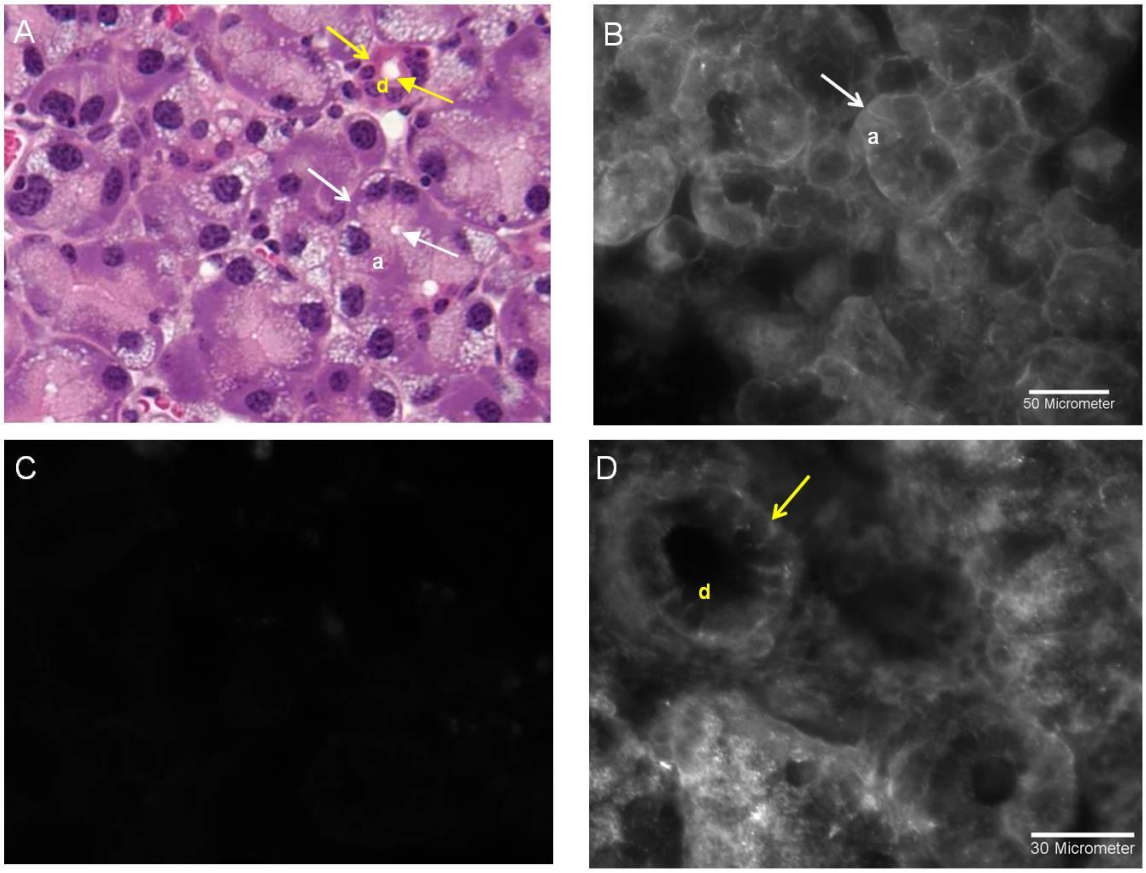

Figure 7-5. A: H&E staining on mouse lacrimal gland section. Acinar cells (a) are arranged into tubuloacinar structure with the apical membranes (large white arrow) organized into a sphere to form the apical lumen. The nucleus is located near the basoalateral membrane (small white arrow). Duct cells (d) are smaller than acinar cells. They are arranged into a tubule structure with the apical membranes (large yellow arrow) facing the lumen. Basolateral membrane is labeled by small yellow arrow. B: immunohisotology staining of mouse lacrimal gland sections reveals expression of pNBC1 on the basolateral membrane of acinar cells. C: The negative control shows there is no nonspecific binding of the secondary antibody. D: In lacrimal duct, pNBC1 is localized on the basolateral membranes but not on the apical membrane.

7.4.3 Muscarinic-Stimulated I_{sc} Response

I_{sc} was measured by Selvam *et al*. when the monolayer was stimulated by carbachol (64). At rest, a positive I_{sc} indicates the epithelium is absorbing solutes from the apical to basolateral side. When stimulated, the monolayer switched to secretion

mode as reflected by the reversal of the sign of I_{sc} (Fig 7-6, top). This process was inhibited by ouabain. The model in voltage-clamp mode was able to simulate this behavior (Fig 7-6, bottom). Several key features of the I_{sc} response are exhibited by the cell model: i) a positive resting I_{sc}, indicating that the epithelial cells are in an absorptive mode; ii) I_{sc} reverses sign when apical K^+ and Cl^- conductances are increased; iii) a small deflection in I_{sc} (noted "Stimulated Phase" in Fig 7-5A) is observed; iv) I_{sc} diminishes after a maximum I_{sc} is achieved; and v) inhibition of the Na^+-K^+-ATPase completely blocks I_{sc} behavior.

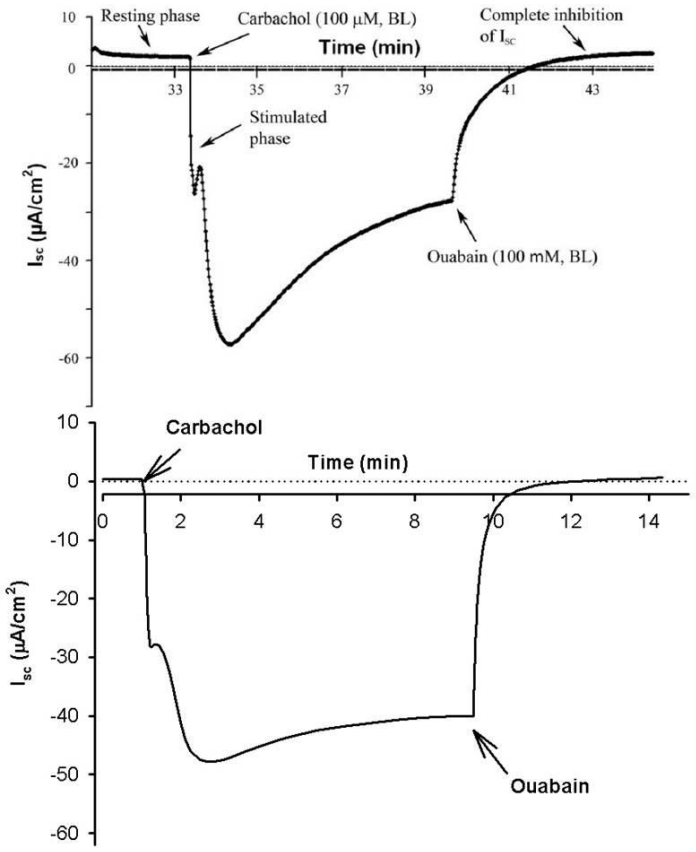

Figure 7-6. In rabbit monlayers, Selvam et al. measured the response of I_{sc} to carbachol (64) (top). This dynamic response can be simulated using the model in voltage-clamp mode (bottom). The time course and magnitude of the predicted I_{sc} changes are comparable to experimental measurements.

The stimulated-I_{sc} response is a dynamic process that involves activation of several different transport systems. Using the cell model, I_{sc} can be analyzed by examining the predicted apical K^+ and Cl^- currents (Fig 7-7A top), which are the predominant currents crossing the apical membrane when the cell is stimulated. Solute loss causes a reduction in cell volume (Fig 7-7A bottom). This, in turn, activates the volume-sensitive NKCC1, NHE, and pNBC1 on the basolateral membrane to replenish cell volume and cytosolic Cl^-. Time delays in the activation of these transporters, mainly NKCC1, causes a small deflection of the rising Cl^- current, and this is the cause of the stimulated phase inflection shown in Figure 6-6. Since membrane Cl^- permeability is much higher than HCO_3^- (36), activation of pNBC1 loads excess HCO_3^- into the cell, and this leads to cell swelling. This eventually leads to activation of volume-sensitive K^+ and Cl^- channels on the basolateral membrane, and facilitates KCl extrusion. This reduces cytosolic Cl^- level and diminishes I_{sc}. When either NKCC1 or pNBC1 is excluded from the simulation, the stimulated-I_{sc} response is altered (Fig 7-7 B and C). Based on these observations, model predictions support the idea that the dynamic I_{sc} response requires coordination of the activation of both NKCC1 and pNBC1. This dynamic process is summarized in Figure 7-8.

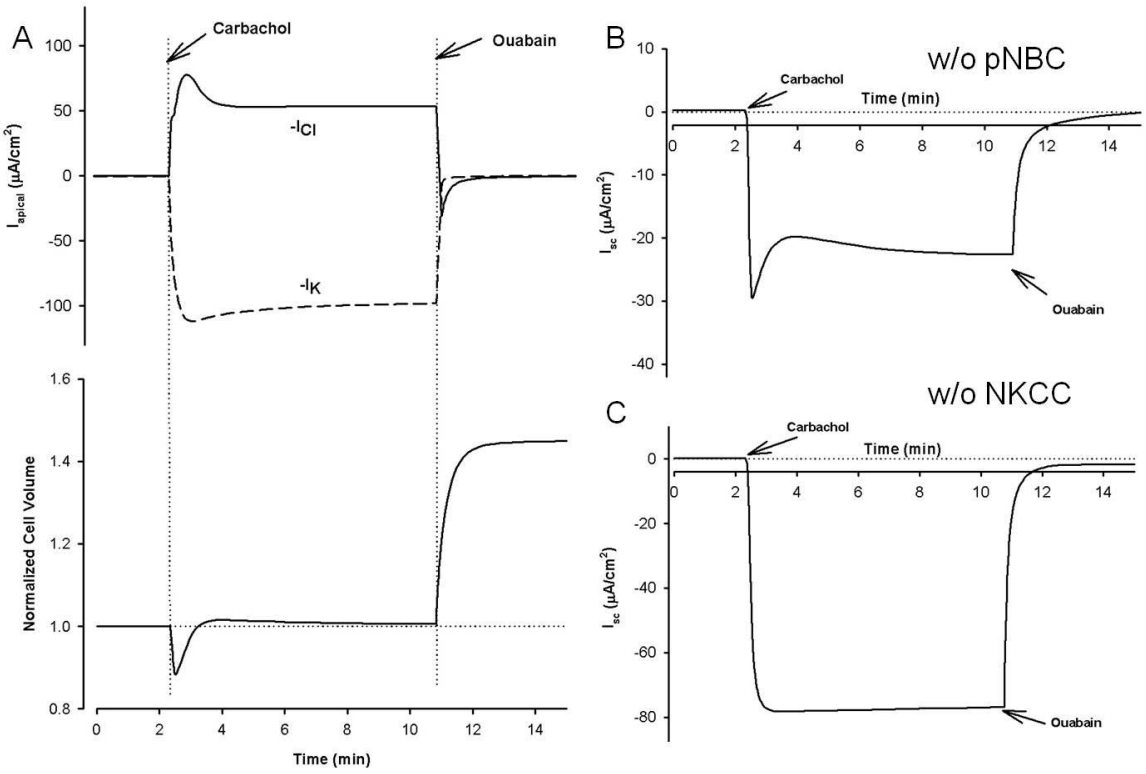

Figure 7-7. The dynamic response of I_{sc} to muscarinic stimulations can be explained by summation of the apical K^+ and Cl^- currents (A, top). Opening of apical K^+ and Cl^- channel leads to solute efflux, and cell shrinkage follows (A, bottom). This activates volume-sensitive NKCC for Cl^- uptake and causes a small fluctuation on the apical Cl^- current, and this accounts for the stimulatory phase inflection in current. However, accumulation of cytosolic HCO_3^- causes cell swelling. This, in turn, activates the volume-sensitive basolateral K^+ and Cl^- channels, which results in the loss of K^+ and Cl^- across the basolateral membrane. Hence, apical K^+ and Cl^- currents are reduced during the I_{sc} recovery phase. The dynamic I_{sc} response requires the coordinated activation of both NKCC and pNBC1 (B and C).

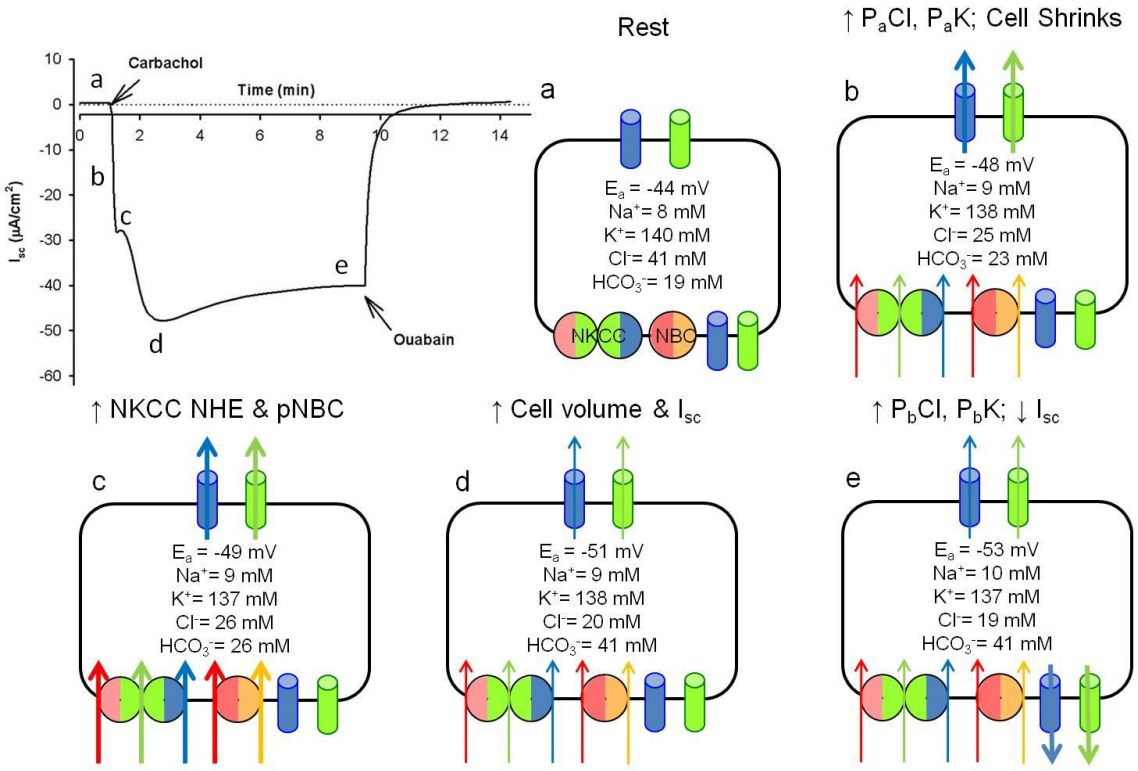

Figure 7-8. This figure summarizes coordinate actions of the different transport systems that result in the complex response of I_{sc} to muscarinic stimulation. The model predicts the stimulatory phase inflection is due to a delay in the activation of cell volume-sensitive transporters. Increased pNBC1 activity causes cell swelling. This activates volume-sensitive K^+ and Cl^- channels for solute removal via the basolateral membrane, and this reduces I_{sc}. Red: Na^+, Blue: K^+, Green: Cl^-, and Orange: HCO_3^-.

7.4.5 In Vivo Fluid Secretion Simulations

It is known that aquaporin 5 is expressed on the apical membrane of lacrimal acinar and duct cells (3, 88). However, tear secretion was not reduced in mice lacking aquaporin 5, although salivary gland secretion was impaired (88). This finding indicates that the apical membrane water permeability of lacrimal duct and acinar cell is relatively low, which is necessary for the secretion of hypertonic tears. Our acinar cell model predicts that the primary secretion of acinar cells is hypertonic and has a K^+ concentration that is much higher than plasma. The only measurement of the composition of the fluid

emerging from the lacrimal acini was done by Alexander, *et al*. (31). The results showed only slightly elevated K^+ and Cl^- concentrations compared to plasma, and the samples were essentially isotonic (31). However, these values are based on the analysis of picoliter-sized samples collected by micropuncture methods, and it is entirely possible that the samples were contaminated with, or consisted of, interstitial fluid.

Nevertheless, it is important to understand what determines acinar cell luminal composition and flow and to see if acinar cells could generate a plasma-like secretion as measured by Alexander *et al*. To this end, simulations were done to characterize the influence of apical membrane water permeability on luminal composition and flow. Simulations were thereby done with the acinar cell model in compartment mode with various apical-to-basolateral water permeability ratios (Fig 7-9). The model predicts that luminal fluid becomes isotonic when $\frac{P_a^W}{P_b^W} \geq 0.1$. This is due to increased transcellular water secretion which dilutes the luminal solutes. When the ratio is lower than 0.1, the luminal fluid is hypertonic. These findings are consistent with the conclusions of Moore, *et al*., that the lacrimal acinar and duct cell have a relatively low apical membrane water permeability ($\frac{P_a^W}{P_b^W} \geq 0.01$) that permits the epithelium to generate hypertonic fluid with Cl^- level similar to measurements (88). Finally, it should be noted that even when the luminal fluid is nearly isotonic, the model predicts that K^+ concentration, 31 mM, is much higher than the K^+ concentration of 12.7 ± 2.4 mM measured by Alexander, *et al*. (31).

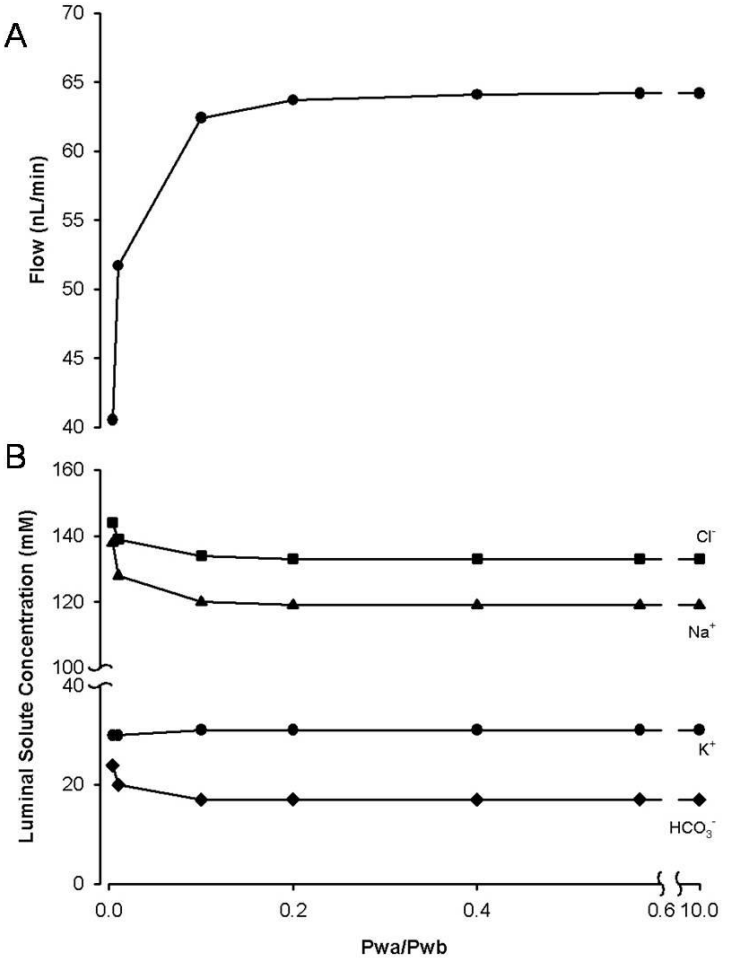

Figure 7-9. Water secretion rate and luminal composition were examined using the acinar cell model in compartment mode with various apical-to-basolateral water permeability ratios. A: At low Pwa/Pwb ratio, water secretion rate is inversely proportional to amount of solute present in lumen. However, when the ratio is higher than 0.1, water flow rate is saturated at ~63 nL/min. B: A hypertonic lumen is predicted with low apical water permeability. Luminal solutes are diluted by the high water flux when the ratio is higher than 0.1, and the luminal space becomes isotonic with a high K^+ concentration.

With the inclusion of the acid-base transporters, it is likely that the acinar cell responses to pharmacological transporter blockade will differ from those exhibited by the simpler model with only cell-volume regulatory transporters (see Fig 7-4). In part, the differences in the responses might arise from interactions and cross compensation

involving common transported ions. Simulations were undertaken to predict acinar cell fluid secretion. It was predicted using the model in compartment mode in which the luminal compartment composition depends on the apical and junctional fluxes. In the simulations, apical K^+ and Cl^- permeabilities were increased to simulate muscarinic stimulation. In addition, NHE and pNBC1 activities were increased (2x and 1000x respectively). The model predicted that 99% NKCC1 inhibition without any compensation of NHE and AE in response to cell shrinkage causes a significant reduction (~70%) of fluid flow rate (Fig 7-10). When compensation by the NHE and AE was included by the amount predicted by the I_{sc} study (Fig 7-4 C), the water secretion was reduced only ~50%. Luminal Cl^- was reduced while HCO_3^-, concentration and pH increased (Table 7-1). These changes were consequences of increased Cl^- uptake via the pH regulatory pathways. Inhibition of NHE by 99% with amiloride did not change fluid flow rate significantly, which reflects increased Cl^- uptake via NKCC1 because of the decrease in cytosolic Cl^-.

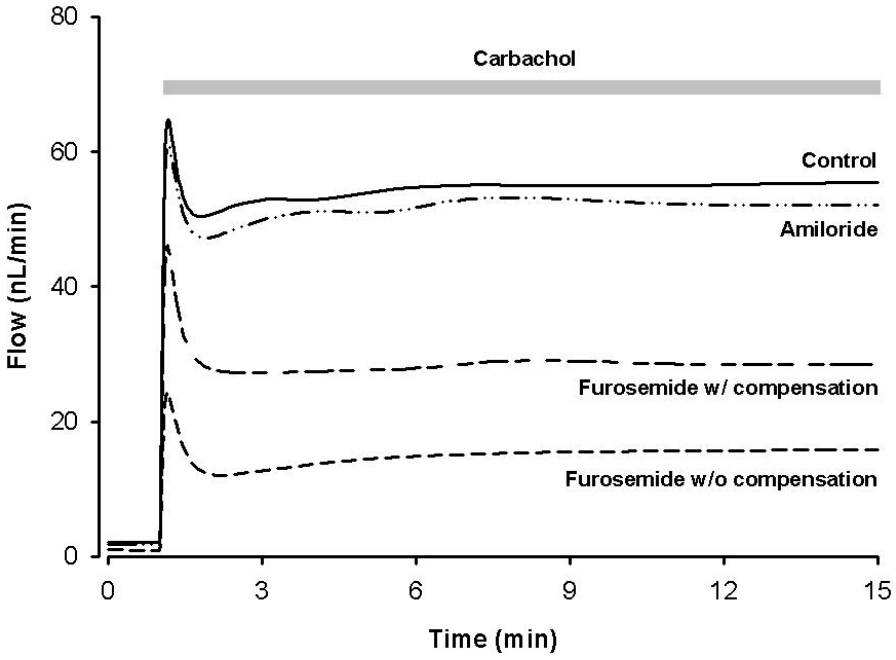

Figure 7-10. Carbachol-induced lacrimal fluid secretion computed using the cell model in compartment mode where apical solute composition is determined by ratio of solute to water fluxes. The simulated results are compared with lacrimal fluid measurements from anesthetized mice in our laboratory (Fig. 5-1).

Table 7-1. Predicted steady-state cell volume, luminal water flow, cytosolic and luminal electrolyte composition using cell model in compartment mode in the presence of transport inhibitors.

		Cytosolic					Luminal					Flow (nL/min)
		Na^+	K^+	Cl^-	HCO_3^-	pH	Na^+	K^+	Cl^-	HCO_3^-	pH	
Control	Rest	8	140	41	19	7.3	118	22	104	32	7.5	2
	Stim	7	140	35	24	7.5	130	34	142	23	7.4	52
Furosemide	Rest	9	138	31	19	7.3	127	23	110	40	7.6	1.8
	Stim	8	139	19	32	7.6	150	27	150	25	7.4	16
Fur w/ Comp	Rest	12	135	26	34	7.8	136	15	96	56	7.9	2
	Stim	10	137	18	34	7.8	138	25	101	62	8.2	28.5
Amiloride	Rest	9	138	50	9	6.9	128	22	124	27	7.4	1.6
	Stim	10	137	32	17	7.2	145	29	150	24	7.3	50

One of the critical requirements for generating fluid with high K^+ and Cl^- concentration is to maintain cytosolic Cl^- concentration above electrochemical equilibrium. As noted earlier, basolateral NKCC1 uptake must be increased to sustain K^+ and Cl^- efflux during secretion. Inhibition of NKCC1 not only reduced lacrimal fluid flow rate, it could affect luminal fluid composition because of interactions with the acid-base transporters. We used the acinar cell model in compartment mode to examine the influence of NKCC1 activity on luminal solute concentrations during secretion (Fig 7-11 A and B). In these simulations, NKCC1 activity was varied while the other membrane transporters were kept constant at their normal activities during muscarinic stimulation. The model predicts that intracellular and luminal Cl^- concentrations increase in parallel as NKCC1 activity is increased. The rise in luminal Cl^- was accompanied by slight elevation of Na^+ and K^+ concentrations, while HCO_3^- concentration was reduced. Despite large increases in NKCC1 activity, cytosolic Cl^- saturated at 42 mM. This reflected in the fact that large increases in NKCC1 activity (up to 10 fold, not shown) were not able to fully restore cell volume.

In addition to cytosolic Cl^-, HCO_3^- is another negatively charged solute that is secreted via Ca^{2+}-activated-Cl^- channels. Here we used the model in compartment mode to examine effect of different cytosolic HCO_3^- concentrations on luminal solute composition. To do this, pNBC1 activity was varied while the other membrane transporters were kept constant (Fig 7-11 C and D). HCO_3^- secretion increased with pNBC1 activity and the rise in intracellular HCO_3^- restores and even increases, cell volume (Fig 7-11 C). However, cytosolic HCO_3^- levels did not have significant effect on

other luminal solutes, except when the cells swell (dotted line), and the volume-sensitive K^+ and Cl^- channels are activated. This permits K^+ and Cl^- efflux through the basolateral membrane which reduces luminal K^+ concentration.

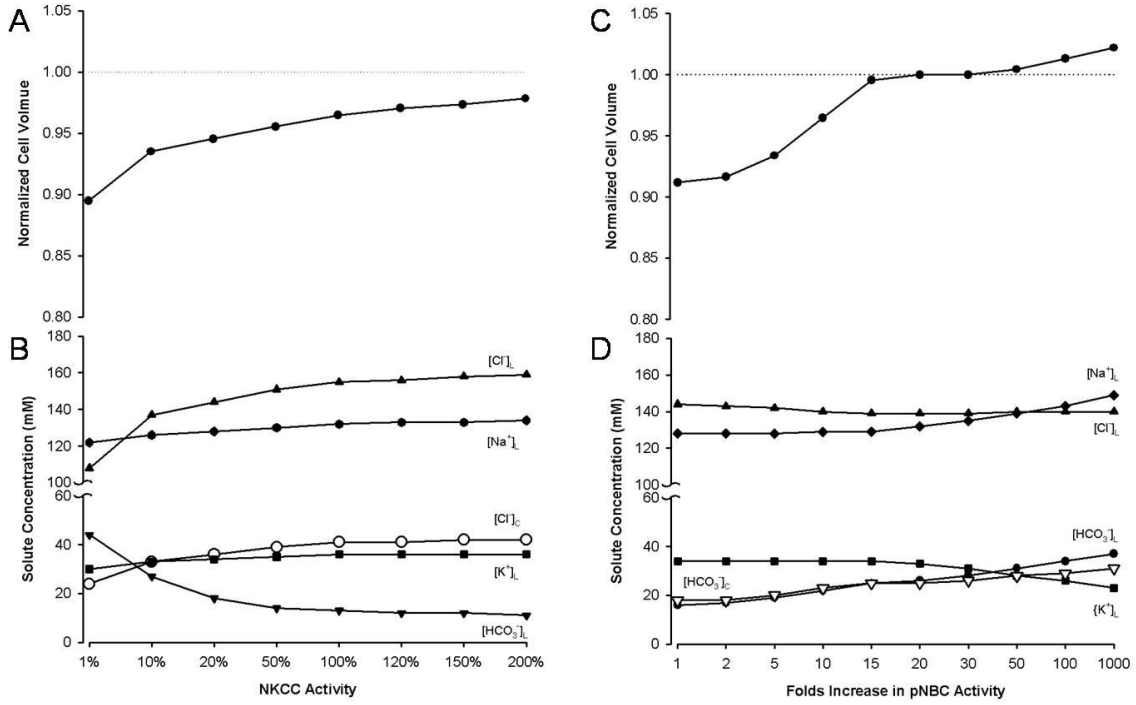

Figure 7-11. Influence of various levels of cytosolic Cl^- and HCO_3^- on acinar cell volume and luminal composition; unfilled circles show cytoplasmic Cl^- concentration. The simulations were done with the model in compartment mode during muscarinic stimulation. A: Cytosolic Cl^- level is modulated with different NKCC1 activities. Cell volume gradually increases toward normal (*Vset*) with increasing NKCC1 uptake. RVI only can restore up to 97% of the cell volume even though NKCC1 activity increases up to 10 fold. B: Increased NKCC1 uptake also increases Cl^- secretion. To maintain electroneutrality, both Na^+ and K^+ secretion rise while luminal HCO_3^- concentration decreases. C: Increased pNBC1 activity increases HCO_3^- uptake and increases cell volume. D: Because of the relatively low apical HCO_3^- permeability, the increase in cytosolic HCO_3^- does not have a significant effect on luminal composition (except for a rise in the HCO_3^- concentration). However, when cell volume is higher than *Vset* (dotted line), activation of volume-sensitive K^+ and Cl^- channels leads to basolateral loss of K^+ and a reduction in the luminal K^+ concentration.

7.5 Discussion and Conclusion

We have developed a mathematical representation of a lacrimal acinar cell which has provided useful insight into the transport mechanisms that generate hypertonic tear fluid. At rest, the model shows that cytosolic Cl^- level is maintained above equilibrium by the basolateral NKCC1; other transport pathways contribute during stimulated secretion. With the volume-sensitive and pH-regulatory systems in the model, we were able to simulate results from different experiments (4, 30, 64). Due to variations in experimental conditions, such as different agonist dosages and different wash-in/wash-off times, the effect of muscarinic exposure on apical K^+-and Cl^--channel permeabilities, and the time delays for the onset of muscarinic activation of ion transporters, were different. After taking these factors into account, the model exhibited behaviors that agreed remarkably well with published measurements.

Selvam *et al*. showed that, in the lacrimal acinar cell monolayers, the carbachol-induced response of I_{sc} is a complex dynamic process (64). Model simulations suggest that rapid changes in I_{sc} arise from several transport components with different activation delays (Fig 7-4). Based on the model simulation, there are at least two components that contributed to the dynamic I_{sc} response, and they are NKCC1 and pNBC1. There are multiple factors that could influence transporter activities, and protein kinase C (PKC) could be one of them. The M_3-receptor is a G-protein coupled receptor. The PKC family consists of 11 isoforms: 1) conventional PKCs (PKCα, βI, βII, and γ) have a Ca^{2+} and DAG dependent kinase activity; 2) novel PKCs (PKCε, δ, θ, η, and μ are only DAG dependent; and 3) atypical PKCs (PKCξ, and ι/ λ) which are independent of both Ca^{2+}

and DAG. There are five PKC isoforms found in rat lacrimal gland: PKCα, ε, δ, ξ, and ι/λ. In rat lacrimal gland, it has been demonstrated that PKCα, ε, and δ are regulatory mechanisms for cholinergic-induced protein secretion (89). The same group showed that different isoforms have different responses to agonist desensitization with PCKδ being the most insensitive, PKCε is moderate insensitivity, and PKCα being the most sensitive. Results from this study suggest that PKCδ is the predominant regulatory mechanism for protein secretion during prolonged tear secretion.

In addition to regulating protein secretion, PKC could also play an important role in modulating membrane transporter activities. Many studies have shown PKC-induced changes of NKCC1 and pNBC1 transport (28-29, 90-93). There is evidence indicating that increased NKCC1 uptake is linked to increased PKCδ expression. Liedtke *et al*. found co-localization of actin filaments with PCKδ in Calu-3 cells, which is a critical requirement for NKCC1 activation (92). Moreover, a study in human tracheal epithelial cells showed that activation of NKCC1 by hyperosmotic stress is associated with PKCδ (91). In contrast, there is evidence that the phorbol ester 12-O-tetradecanoylphorbol-13-acetate (PMA) increases PKC activity leading to a reduction of NKCC1 activity. Farokhzad *et al*. reported that in the human T84 cell line, exposure to forskolin only caused a transient increase (~30 minutes) of NKCC1 uptake followed by prolonged suppression of the transporter activities (up to 10 hours). They also showed that PMA treatment caused a reduction in NKCC1 mRNA level which suggests that NKCC1 surface expression might be reduced (28). In agreement with the previous study in the same cell line, Del Castillo *et al*. showed that in the presence of carbachol, the cell

surface expression of NKCC1 is reduced due to internalization. They further showed that membrane endocytosis is associated with PKCε activity (90). Like NKCC1, pNBC1 activity is also modulated by PKC. In murine colonic crypts, Bachmann *et al*. showed carbachol-induced increase of dimethylamiloride insensitive proton flux mediated by pNBC (29). In the presence of agonist, the proton flux was reduced to basal level is when both conventional and novel PKCs are inhibited, suggesting that pNBC1 activity is regulated by both types of PKC. However, in rat salivary gland, Perry *et al*. found that prolonged carbachol exposure caused internalization of surface pNBC1 (93). There are opposing findings regarding PKC regulation on NKCC1 and pNBC1 activities, but this could be due to the fact that experiments were conducted using different cell lines. Since there are many different PKC isoforms, and it is possible that more than one isoform is activated by cholinergic agonists, then membrane transporter expression or activity could be determined by the relative levels of stimulatory and inhibitory PKCs. In the rabbit lacrimal acinar monolayer, prolonged carbachol stimulation (up to an hour) resulted in I_{sc} slowly returning to resting levels (personal communication with Dr. Shivaram Selvam). It could be due to receptor desensitization or internalization of membrane transporters as a cellular protective mechanism from overloading of cytosolic HCO_3^-, as suggested by Perry *et al*. (93). The difference in response times of NKCC1 and pNBC1, which we postulate can explain key parts of the I_{sc} response, could be due to activation or inactivation of different PKC isoforms. This idea is supported by a study on PMA-induced basolateral endocytosis in the T84 cell line (93). This study showed a biphasic endocytotic response, where an early phase is associated with PKCε and δ and a late

phase is linked to PKCα. Yet, the mechanisms of how PKC influence NKCC1 and pNBC1 expression or transport activities are not clear, and more studies are needed to elucidate the functions of different PKC isoforms.

The acinar cell model in compartment mode was used to examine the influence of the apical-to-basolateral water permeability ratio on luminal composition and water secretion rate (Fig 7-7). The results showed that luminal hypertonicity is very sensitive to apical water permeability. P_a^W has to be much lower than P_b^W in order to generate hypertonic fluid, a finding that agrees with work by Moore *et al*. (88). Based on these results, we concluded that aquaporin expression is not a critical requirement for the production of a hypertonic secretion in lacrimal gland. Even with high apical water permeability, the model predicts luminal composition with high K^+ (>30 mM) and Cl^- (>130 mM) even though the primary secretion is isotonic (Fig 7-7B). The predicted solute concentrations are close to the measurements reported from final lacrimal secretion (30-32). However, the model predictions disagree with measurements of composition of the primary acinar secretion reported by Alexander *et al*. (31). They found an isotonic primary secretion with slightly increased of luminal K^+ and Cl^- concentrations of (in mM): Na^+ 132 ± 3, K+: 12.7 ± 2.4, and Cl^- 102 ± 2. They reported final secretion with composition of (in mM): Na^+ 135 ± 5, K+ 46 ± 3, and Cl^- 123 ± 1. They also found that the composition of the final lacrimal secretion was independent of tear flow, except at very low flow rates (31). However, lacrimal acinar cells comprise 80% of total gland mass while duct cells are only 15% (1). Although there is no direct measurement of water secretion by duct cells, it was estimated that lacrimal ducts

contribute roughly 30% of the final lacrimal fluid volume (94). If the primary secretion composition measurements of Alexander *et al*. are valid, this means that the duct cells would have to secrete a lot of KCl in just the right amounts to produce constant tear composition at widely varying flow rates. This scenario could only be possible at low secretion rates, where the transit time through the ducts is long enough for KCl secretion to raise luminal fluid levels. However, at high flow rates, it is unlikely that ductal modification of luminal composition would be complete. A more plausible explanation to account for the generation of hypertonic tear fluid with a K^+ concentration that is relatively flow independent would be that the acinar cells secrete a fluid similar to duct cells. This issue is the subject of the next chapter, where a duct cell model is presented, along with measurements of the composition of final rat tear fluid and different flow rates.

The acinar cell model predicts a ~70% drop in water secretion when in the presence of 99% NKCC1 inhibition. This indicates that, during stimulated secretion, the NHE, AE1, and pNBC1 activities contributed 30% to water flow rate, and it suggests that the pH regulatory systems are not the predominant mechanism for water secretion. However, they play an important role in the regulation of luminal pH, which is another critical requirement for ocular health. With compensatory upregulation of NHE and AE activities during NKCC1 inhibition, the fluid secretion rate was restored to 50% of normal, which agrees with experimental measurements. However, the luminal fluid became alkalized due to a significant increase in HCO_3^- secretion (Table 7-1). Sensitivity studies on cytosolic Cl^- and HCO_3^- showed that carbachol-induced high KCl

secretion depends on cytosolic Cl^- levels rather than HCO_3^-. However, luminal K^+ saturated at 36 mM even though NKCC1 activity was doubled. This suggests that duct cells may play an important role in K^+ secretion. Ubels *et al*. showed that there is apical KCC1 expression in lacrimal duct cells in rats (3). Also, duct cells express a similar array of proteins like acinar cells. It is possible that they behave the same as acinar cells in response to muscarinic stimulation to produce a fluid containing high K^+ and Cl^-. In the next chapter, we will explore these issues.

Chapter 8. Water and Electrolyte Secretion in Lacrimal Duct Cells and the Role of Apical KCC1

8.1 Introduction

Little is known about the function of lacrimal duct cells in fluid secretion. Immunocytochemistry shows that these cells express similar transport proteins as acinar cells. This suggests that acinar and duct cells could have similar function in fluid secretion. Our apical cell model predicts that exposure to muscarinic agonists result in the formation of a hypertonic primary secretion from acinar cells. This high K^+ and Cl^- fluid passes through the ductal epithelium and it remains hypertonic when secreted onto the cornea. The mechanism of how duct cells maintain the hypertonic primary secretion is not clear. Apical expression of AQP5 in duct cell membranes suggests that duct cells are involved in fluid secretion. Moreover, higher expression of basolateral NKCC1 is found in ducts cells than in acini, and apical KCC1 is expressed only in lacrimal duct cells. These findings suggest that duct cells could have more transport capacity than acinar cells (3). During stimulation, hypertonic fluid containing high K^+ and Cl^- could be secreted from duct cells to maintain constant fluid composition while increasing tear flow. Since it is technically challenging to measure ductal epithelium function in tear secretion, a mathematical model containing both acinar and duct cells was developed to examine the ionic composition in various tear flow rates and to determine the role of duct cells in tear production. The model is based on mass conservation, electroneutrality constraints, and includes kinetic models of Na^+-K^+-ATPase, NKCC1, KCC1, NHE, AE1, CO_2 hydration, pNBC1, and passive fluxes of ions, non-electrolytes and water. The

effects of muscarinic stimulation to enhance apical Cl^- and K^+ permeabilities and NHE activity are also included, as are the effects of cell volume changes on the NKCC1 and KCC1. In addition, experiments were performed to characterize the flow dependence of tear fluid composition for comparison to the model predictions.

8.2 Materials and Methods

8.2.1 In vivo Lacrimal Fluid Secretion Measurement

Experiments were conducted using Sprague-Dawley (SD) rats. The animals were housed in an approved animal facility, and all procedures were approved by IACUC Committee at SUNY Stony Brook.

Male SD rats (n = 10, 200—350 g in weight) were anesthetized with inactin and ketamine (135 mg/Kg Inactin, intraperitoneal; 20 mg/Kg xylazine, intraperitoneal if necessary) and placed on a temperature-controlled surgical table. Animal body temperature was monitored by rectal temperature probe and maintained at ~ 37^{o}C. A tracheal cannula was inserted to prevent saliva aspiration. Catheters were inserted into left femoral vein for isotonic saline infusion (0.6 mL/hour), and into the left femoral artery for blood pressure monitoring. Heparin was added to the fluid in the artery line to prevent formation of blood clots.

Tear flow rate measurements and sample collection follow the procedures previously used by Walcott *et al*. (30). The animal was placed on its side with its head immobilized by non-penetrating steel pins. The lacrimal duct was exposed with a small incision along an axis between the outer junction of eyelids and the ear. The tissue surrounding the duct was then removed by blunt dissection. The lacrimal duct was

sectioned as far distally as possible and the end of the duct was placed into a constant-bore microcapillary tube with known volume for tear collection. The tear flow rate was then measured by monitoring the movement of fluid meniscus in the tube. The experimental procedure starts with the intraperitoneal injection of carbachol (125—180 g/Kg body weight) to induce tear secretion following procedures described by Alexander *et al*. (31). The average flow rate was computed.

8.2.2 Lacrimal Fluid Composition Measurements

Animal tear samples were collected using microcapillary tube and emptied into pre-weighted Thin-Wall Microtubes (United Scientific Products). For all the tear samples, 20 L distilled water was added to increase the sample volume. Then the fluid-filled microtubes were weighed again to determine the sample mass, which was used to correct for fluid evaporation. Then the samples were stored in -20^{o}C until measurements. Na^{+} and K^{+} concentrations were measured using microelectrodes that are commercially available (Microelectrodes, Inc.). The microelectrodes were calibrated using our standard solutions, and the measured ion concentrations were calculated based on the calibration curves. Cl^{-} concentration was measured using custom-made, nanoliter-scale Cl^{-} titrator (95). The titrations were done in nanoliter size samples placed on a silver platform under water-equilibrated mineral oil (95).

8.2.3 Duct Cell Model Description and Simulations

The key difference between the acinar and duct cell models is the apically expressed KCC1 in duct cell. This volume-sensitive membrane cotransporter is activated

when the cell swells, and it facilitates KCl extrusion into the luminal space. This could be one of the mechanisms duct cells use to maintain high KCl secretion.

The first set of simulations was done to examine pH regulation pathways in lacrimal duct. This was accomplished by simulating acid-loading experiments published by Tóth-Molnar *et al*. (5). The second set of simulation was done to examine the role that apical KCC1 might play in generating hypertonic fluid with high KCl concentrations. In compartment mode, the primary secretion from the acinar cell model (one acinar cell) with various flow rates is treated as input into the ductal luminal space. This fluid passes through the lumen and gets modified by the duct cell model (one duct cell) (Fig 8-1). The output luminal compositions are obtained with the same apical membrane areas in both acinar and duct cell models.

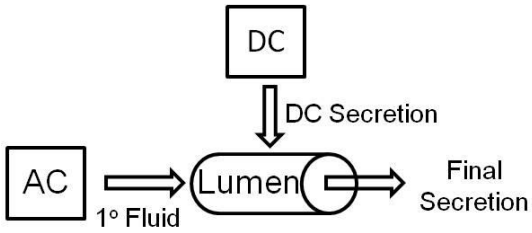

Figure 8-1. A schematic illustration of the combined model used in the second set of simulation experiment. Primary secretions from acinar cell model enter the ductal lumen. There, the duct cell model modifies the fluid composition with respect to flow rate. The degree of ductal modification was examined by comparing the composition and flow of the final secretion to the secretion of the acinar cell.

8.3 Results

8.3.1 Carbachol-Induced Tear Secretion

Tear flow experiments were conducted in 10 rats. In each rat, multiple samples were collected at different flow rates. Depending on the flow, the sample interval varied from 5 to 90 minutes. Tear secretion rates ranged from 0.12 – 3.8 L per minute. Tear

samples were then separated into two groups based on the secretion rates: low flow (< 1 L/min) and high flow (≥ 1 L/min). Mean tear fluid composition is reported in Figure 8-2. At low flow, the mean solute concentrations (in mM) were Na^+ 127 ± 6, K^+ 55 ± 3, and Cl^- 105 ± 6, respectively. At high flow, they were (in mM): Na^+ 148 ± 6, K^+ 35 ± 2, and Cl^- 126 ± 12. Tear fluid osmolarity, which was estimated by doubling the sum of the concentrations of K^+ and Na^+, was 365 ± 12 mOsm and 367 ± 10 at low and high flows, respectively.

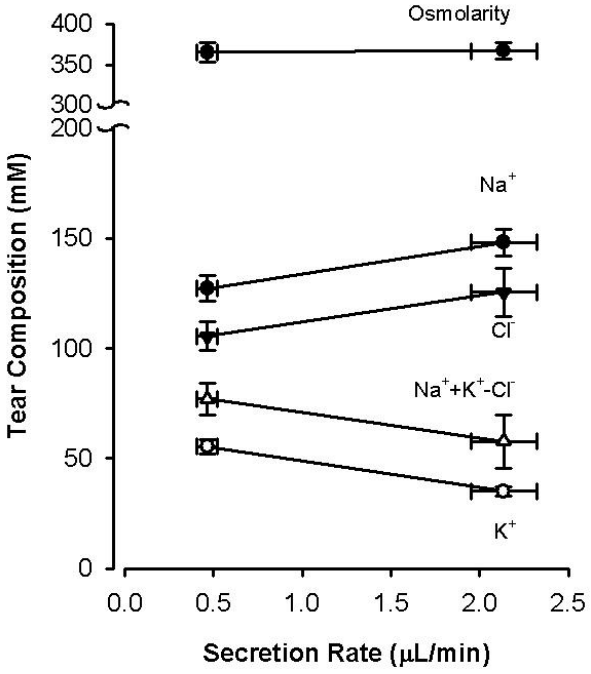

Figure 8-2. Tear samples were collected from 10 animals and ion composition measured. The samples were divided into two groups, low flow (< 1 L/min, n=19) and high flow (≥ 1 L/min, n=14). Results showed a flow rate dependency of fluid composition. Na^+ and Cl^- concentrations increase with increasing secretion rate, while and K^+ concentration decreases. Note that estimated tear fluid osmolarity was unchanged.

8.3.2 Duct Cell Model Predictions

The model in compartment mode was used to simulate acid-loading experiments conducted by Tóth-Molnar *et al*. (Fig 8-3) (5). The pH recovery *in vitro* was reported to be significantly reduced when extracellular Na^+ is removed or in the presence of amiloride. These behaviors are consistent with model predictions that 3 minutes of 20 mM NH_4^+ loading cause a three-fold increase in NHE activity (E_T NHE) (Fig 8-3). Removal of external Na^+ abolishes NHE and pNBC transport, thus the rate of pH recovery is reduced. The relative contribution of NHE and pNBC in the pH recovery response was tested by simulating the effects of amiloride by reducing E_T NHE. With NHE inhibition, the rate of pH recovery is significantly reduced, and this suggests that NHE is the predominant pH regulatory protein in lacrimal duct cells. Furthermore, the influence of carbachol on the acid-loading response was examined by the same group (Fig 8-3 B), and this behavior was simulated by the model (Fig 8-3 D). The model also predicts that pH recovery rate in a stimulated cell is significantly reduced in the presence of amiloride and Na^+-free solutions.

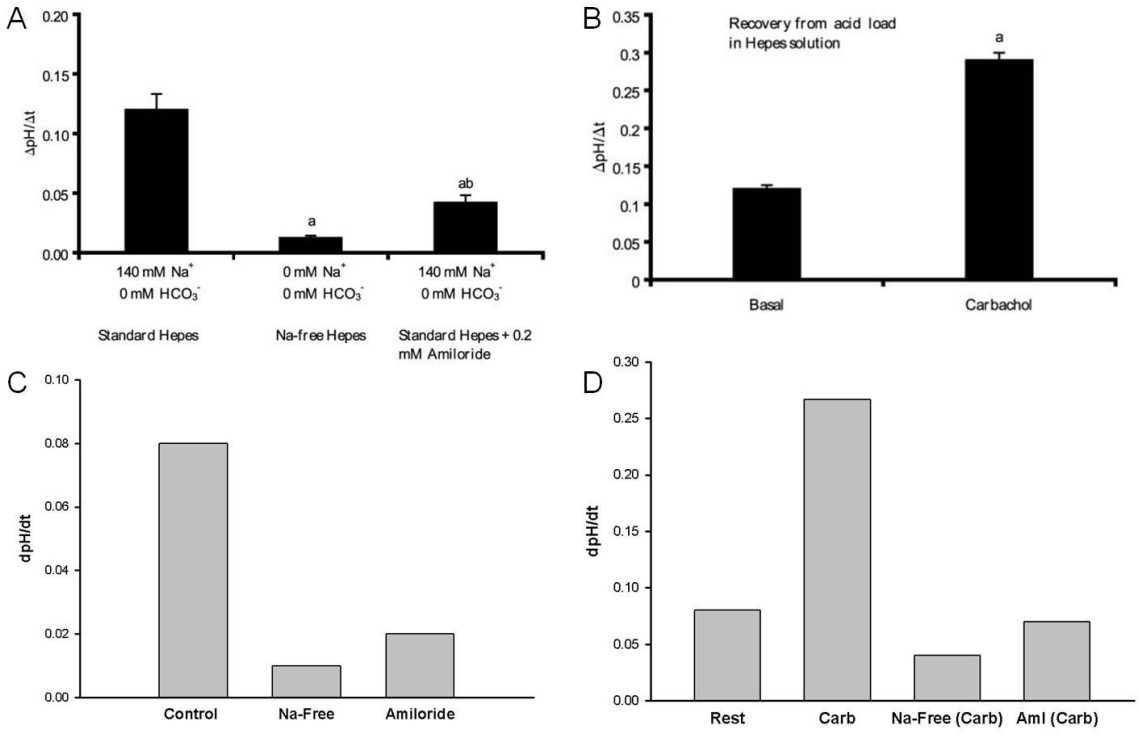

Figure 8-3. Lacrimal duct cell model in compartment mode with same apical and basolateral bathing solutions were use to simulate acid-loading experiments conducted by Tóth-Molnar *et al*. (5). In the model, 3 minutes NH_4^+ loading causes a three-fold increase in NHE activity (C). The pH response is markedly blunted with Na^+-free solutions and amiloride exposure. Changes in the pH response in the model match experimental measurements (A). Muscarinic agonist exposure increases pH recovery in isolated rabbit lacrimal ducts (B). This behavior is simulated by the model with a six-fold increase in NHE activity (D).

Hypertonic fluid produced by acinar cells (Fig 8-4 A) enters the ductal lumen and fluid flow and composition are modified by the duct cells (Figure 8-4B). At basal flow, the model predicts that the luminal fluid is slightly hypertonic with 110 mM Na^+, 45 mM K^+, and 133 mM Cl^-. As secretion rate increases, the luminal fluid becomes more hyperosmotic due to increased NaCl secretion; however, K^+ concentration decreases (to 33 mM at maximum flow rate).

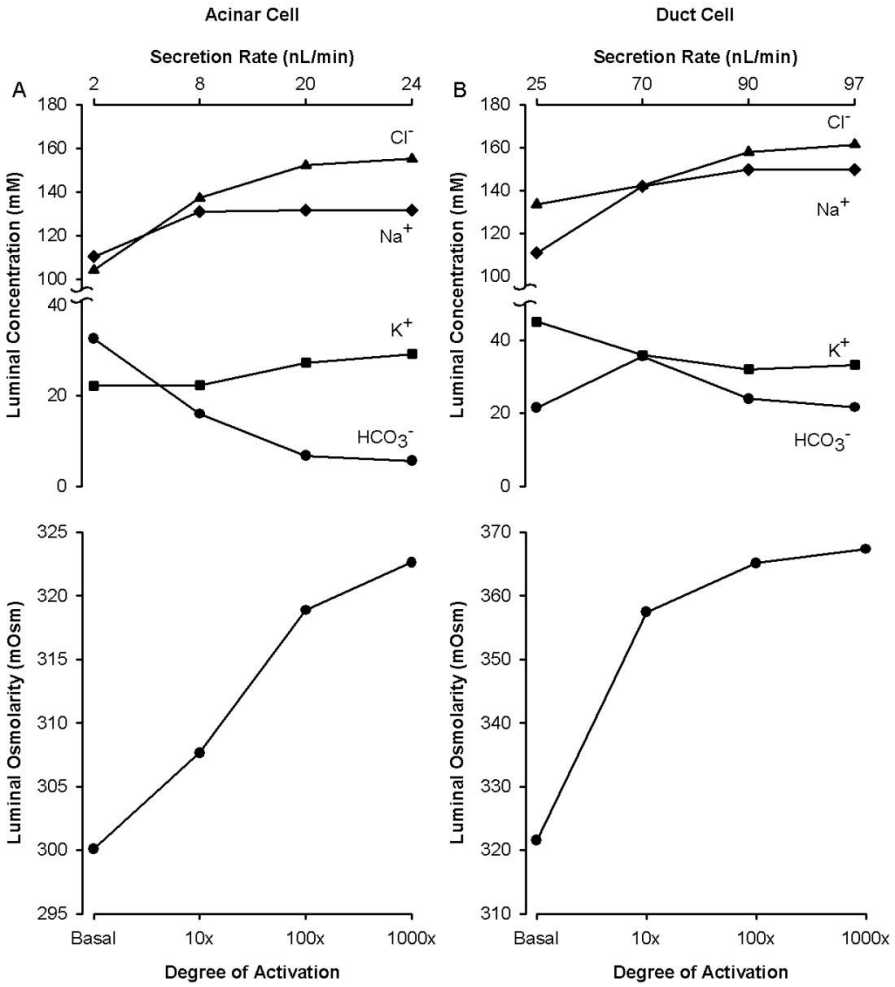

Figure 8-4. Degree of activation indicates different levels of muscarinic stimulated water secretion in both models. Secretion rates achieved by muscarinic agonist exposure are shown on the upper x-axes. The acinar cell model predicted that the primary secretion is hypertonic even at basal secretion rate (A, top). Luminal hypertonicity increased with increasing water flow (A, bottom). This is accompanied with increased Na^+, K^+, and Cl^- secretion. The primary secretion enters the ductal lumen and modified by duct cells. Duct cell model simulation showed a significant increase in luminal NaCl secretion by the duct, and K^+ concentration decreases with increasing flow rate (B, top). Also, ductal lumen osmolarity increases (B, bottom). Notice that the model predicted that water secretion is much larger in duct cells as compared to acinar cells.

8.3.3 Role of Apical KCC1 in Fluid Secretion

Apical KCC1 expression provides an additional KCl exit pathway in duct cells that might enhance secretion. However, both experimental measurements and duct cell

model predictions suggest that luminal K^+ levels decreases with increasing water flow rate. Therefore, the effect of different levels of KCC1 activities on luminal K^+ concentration, osmolarity, and water secretion rates with basal and maximal flow were examined using the duct cell model in compartment mode (Fig 8-5).

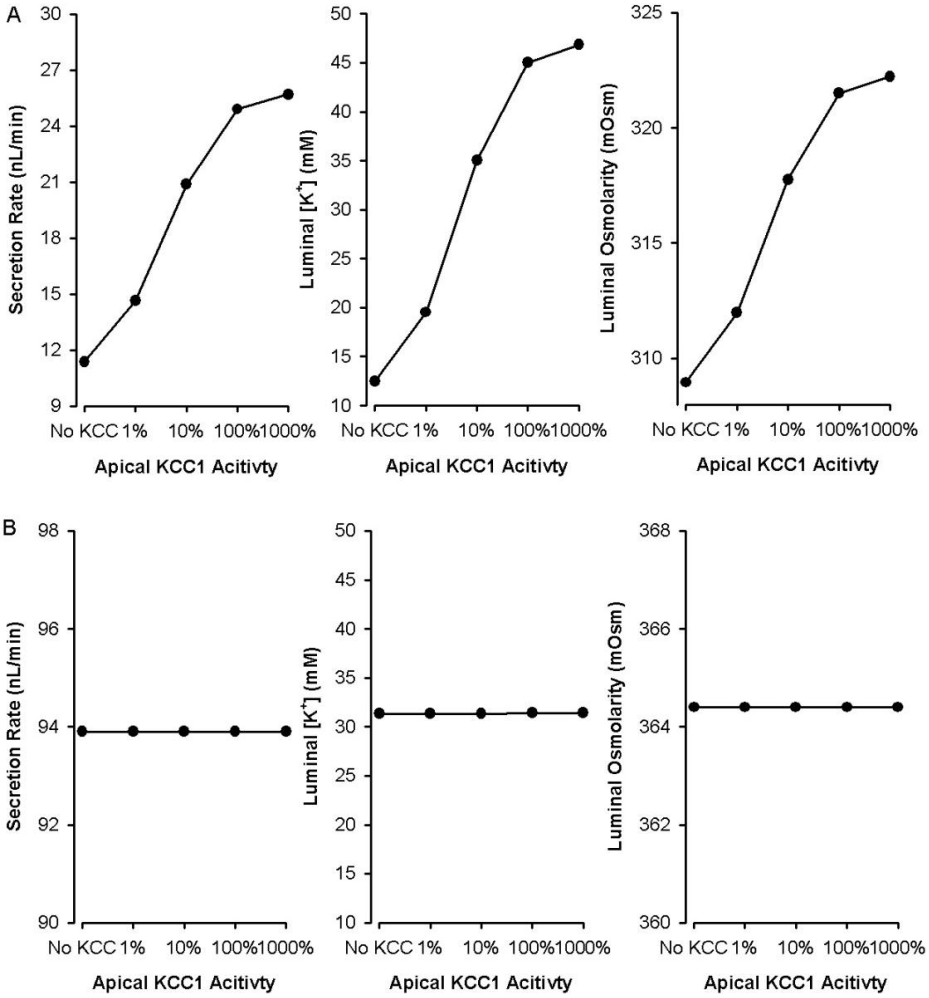

Figure 8-5. The influence of apical KCC1 on ductal luminal composition. At basal flow (A), the model predicted that water secretion rate increases with increasing apical KCC1 activity. This is due to increased K^+ and Cl^- secretion into the lumen (A, middle); thus, luminal osmolarity is elevated (A, right). However, at maximal stimulation, the model shows that increasing KCC1 activity has no effect on secretion (B). This is due to the fact that as luminal K^+ rises because of passive K^+ efflux, the net driving force for KCl extrusion via KCC1is eliminated.

The results show that the apical KCC1 transporter influences fluid composition only in resting cells where it increases the secretion of water, K^+, and Cl^-, which raise tear fluid osmolarity. When the cell is stimulated, the KCC1 transporter has little influence on tear composition or flow, because luminal K^+ and Cl^- are sufficiently high to eliminate the net chemical potential that drives the KCC1 transporter. These findings suggest that the most important role of the apical KCC1 transporter may be to produce tear fluid at a steady basal rate with high K^+ content.

8.3.4 Influence of Duct-to-Acinar Cells Apical Membrane Area on Secretion

Based on cell population, Mircheff suggests that lacrimal ducts contribute ~30% of total fluid volume (94). This disagrees with the predictions from the combined model simulation in Figure 8-4. To address this issue, we used the combined model to simulate water secretion at basal and maximum flow with varying of duct-to-acinar apical membrane (*Aa*) area ratio (Fig 8-6). Model simulations suggest that tear secretion is sensitive to the duct cell area such that lower flow and less hypertonic fluid are predicted with the smaller ratio. As a result, luminal solute secretion is reduced (Table 8-1). At maximum flow, the acinar cell model predicts water secretion rate is 24 nL/min, which is 70% of total fluid volume. This implies that the duct cells fluid secretion rate is 10 nL/min. Based on the combined model simulations, the duct cell A_a could be between 20% to 40% of the acinar cell A_a.

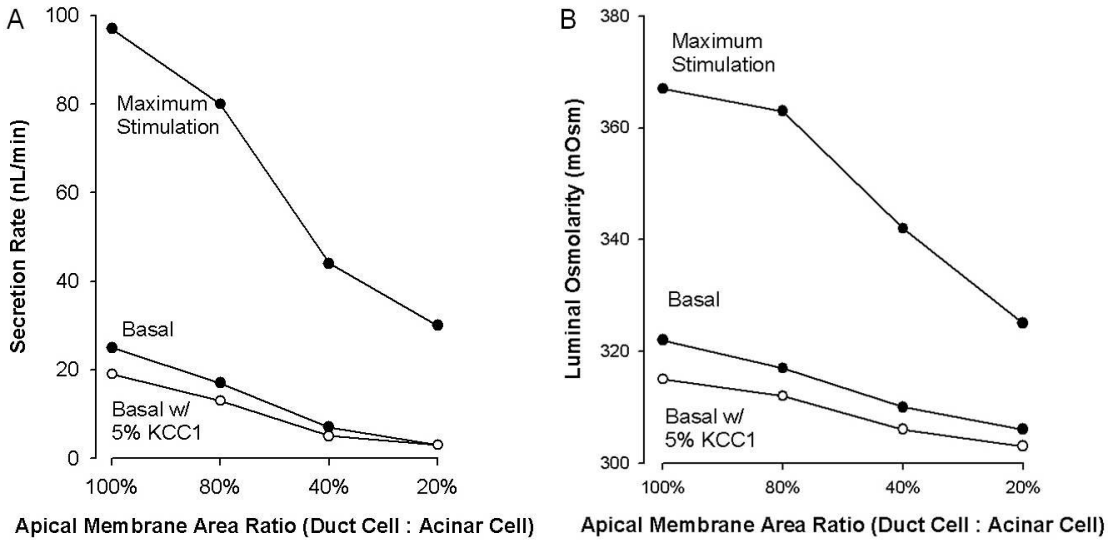

Figure 8-6. Influence of the duct-to-acinar cells apical membrane area ratio on flow and luminal osmoarlity. A: As the apical membrane area decreases in the duct cells, both the basal and maximum stimulated secretion rates decreased. Reduction of apical KCC1 activity to 5% slows basal water flow even more, but this does not have an effect on maximum stimulation. B: Decreased duct cell apical membrane area also causes reduction of luminal osmolarity during both basal and maximum stimulation. This is due to decreased Na^+ and Cl^- secretion from the duct cells. Reducing apical KCC1 activity to 5% makes the lumen even less hypertonic.

Table 8-1. Predicted luminal solute concentration by the combined model.

		DC:AC Aa Ratio			
		100%	80%	40%	20%
Na^+	Basal	111	108	101	96
	Basal 5% KCC1	122	120	116	115
	Max Stim	150	143	130	119
K^+	Basal	45	46	49	50
	Basal 5% KCC1	30	30	30	28
	Max Stim	33	38	41	43
Cl^-	Basal	134	131	125	120
	Basal 5% KCC1	124	121	115	110
	Max Stim	161	145	144	143
HCO_3^-	Basal	21	22	23	24
	Basal 5% KCC1	27	27	27	30
	Max Stim	22	36	27	19

8.4 Discussion

We have developed a mathematical model of lacrimal duct cell with cell volume regulation and pH regulation. This model provides useful insights into the physiologic function of the lacrimal ducts. As discussed in Chapter 7, acinar cell model predicts that the primary secretion is hypertonic with a high K^+ and Cl^- concentrations. Primary fluid is then modified by duct cell secretion, which is included in the combined acinar and duct cell model. Model predictions suggest that there is a flow rate dependency of luminal composition. Luminal Na^+ and Cl^- levels increased, and K^+ concentration decreased, with increasing secretion rate. The model simulations were in agreement with ion composition measurements in rat tear samples showed flow rate dependency as well. These findings suggest that duct cells are involved in fluid modification. In contrast, these findings disagree with results of Alexander *et al*. (31), which show no flow-dependence of tear compositions except at very low flow. Our tear secretion data shows that the duct cell maintains a high K^+ and Cl^- concentrations in tear fluid. These results demonstrate that similar transport function is obtained in duct and acinar cell models when the models incorporate the findings of Ubels *et al*. (3), who found that that duct cells express an array of transport proteins similar to acinar cells. Taken together, this evidence supports the notion that duct cells behave like acinar cells when stimulated.

Model simulations suggest that apical KCC1 expression only plays an important role in establishing a basal tear secretion rate. Increasing KCC1 activity facilitates luminal KCl efflux, and therefore increases luminal osmolarity; thus water secretion goes

up. However at maximal stimulation, varying KCC1 activities showed very little effect on secretion. This is due to the fact that the luminal K^+ concentration is sustained at a high level by diffusion. The high luminal K^+ level is sufficient to slow down or reverse K^+ transport via KCC1. Indeed, the model predicts that passive KCl efflux into the lumen is reduced when the activity of the KCC1 transporter is increased. Therefore, no net change in K^+ secretion is predicted.

While our model is sufficient to reveal a possible role for the KCC1 transporter, it does not, at present, reflect the relative contribution of the acinar cell and duct cell in water secretion. For example, the model predicts that more water is secreted by the duct cells than the acinar cells. In contrast, Mircheff has concluded that lacrimal duct cells only contribute ~30% of total fluid volume (94). This estimate is based on different numbers of acinar and duct cells, but does not take into account the differences in apical membrane area between the two cell types. The current study initially used the simplest representation of water and electrolyte secretion in lacrimal gland, which only consists of one acinar and one duct cell with equivalent apical membrane areas. When the apical membrane area ratio between duct and acinar cells was decreased, flow was reduced and tear fluid composition was altered. However, reasonable predictions for tear fluid osmolarity, compostion, and flow were obtained when the relative contributions of the acinar and ducts cells were set to the value estimated by Mircheff (94). Nevertheless the current model is clearly this is insufficient to represent the whole lacrimal system. The lacrimal duct system has complex geometry and is not homogeneous in size or function. This is demonstrated by recent findings that the rabbit lacrimal duct can be divided into

different segments based on different anatomical characteristics (96) and transport protein expression levels (e.g. KCC1, NKCC1, Na^+-K^+-ATPase, etc). More anatomical and functional data are needed about ductal structure and function before a detailed model of the lacrimal duct system can be constructed. Such a model would explicitly model advection of solutes through the ductal lumen using partial differential equations, while the walls of the ducts would consist of an ensemble of duct cell models with differing transport parameters. Nevertheless, the results obtained in this dissertation research project provide new insights into the mechanisms of tear secretion, and has identified a number of key issues that can be evaluated experimentally.

References:

1. Hodges RR, Dartt DA. Regulatory pathways in lacrimal gland epithelium. Int Rev Cytol. 2003;231:129-96.
2. Dartt DA HR, Zoukhri D. Tears and Their Secretion. Advances in Organ Biology. 2005;10:21-82.
3. Ubels JL HH, Srikanth S, Resau JH, and Webb CP. Gene expression in rat lacrimal gland duct cells collected using laser capture microdissection: evidence for K+ secretion by duct cells. Invest Ophthalmol Vis Sci 2006;47:1876-85.
4. Saito Y, Ozawa T, Suzuki S, Nishiyama A. Intracellular pH regulation in the mouse lacrimal gland acinar cells. J Membr Biol. 1988;101(1):73-81.
5. Toth-Molnar E VV, Ozsvari B, Rakonczay Z, Jr., Varro A, Papp JG, Toth A, Lonovics J, Takacs T, Ignath I, Ivanyi B, and Hegyi P. New experimental method to study acid/base transporters and their regulation in lacrimal gland ductal epithelia. Invest Ophthalmol Vis Sci. 2007;48:3746-55.
6. Walcott B, Matthews G, Brink P. Differences in stimulus induced calcium increases in lacrimal gland acinar cells from normal and NZB/NZW F1 female mice. Curr Eye Res. 2002;25(4):253-60.
7. Zoukhri D HR, Sergheraert C, Dartt DA. Cholinergic-induced Ca2+ elevation in rat lacrimal gland acini is negatively modulated by PKCdelta and PKCepsilon. Invest Ophthalmol Vis Sci. 2000;41(2):386-92.
8. Mauduit P, Herman G, Rossignol B. Protein secretion induced by isoproterenol or pentoxifylline in lacrimal gland: Ca2+ effects. Am J Physiol. 1984;246(1 Pt 1):C37-44.
9. Ding CQ WB, Keyser KT. The a1- and b1 Adrenergic Modulation of Lacrimal Gland Function in the Mouse. Invest Ophthalmol Vis Sci. 2007;48:1504-10.
10. Arreola J, Melvin JE, Begenisich T. Activation of calcium-dependent chloride channels in rat parotid acinar cells. J Gen Physiol. 1996;108(1):35-47. PMCID: 2229297.
11. Azzarolo AM, Wood RL, Mircheff AK, Richters A, Olsen E, Berkowitz M, et al. Androgen influence on lacrimal gland apoptosis, necrosis, and lymphocytic infiltration. Invest Ophthalmol Vis Sci. 1999;40(3):592-602.
12. Azzarolo AM, Mircheff AK, Kaswan RL, Stanczyk FZ, Gentschein E, Becker L, et al. Androgen support of lacrimal gland function. Endocrine. 1997;6(1):39-45.
13. McCabe E, Narayanan S. Advancements in anti-inflammatory therapy for dry eye syndrome. Optometry. 2009;80(10):555-66.
14. Sullivan DA, Wickham LA, Rocha EM, Krenzer KL, Sullivan BD, Steagall R, et al. Androgens and dry eye in Sjogren's syndrome. Ann N Y Acad Sci. 1999;876:312-24.
15. Verthelyi D. Sex hormones as immunomodulators in health and disease. Int Immunopharmacol. 2001;1(6):983-93.

16. Konttinen YT, Porola P, Konttinen L, Laine M, Poduval P. Immunohistopathology of Sjogren's syndrome. Autoimmun Rev. 2006;6(1):16-20.
17. Hu Y, Purushotham KR, Wang P, Dawson R, Jr., Humphreys-Beher MG. Downregulation of beta-adrenergic receptors and signal transduction response in salivary glands of NOD mice. Am J Physiol. 1994;266(3 Pt 1):G433-43.
18. Bacman S, Perez Leiros C, Sterin-Borda L, Hubscher O, Arana R, Borda E. Autoantibodies against lacrimal gland M3 muscarinic acetylcholine receptors in patients with primary Sjogren's syndrome. Invest Ophthalmol Vis Sci. 1998;39(1):151-6.
19. Zoukhri D HR, Rawe IM, Dartt DA. Ca2+ signaling by cholinergic and alpha1-adrenergic agonists is up-regulated in lacrimal and submandibular glands in a murine model of Sjögren's syndrome. Clin Immunol Immunopathol. 1998;89(2):134-40.
20. Borda ES, Sterin-Borda L. Antiadrenergic and muscarinic receptor antibodies in Chagas' cardiomyopathy. Int J Cardiol. 1996;54(2):149-56.
21. Konttinen YT, Hukkanen M, Kemppinen P, Segerberg M, Sorsa T, Malmstrom M, et al. Peptide-containing nerves in labial salivary glands in Sjogren's syndrome. Arthritis Rheum. 1992;35(7):815-20.
22. Zoukhri DK, C. L. Impaired neurotransmitter release from lacrimal and salivary gland nerves of a murine model of Sjogren's syndrome. Invest Ophthalmol Vis Sci. 2001;42(5):925-32.
23. Fox RI, Luppi M, Pisa P, Kang HI. Potential role of Epstein-Barr virus in Sjogren's syndrome and rheumatoid arthritis. J Rheumatol Suppl. 1992;32:18-24.
24. St Clair EW. New developments in Sjogren's syndrome. Curr Opin Rheumatol. 1993;5(5):604-12.
25. Paranyuk Y, Claros N, Birzgalis A, Moore LC, Brink PR, Walcott B. Lacrimal gland fluid secretion and lymphocytic infiltration in the NZB/W mouse model of Sjogren's syndrome. Curr Eye Res. 2001;23(3):199-205.
26. Tsubota K, Hirai S, King LS, Agre P, Ishida N. Defective cellular trafficking of lacrimal gland aquaporin-5 in Sjogren's syndrome. Lancet. 2001;357(9257):688-9.
27. Tornwall J, Konttinen YT, Tuominen RK, Tornwall M. Protein kinase C expression in salivary gland acinar epithelial cells in Sjogren's syndrome. Lancet. 1997;349(9068):1814-5.
28. Farokhzad OC, Sagar GD, Mun EC, Sicklick JK, Lotz M, Smith JA, et al. Protein kinase C activation downregulates the expression and function of the basolateral Na+/K+/2Cl(-) cotransporter. J Cell Physiol. 1999;181(3):489-98.
29. Bachmann O, Reichelt D, Tuo B, Manns MP, Seidler U. Carbachol increases Na+-HCO3- cotransport activity in murine colonic crypts in a M3-, Ca2+/calmodulin-, and PKC-dependent manner. Am J Physiol Gastrointest Liver Physiol. 2006;291(4):G650-7.

30. Walcott B, Birzgalis A, Moore LC, Brink PR. Fluid secretion and the Na+-K+-2Cl- cotransporter in mouse exorbital lacrimal gland. Am J Physiol Cell Physiol. 2005;289(4):C860-7.
31. Alexander JH, van Lennep EW, Young JA. Water and electrolyte secretion by the exorbital lacrimal gland of the rat studied by micropuncture and catheterization techniques. Pflugers Arch. 1972;337(4):299-309.
32. Botelho SY ME. Electrolytes in lacrimal gland fluid and in tears at various flow rates in the rabbit. Am J Physiol. 1973;225(3):606-9.
33. Thaysen JH, Thorn NA. Excretion of urea, sodium, potassium and chloride in human tears. Am J Physiol. 1954;178(1):160-4.
34. Marty A, Tan YP, Trautmann A. Three types of calcium-dependent channel in rat lacrimal glands. J Physiol. 1984;357:293-325. PMCID: 1193259.
35. Evans MG, Marty A. Calcium-dependent chloride currents in isolated cells from rat lacrimal glands. J Physiol. 1986;378:437-60. PMCID: 1182874.
36. Nilius B, Droogmans G. Amazing chloride channels: an overview. Acta Physiol Scand. 2003;177(2):119-47.
37. Tan YP, Marty A, Trautmann A. High density of Ca(2+)-dependent K+ and Cl-channels on the luminal membrane of lacrimal acinar cells. Proc Natl Acad Sci U S A. 1992;89(23):11229-33. PMCID: 50523.
38. Park K, Brown PD. Intracellular pH modulates the activity of chloride channels in isolated lacrimal gland acinar cells. Am J Physiol. 1995;268(3 Pt 1):C647-50.
39. Begenisich T, Melvin JE. Regulation of chloride channels in secretory epithelia. J Membr Biol. 1998;163(2):77-85.
40. Walcott B, Moore L, Birzgalis A, Claros N, Brink PR. A model of fluid secretion by the acinar cells of the mouse lacrimal gland. Adv Exp Med Biol. 2002;506(Pt A):191-7.
41. Edelman JL, Loo DD, Sachs G. Characterization of potassium and chloride channels in the basolateral membrane of bovine nonpigmented ciliary epithelial cells. Invest Ophthalmol Vis Sci. 1995;36(13):2706-16.
42. Petersen OH. Calcium-activated potassium channels and fluid secretion by exocrine glands. Am J Physiol. 1986;251(1 Pt 1):G1-13.
43. Trautmann A, Marty A. Activation of Ca-dependent K channels by carbamoylcholine in rat lacrimal glands. Proc Natl Acad Sci U S A. 1984;81(2):611-5. PMCID: 344729.
44. Padfield PJ, Garner A, Case RM. Patterns of pancreatic secretion in the anaesthetised guinea pig following stimulation with secretin, cholecystokinin octapeptide, or bombesin. Pancreas. 1989;4(2):204-9.
45. McManaman JL, Reyland ME, Thrower EC. Secretion and fluid transport mechanisms in the mammary gland: comparisons with the exocrine pancreas and the salivary gland. J Mammary Gland Biol Neoplasia. 2006;11(3-4):249-68.
46. Gimenez I. Molecular mechanisms and regulation of furosemide-sensitive Na-K-Cl cotransporters. Curr Opin Nephrol Hypertens. 2006;15(5):517-23.
47. Darman RB, Forbush B. A regulatory locus of phosphorylation in the N terminus of the Na-K-Cl cotransporter, NKCC1. J Biol Chem. 2002;277(40):37542-50.

48. Chen H, Sun D. The role of Na-K-Cl co-transporter in cerebral ischemia. Neurol Res. 2005;27(3):280-6.
49. Galan A, Cervero F. Painful stimuli induce in vivo phosphorylation and membrane mobilization of mouse spinal cord NKCC1 co-transporter. Neuroscience. 2005;133(1):245-52.
50. Liedtke CM, Wang X, Smallwood ND. Role for protein phosphatase 2A in the regulation of Calu-3 epithelial Na+-K+-2Cl-, type 1 co-transport function. J Biol Chem. 2005;280(27):25491-8.
51. Piechotta K, Lu J, Delpire E. Cation chloride cotransporters interact with the stress-related kinases Ste20-related proline-alanine-rich kinase (SPAK) and oxidative stress response 1 (OSR1). J Biol Chem. 2002;277(52):50812-9.
52. Kahle KT, Rinehart J, Ring A, Gimenez I, Gamba G, Hebert SC, et al. WNK protein kinases modulate cellular Cl- flux by altering the phosphorylation state of the Na-K-Cl and K-Cl cotransporters. Physiology (Bethesda). 2006;21:326-35.
53. Lionetto MG, Schettino T. The Na+-K+-2Cl- cotransporter and the osmotic stress response in a model salt transport epithelium. Acta Physiol (Oxf). 2006;187(1-2):115-24.
54. Delpire E, Gagnon KB. SPAK and OSR1, key kinases involved in the regulation of chloride transport. Acta Physiol (Oxf). 2006;187(1-2):103-13.
55. Tsutsumi T UH, Kosaka T, Kayahara T, Nakano K. Proline- and alanine-rich Ste20-related kinase associates with F-actin and translocates from the cytosol to cytoskeleton upon cellular stresses. J Biol Chem. 2000;275(13):9157-62.
56. Grinstein S, Rothstein A, Cohen S. Mechanism of osmotic activation of Na+/H+ exchange in rat thymic lymphocytes. J Gen Physiol. 1985;85(5):765-87. PMCID: 2215819.
57. Douglas IJ, Brown PD. Regulatory volume increase in rat lacrimal gland acinar cells. J Membr Biol. 1996;150(2):209-17.
58. Kotera T, Brown PD. Calcium-dependent chloride current activated by hyposmotic stress in rat lacrimal acinar cells. J Membr Biol. 1993;134(1):67-74.
59. Park KP, Beck JS, Douglas IJ, Brown PD. Ca(2+)-activated K+ channels are involved in regulatory volume decrease in acinar cells isolated from the rat lacrimal gland. J Membr Biol. 1994;141(2):193-201.
60. Sarkadi B, Parker JC. Activation of ion transport pathways by changes in cell volume. Biochim Biophys Acta. 1991;1071(4):407-27.
61. Garay RP, Nazaret C, Hannaert PA, Cragoe EJ, Jr. Demonstration of a [K+,Cl-]-cotransport system in human red cells by its sensitivity to [(dihydroindenyl)oxy]alkanoic acids: regulation of cell swelling and distinction from the bumetanide-sensitive [Na+,K+,Cl-]-cotransport system. Mol Pharmacol. 1988;33(6):696-701.
62. Mircheff AK, Ingham CE, Lambert RW, Hales KL, Hensley CB, Yiu SC. Na+/H+ antiporter in lacrimal acinar cell basal-lateral membranes. Invest Ophthalmol Vis Sci. 1987;28(10):1726-9.

63. Bromberg BB, Welch MH, Beuerman RW, Chew SJ, Thompson HW, Ramage D, et al. Histochemical distribution of carbonic anhydrase in rat and rabbit lacrimal gland. Invest Ophthalmol Vis Sci. 1993;34(2):339-48.
64. Selvam ST, P. B. Gukasyan, H. J. Yu, A. S. Stevenson, D. Trousdale, M. D. Mircheff, A. K. Schechter, J. E. Smith, R. E. Yiu, S. C. Transepithelial bioelectrical properties of rabbit acinar cell monolayers on polyester membrane scaffolds. Am J Physiol Cell Physiol. 2007;293(4):C1412-9.
65. Ogawa Y, Toyosawa S, Inagaki T, Hong SS, Ijuhin N. Carbonic anhydrase isozyme VI in rat lacrimal gland. Histochem Cell Biol. 1995;103(5):387-94.
66. Ogawa Y, Hong SS, Toyosawa S, Kuwahara H, Shimazaki M, Yagi T. Immunoelectron microscopy of carbonic anhydrase isozyme VI in human submandibular gland: comparison with isozymes I and II. J Histochem Cytochem. 1993;41(3):343-51.
67. Sterling D, Reithmeier RA, Casey JR. A transport metabolon. Functional interaction of carbonic anhydrase II and chloride/bicarbonate exchangers. J Biol Chem. 2001;276(51):47886-94.
68. Nguyen HV S-TA, Alper SL, and Melvin JE. Cl(-)/HCO(3)(-) exchange is acetazolamide sensitive and activated by a muscarinic receptor-induced [Ca(2+)](i) increase in salivary acinar cells. Am J Physiol Gastrointest Liver Physiol. 2004;286:G312-20.
69. Orlowski JG, S. Na1/H1 Exchangers of Mammalian Cells. J Biol Chem. 1997;272(36):22373-6.
70. Slepkov ER, Rainey JK, Sykes BD, Fliegel L. Structural and functional analysis of the Na+/H+ exchanger. Biochem J. 2007;401(3):623-33. PMCID: 1770851.
71. Grinstein S, Cohen S, Goetz JD, Rothstein A. Osmotic and phorbol ester-induced activation of Na+/H+ exchange: possible role of protein phosphorylation in lymphocyte volume regulation. J Cell Biol. 1985;101(1):269-76. PMCID: 2113623.
72. Saito Y, Ozawa T, Nishiyama A. Effects of intra- and extracellular H+ and Na+ concentrations on Na(+)-H+ antiport activity in the lacrimal gland acinar cells. Pflugers Arch. 1990;417(4):382-90.
73. Alper SL. Molecular physiology of SLC4 anion exchangers. Exp Physiol. 2006;91(1):153-61.
74. Lambert RW, Bradley ME, Mircheff AK. Cl(-)-HCO3- antiport in rat lacrimal gland. Am J Physiol. 1988;255(3 Pt 1):G367-73.
75. Lambert RW, Bradley ME, Mircheff AK. pH-sensitive anion exchanger in rat lacrimal acinar cells. Am J Physiol. 1991;260(3 Pt 1):G517-23.
76. Kim YB, Yang BH, Piao ZG, Oh SB, Kim JS, Park K. Expression of Na+/HCO3- cotransporter and its role in pH regulation in mouse parotid acinar cells. Biochem Biophys Res Commun. 2003;304(4):593-8.
77. Li J, Koo NY, Cho IH, Kwon TH, Choi SY, Lee SJ, et al. Expression of the Na+-HCO3- cotransporter and its role in pHi regulation in guinea pig salivary glands. Am J Physiol Gastrointest Liver Physiol. 2006;291(6):G1031-40.

78. Bok D, Schibler MJ, Pushkin A, Sassani P, Abuladze N, Naser Z, et al. Immunolocalization of electrogenic sodium-bicarbonate cotransporters pNBC1 and kNBC1 in the rat eye. Am J Physiol Renal Physiol. 2001;281(5):F920-35.
79. Sun XC, Bonanno JA, Jelamskii S, Xie Q. Expression and localization of Na(+)-HCO(3)(-) cotransporter in bovine corneal endothelium. Am J Physiol Cell Physiol. 2000;279(5):C1648-55.
80. Gross E AN, Pushkin A, Kurtz I, and Cotton CU. The stoichiometry of the electrogenic sodium bicarbonate cotransporter pNBC1 in mouse pancreatic duct cells is 2 HCO(3)(-):1 Na(+). J Physiol 2001;531:375-82.
81. Gross E, Hawkins K, Pushkin A, Sassani P, Dukkipati R, Abuladze N, et al. Phosphorylation of Ser(982) in the sodium bicarbonate cotransporter kNBC1 shifts the HCO(3)(-) : Na(+) stoichiometry from 3 : 1 to 2 : 1 in murine proximal tubule cells. J Physiol. 2001;537(Pt 3):659-65. PMCID: 2278987.
82. Latta R, Clausen C, Moore LC. General method for the derivation and numerical solution of epithelial transport models. J Membr Biol. 1984;82(1):67-82.
83. Hund TJ, Rudy Y. Rate dependence and regulation of action potential and calcium transient in a canine cardiac ventricular cell model. Circulation. 2004;110(20):3168-74. PMCID: 1851913.
84. Lytle C, McManus TJ, Haas M. A model of Na-K-2Cl cotransport based on ordered ion binding and glide symmetry. Am J Physiol. 1998;274(2 Pt 1):C299-309.
85. Weinstein A. A kinetically defined Na+/H+ antiporter within a mathematical model of the rat proximal tubule. J Gen Physiol 1995;105:617-41.
86. Chang H, Fujita T. A numerical model of acid-base transport in rat distal tubule. Am J Physiol Renal Physiol. 2001;281(2):F222-43.
87. Gross E, Hopfer U. Effects of pH on kinetic parameters of the Na-HCO3 cotransporter in renal proximal tubule. Biophys J. 1999;76(6):3066-75. PMCID: 1300276.
88. Moore M MT, Yang B, Verkman AS. Tear secretion by lacrimal glands in transgenic mice lacking water channels AQP1, AQP3, AQP4 and AQP. Exo Eye Res. 2000;70(5):557-62.
89. Zoukhri DH, R. R. Dicker, D. M. Dartt, D. A. Role of protein kinase C in cholinergic stimulation of lacrimal gland protein secretion. FEBS Lett. 1994;351(1):67-72. PMCID: 1698268.
90. Del Castillo IC, Fedor-Chaiken M, Song JC, Starlinger V, Yoo J, Matlin KS, et al. Dynamic regulation of Na(+)-K(+)-2Cl(-) cotransporter surface expression by PKC-{epsilon} in Cl(-)--secretory epithelia. Am J Physiol Cell Physiol. 2005;289(5):C1332-42.
91. Liedtke CM, Cole TS. Activation of NKCC1 by hyperosmotic stress in human tracheal epithelial cells involves PKC-delta and ERK. Biochim Biophys Acta. 2002;1589(1):77-88.
92. Liedtke CM, Hubbard M, Wang X. Stability of actin cytoskeleton and PKC-delta binding to actin regulate NKCC1 function in airway epithelial cells. Am J Physiol Cell Physiol. 2003;284(2):C487-96.

93. Perry C, Baker OJ, Reyland ME, Grichtchenko, II. PKC{alpha}{beta}{gamma}- and PKC{delta}-dependent endocytosis of NBCe1-A and NBCe1-B in salivary parotid acinar cells. Am J Physiol Cell Physiol. 2009;297(6):C1409-23. PMCID: 2793054.
94. Mircheff A, editor. Water and electrolyte secretio nand fluid modification. Philadelphia: Saunders Publishing; 1994.
95. Ramsay J BR, and Croghaw P. Electrometric titration of Cl in small volumes. J Exp Biol. 1955;32:822-9.
96. Ding C, Parsa L, Nandoskar P, Zhao P, Wu K, Wang Y. Duct system of the rabbit lacrimal gland: structural characteristics and role in lacrimal secretion. Invest Ophthalmol Vis Sci. 2010;51(6):2960-7. PMCID: 2891459.

Appendix:

I. Variables and parameter values for acinar and duct cell models

Name	Symbol	Value	Units
Cell Volume	Vc		cm^3
Solute Concentration	C		mM
Apical Membrane Potential	E_a		mV
Basolateral Membrane Potential	E_b		mV
Transepithelial Potential	E_t		mV
Ion Currents	I		$\mu A/cm^2$
Ion Fluxes	J		$\mu mole/(cm^2 \times s)$
Water Fluxes	J^w		$cm^3/(cm^2 \times s)$
Apical Membrane Solute Permeability	P_a		cm/s
Basolateral Membrane Solute Permeability	P_b		cm/s
Junctional Solute Permeability	P_j		cm/s
Cell Volume Set Point	V_{set}		cm^3
Amount of Enzyme	E_T		unitless
Apical Membrane Area	A_a	1.8	cm^2
Basolateral Membrane Area	A_b	8.8	cm^2
Reflection Constant	Σ	1	unitless
RT/F	RT/F	26.7	mV
Faraday's Constant	F	96500	coul/mole
Maximum Pump Current	I_{max}	100	A/cm^2
Pump Parameter	K_{Na}	10	mM
Pump Parameter	K_K	1.5	mM
Apical Water Permeability	Pw_a	1×10^{-8}	$cm/(s \times mM)$
Basolateral Water Permeability	Pw_b	2.6×10^{-6}	$cm/(s \times mM)$
Luminal Space Area	A_o	1	cm^2
Luminal Space Volume	V_a	3×10^{-5}	cm^3

II. Membrane solute permeabilities for acinar and duct cell models

Membrane Permeability	Symbol	Value (cm/s)	
		Rest	Maximum Stimulation
Apical	P_{Na}	1×10^{-8}	1×10^{-8}
	P_{K}	5×10^{-8}	5×10^{-5}
	P_{Cl}	5×10^{-8}	5×10^{-5}
	P_{HCO3}	2.5×10^{-8}	2.5×10^{-7}
Basolateral	P_{na}	3×10^{-6}	3×10^{-6}
	P_{K}	9.26×10^{-6}	9.26×10^{-6}
	P_{Cl}	1×10^{-7}	1×10^{-7}
	P_{HCO3}	5×10^{-8}	5×10^{-8}
Junctional	P_{Na}	5×10^{-6}	5×10^{-6}
	P_{K}	1×10^{-8}	1×10^{-8}
	P_{Cl}	1×10^{-8}	1×10^{-8}

III. Volume regulation parameters for both acinar and duct cell models

Name	Value	Unit
Maximum *NKCC* E_T	5×10^{-5}	unitless
Minimum *NKCC* E_T	1×10^{-5}	unitless
Maximum NKCC Tolerance	5×10^{-5}	cm^3
NKCC Delay	100	sec^{-1}
Maximum P_bK	9.26×10^{-5}	cm/s
Minimum P_bK	9.26×10^{-6}	cm/s
Maximum K Tolerance	5×10^{-5}	cm^3
Maximum P_bCl	1×10^{-6}	cm/s
Minimum P_bCl	1×10^{-7}	cm/s
Maximum Cl Tolerance	5×10^{-5}	cm^3
Cell Volume Set Point	2.96×10^{-4}	cm^3
Maximum *KCC* E_T (Duct Cell)	1×10^{-5}	unitless
Minumum *KCC* E_T (Duct Cell)	1×10^{-6}	untiless
Maximum KCC Tolerance (Duct cell)	5×10^{-5}	cm^3

IV. pH Regulation parameters for both acinar and duct cell models

Name	Symbol	Value	Unit
CO_2 Hydration Constant	K_h	0.725	s^{-1}
CO_2 Dehydration Constant	K_d	248	s^{-1}
NH_4^+ Dissociation Constant	Ka	5.62×10^{-7}	s^{-1}
H_2CO_3 Dissociation Constant	Kb	0.269	s^{-1}
$H_2PO_4^-$ Dissociation Constant	Kc	1.5×10^{-4}	s^{-1}
NHE E_T (Resting)	$NHE\ E_T$	0.4	unitless
NHE E_T (Stimulated)	$NHE\ E_T$	0.8	unitless
NHE Delay	NHE_τ	100	s^{-1}
AE E_T	$AE\ E_T$	1×10^{-10}	unitless
NBC E_T (Rest)	$NBC\ E_T$	1×10^{-6}	unitless
NBC E_T (Stimulated)	$NBC\ E_T$	1×10^{-3}	unitless